Investigating the therapeutic potential of IAP antagonism for the treatment of Duchenne muscular dystrophy

Noah Robert

A thesis submitted to the University of Ottawa in partial fulfillment of the requirements for the Master's degree in Microbiology and Immunology

Department of Biochemistry, Microbiology and Immunology
Faculty of Medicine
University of Ottawa

کز دیو و دد ملولم و مطالعه موشی خویم آرزوست

"*I am tired of demons and monsters, and I wish I could study a good mouse*"

-

Salar Pashangzadeh

PhD Candidate

Table of Contents

ABSTRACT ..... *v*

ACKNOWLEDGEMENTS ..... *vi*

LIST OF FIGURES ..... *viii*

LIST OF TABLES ..... *x*

LIST OF TERMS & ABBREVIATIONS ..... *xi*

CHAPTER ONE: INTRODUCTION *1*

1.1 Skeletal Muscle: Overview **2**

1.2 Post-Natal Skeletal Muscle Regeneration: **3**

1.2.1 Satellite Cells 3

1.3 The Extracellular Matrix **4**

1.4 Immune-Mediated Muscle Regeneration **5**

1.5 Duchenne Muscular Dystrophy: Overview **7**

1.5.1 Mouse Models of DMD 10

1.5.2 Satellite Cell Dysfunction in DMD 12

1.5.3 Immune Cell-Mediated Fibrosis in DMD: Innate effector cells 12

1.5.4 Current and Emerging Therapeutic Strategies for DMD: Challenges and Limitations: 14

1.6 The NF-κB Pathway **16**

1.6.1 The NF-κB Pathway in Skeletal Muscle Regeneration and Disease 17

1.7 Inhibitors of Apoptosis Proteins **22**

1.7.1 cIAP1/2 in Skeletal Muscle Biology and Disease 23

1.7.2 Targeting the IAPs: SMAC Mimetics 24

1.7.3 SMAC Mimetics Effects on Macrophages 24

1.8 Rationale and Hypothesis **27**

CHAPTER TWO: MATERIALS AND METHODS *29*

2.1 Animal Care and Experimental Design **30**

2.2 Creatine Kinase Assay: **32**

2.3 Histology: **32**

2.4 Picrosirius Red Staining **32**

2.5 Multiplex Immunohistochemistry (mIHC) **33**

2.6 Embryonic Myosin Heavy Chain (eMyHC) Staining: **34**

2.7 Image Acquisition and Analysis: **35**

2.7.1 Quantification of Fibrosis 35

2.7.2 mIHC Analysis 36

2.8 Total Collagen Assay: **36**

2.9 Cytokine and Chemokine Array **37**

2.10 Gene Expression Analysis: 38

2.11 Western Blot Analysis: 38

2.12 Statistical Analyses: 39

CHAPTER THREE: RESULTS 42

3.1 Aim 1: Evaluation of fibrosis and the inflammatory response in adult D2.*mdx* mice treated with LCL161 43

3.2 Aim 2: Evaluation of fibrosis and the inflammatory response in juvenile D2.*mdx* mice treated with LCL161 58

CHAPTER FOUR: DISCUSSION 71

Overview: 72

4.1 Muscle Preservation and Functional Outcomes. 72

4.2 LCL161's impact on muscle regeneration may be dependent on disease severity and regulation of MuSCs. 75

4.3 Is fibrosis secondary to the regenerative benefits of LCL161? 77

4.4 LCL161 influences inflammation in D2.*mdx* mice. 80

4.5 Investigating T-Cell dynamics in response to LCL161. 84

4.6 Conclusion 87

REFERENCES: 89

ABSTRACT

Duchenne muscular dystrophy (DMD) is a severe, X-linked genetic disorder characterized by progressive muscle degeneration and fibrosis due to the absence of dystrophin. Despite advancements in supportive care, current treatments remain palliative, underscoring the urgent need for therapies targeting fibrosis and inflammation to improve patient outcomes. While the role of inhibitor of apoptosis proteins (IAPs), particularly cellular-IAPs 1 and 2 (cIAP1/2) in skeletal muscle pathology are increasingly recognized, their specific contribution to muscle fibrosis and the inflammatory response in DMD remains poorly understood. This study investigated the therapeutic potential of LCL161, a Second Mitochondria-derived Activator of Caspases (SMAC) mimetic targeting cIAP1/2, in both adult and juvenile D2.mdx mice, a severe mouse model of DMD. Using a comprehensive approach combining functional, histological and biochemical analyses, I evaluated the impact of LCL161 on muscle pathology. In adult D2.*mdx* mice, LCL161 treatment showed marginal effects on muscle damage and strength, with a trend toward reduced fibrosis in the gastrocnemius muscle and modulation of the cytokine/chemokine profile. Conversely, juvenile D2.*mdx* mice exhibited reduced muscle damage without improved grip strength, accompanied by increased necrosis in the gastrocnemius and significant decreases in *Tnfα* and *Pax7* expression. The muscle and age-dependent responses suggest that the therapeutic efficacy of LCL161 is influenced by the timing and severity of disease progression. This warrants further investigation into the mechanisms by which IAP inhibition influences muscle regeneration, inflammation, and fibrosis in DMD.

ACKNOWLEDGEMENTS

First and foremost, I'd like to thank my supervisors, Drs. Robert Korneluk and Shawn Beug. Shawn, for first taking a chance on me with my Honours project and then convincing Bob to let me stick around for a Master's. Your mentorship gave me a unique opportunity to grow and deepen my interest in research while benefiting from the depth of knowledge that is Dr. Eric. Additional thanks to my TAC members, Dr. Subash Sad and Dr. Luc Sabourin, for their valuable insight and expertise.

To Dr. Neena Lala-Tabbert, thank you for your guidance, support, and invaluable feedback over the past two years. I'm endlessly grateful that you gave me the chance to work on this project, after I spent the first few months running around like a chicken with its head cut off. Under your supervision, I've gained incredible knowledge and encountered opportunities that have shaped me into a better researcher—opportunities I might have otherwise overlooked. Anyone in a mentorship position should strive to be like you and future students will be incredibly fortunate to learn from you.

I am immensely grateful to the technicians who keep our lab—and much of the RI—running smoothly. Martine, your patience, expertise, and support have been invaluable. From hammering in the basics during my undergraduate days to troubleshooting experiments better than Google (or perhaps my ability to Google), your guidance has been crucial. I'm fortunate to have overlapped with your final years at the RI; your retirement leaves big shoes to fill. To Nathalie Earl, thank you for teaching me everything about working with mice, always lending a hand, and tirelessly ensuring the well-being of everyone's animals. Your efforts save us from countless headaches that often go unnoticed.

To the rest of our muscle group—Allan, Diana, and Rachael—thank you for helping with my mice, experiments, and sharing reagents and materials. Beyond research, special thanks to Allan (and by extension the CHEO Student Wellness Committee) for organizing activities and games that reminded us to take a break from our work. I'd also like to acknowledge Keith Wilson for everything he does behind the scenes to let us focus on our research.

A special thanks to Melanie Dugas, our lab's mIHC guinea pig, saving me countless months of optimization but also helping me over the months it did take to get everything down and ready. Also, for speedrunning NYT crossword games in the microscope room to help drown out the incessant buzzing and beeping from tiling hundreds of slides. To Kyle Malone for immediately making me feel welcome in the lab by disclosing incredibly personal information between sips of coffee during my first week or so and helping simplify my scattered ideas and approach new techniques with greater confidence. Lastly, to Mariam Hakoum, your kindness, patience, and generosity in sacrificing your time to help others, including me, did not go unnoticed.

Of course, I'd like to thank my family for supporting me through my degrees and attempting to understand what I was doing but accepted that I was too lazy to explain and mostly received some form of mumble as an answer. Finally, to Emma, for her unwavering support, encouragement, and for trying to answer my statistical questions, which were often just hypothetical incoherent ramblings.

LIST OF FIGURES

Figure 1. The dystrophin-associated protein complex (DAPC). 9

Figure 2. Classical and alternative NF-κB Signalling Pathways 20

Figure 3. NF-κB Signalling Regulates Skeletal Muscle Regeneration and Diseases 21

Figure 4. Schematic representation of selected human inhibitor of apoptosis domain structures 26

Figure 5. The IAP antagonist, LCL161, reduces fibrosis in the diaphragm of *mdx* mice 28

Figure 6. Schematic of treatment schedule for the adult and juvenile mice 31

Figure 7. LCL161 treatment does not significantly affect body weight or muscle mass in adult D2.*mdx* mice but induces splenomegaly 45

Figure 8. LCL161 treatment shows marginal effects on muscle damage and strength but significantly improves resistance to fatigue in adult D2.*mdx* mice 46

Figure 9. Gastrocnemius muscle from LCL161-treated adult D2.*mdx* mice demonstrates a more notable presence of larger fibres 50

Figure 10. LCL161 treatment trends towards reduced fibrosis in the gastrocnemius of adult D2.*mdx* mice 51

Figure 11. LCL161 treatment trends towards increased regeneration in the gastrocnemius and diaphragm of adult D2.*mdx* mice. 52

Figure 12. LCL161 has no apparent impact on macrophage infiltrate or phenotype in adult D2.*mdx* gastrocnemius. 53

Figure 13. Difference in immune response modulation by LCL161 in the gastrocnemius muscle of D2.*mdx* mice through cytokine and chemokine profiling 56

Figure 14. Expression of fibrotic, inflammatory, and myogenic markers in the diaphragm of LCL161-treated Adult D2.*mdx* mice. 57

Figure 15. LCL161 treatment alters select muscle weights and induces splenomegaly without affecting body weight in juvenile D2.*mdx* mice. 60

Figure 16. Functional assessments reveal reduced muscle damage in LCL161-Treated juvenile D2.*mdx* mice despite no improvement in grip strength. 61

Figure 17. LCL161 has no effect on fibre size distribution in the gastrocnemius and diaphragm of D2.*mdx* mice. 64

Figure 18. LCL161 has no effect on fibrosis, but significantly increases necrosis in the gastrocnemius of D2.*mdx* mice 65

Figure 19. LCL161 treatment increases macrophage infiltrate in juvenile D2.*mdx* mice but has no effect on macrophage polarization**.** 66

Figure 20. LCL161 treatment reduces *Tnfα* and *Pax7* levels in the gastrocnemius muscle of juvenile D2.*mdx* mice 69

Figure 21. LCL161 leads to degradation of cIAP1 and cIAP2 in juvenile D2.*mdx* gastrocnemius muscle 70

LIST OF TABLES

Table 1. Optimized Antibody Order, Antigen Retrieval Conditions and Fluorophore Pairing for Multiplex Immunohistochemistry Panel of Macrophage Markers 40

Table 2. List of primer sequences used for RT-qPCR..... 41

LIST OF TERMS & ABBREVIATIONS

ASO	Antisense Oligonucleotide
BAFFR	B-cell Activating Factor Receptor
BCR	B Cell Receptor
BIR	Baculoviral Inhibitor of Apoptosis Protein Repeat
BIRC	Baculoviral IAP Repeat Containing
CARD	Caspase Activation and Recruitment Domain
CCR2	C-C Motif Chemokine Receptor 2
CD(x)	Cluster of Differentiation (specific marker depends on x)
cIAP1	Cellular Inhibitor of Apoptosis Protein 1
cIAP2	Cellular Inhibitor of Apoptosis Protein 2
CK	Creatine Kinase
COL1A1	Collagen Type I Alpha 1 Chain
CTGF	Connective Tissue Growth Factor
CTX	Cardiotoxin
CXCL(#)	C-X-C Motif Chemokine Ligand (specific ligand depends on #)
CXCR(#)	C-X-C Motif Chemokine Receptor (specific receptor depends on #)
DIA	Diaphragm
DMD	Duchenne Muscular Dystrophy
ECM	Extracellular Matrix
EDL	Extensor Digitorum Longus
EGFR	Epidermal Growth Factor Receptor
eMyHC	Embryonic Myosin Heavy Chain
F4/80	EGF-like module-containing mucin-like hormone receptor-like 1
FAPs	Fibro/Adipogenic Progenitors
FGF	Fibroblast Growth Factor
FN1	Fibronectin 1
GAS	Gastrocnemius
GAS6	Growth Arrest-Specific 6
Gr1	Granulocyte Marker 1
IAPs	Inhibitors of Apoptosis Proteins
IFN$_\gamma$	Interferon Gamma
IGF1	Insulin-Like Growth Factor 1
IKK(#)	IκB Kinase (IKK complex component, x indicates specific type)
IL-(#)	Interleukin (specific interleukin depends on #)
IL-1R	Interleukin-1 Receptor
iNOS	Inducible Nitric Oxide Synthase
LCN2	Lipocalin 2
LIX	C-X-C motif chemokine ligand 5

LTBP4	Latent Transforming Growth Factor Beta-Binding Protein 4
LTβR	Lymphotoxin Beta Receptor
Ly6C	Lymphocyte Antigen 6 Complex, locus C
Lyve1	Lymphatic Vessel Endothelial Hyaluronan Receptor 1
MCP-1/CCL2	Monocyte Chemoattractant Protein-1 / C-C Motif Chemokine Ligand 2
MHCII	Major Histocompatibility Complex Class II
mIHC	Multiplex immunohistochemistry
MPO	Myeloperoxidase
MRF	Myogenic Regulatory Factor
MuSC	Muscle Stem Cell; satellite cell
MyoD	Myogenic Differentiation/Myogenic Differentiation 1
MyoG	Myogenin
NEMO	NF-κB Essential Modulator
NF-κB	Nuclear factor kappa-light-chain-enhancer of activated B cells
PAX7	Paired Box protein 7
PDGF	Platelet-Derived Growth Factor
POSTN	Periostin
PTX3	Pentraxin 3
Rag(#)	Recombination Activating Gene (x indicates specific type)
RANK	Receptor Activator of Nuclear Factor Kappa-B
RING	Really Interesting New Gene
ROS	Reactive Oxygen Species
SERPINE1	Serpin family E member 1
SMAC	Second Mitochondrial Activator of Caspases
SMCs	SMAC Mimetics
TAK1	Transforming Growth Factor Beta-Activated Kinase 1
TCR	T Cell Receptor
TGFβ	Transforming Growth Factor Beta
TIMPs	Tissue Inhibitors of Metalloproteinases
TLR	Toll-like Receptor
TNFα	Tumor Necrosis Factor Alpha
TNFR1	Tumor Necrosis Factor Receptor 1
TRAF6	TNF Receptor-Associated Factor 6
TWEAK	Tumor Necrosis Factor-Like Weak Inducer of Apoptosis
UBA	Ubiquitin-Associated
VEGF	Vascular Endothelial Growth Factor
XIAP	X-Linked Inhibitor of Apoptosis Protein

CHAPTER ONE: INTRODUCTION

1.1 Skeletal Muscle: Overview

Skeletal muscle is a highly dynamic tissue that constitutes approximately 40% of human body mass. Attached to bones by tendons, skeletal muscle primarily functions to convert chemical energy into mechanical energy, generating the force and contraction needed for movement and posture maintenance. Beyond facilitating mobility, skeletal muscle is also an essential metabolic and endocrine organ. At a fundamental level, muscle supports basal energy metabolism through the storage of essential nutrients such as carbohydrates and amino acids. Additionally, it contributes to the homeostasis of body temperature. In response to various physiological and environmental stimuli, skeletal muscle produces signalling factors, known as myokines, which promote inter-organ communication and influence overall health.

Skeletal muscle tissue is composed of bundles of muscle fascicles which individually contain groupings of multinucleated cells termed myofibres which are composed of several hundred contractile units known as myofibrils. The hierarchical organization of muscle tissue, from muscle fascicles to myofibrils, enables the coordinated and precise contraction of skeletal muscles. As such, maintaining the health of each of these units is critical for physical function, metabolic regulation, disease prevention, and overall well-being.

1.2 Post-Natal Skeletal Muscle Regeneration:

1.2.1 Satellite Cells

Skeletal muscle has a remarkable capacity for regeneration. The postnatal growth and repair of skeletal muscle depends on a heterogenous population of muscle stem cells (MuSC), called satellite cells, that reside between the basal lamina and plasma membrane of myofibres and are characterized by the expression of paired-box transcription factor 7 (Pax7)[1]. Upon injury, these normally quiescent cells become activated, re-enter the cell cycle, and proceed to differentiate under the controlled expression of muscle-specific transcription factors known as the myogenic regulatory factors (MRFs)[2,3]. Activated or committed satellite cells upregulate myogenic determination protein 1 (MyoD) and myogenic factor 5 (Myf5) and begin to proliferate as myoblasts[4–7]. Following successive rounds of proliferation, myoblasts then upregulate myogenin (MyoG), followed by MRF4 and withdraw from the cell-cycle to differentiate into myocytes[5,8–10]. These terminally differentiated myocytes fuse to one another or existing myofibres to give rise to new fibres and repair damaged ones, respectively. In addition to their capacity for terminal differentiation, satellite cells also have the ability to self-renew to maintain the stem cell population[11].

1.3 The Extracellular Matrix

The extracellular matrix (ECM) within the MuSC niche plays a vital role in supporting regeneration, providing structural integrity, and facilitating communication between muscle cells and their microenvironment (i.e., fibroblasts, immune cells, blood capillaries, and nerves). The ECM can be subdivided into three protein classes: collagenous glycoproteins, non-collagenous proteins, and proteoglycans[12,13]. Together, they function to maintain mechanical homeostasis, muscle elasticity, and serve as signalling intermediates during muscle injury and repair[14,15]. This ECM scaffold influences myoblast differentiation and myofibre regeneration by regulating cell proliferation, adhesion, migration, and ECM remodelling[16–19]. The transient deposition and subsequent degradation of ECM during the regenerative phase are crucial for allowing the growth of new fibres. The balance of the extracellular matrix (ECM) within healthy skeletal muscle is meticulously regulated by various growth factors (e.g., transforming growth factor beta (TGFβ), connective tissue growth factor (CTGF), fibroblast growth factor (FGF), and matrix metalloproteinases (MMP), along with their inhibitors, tissue inhibitors of metalloproteinases (TIMPs)[20,21]. These regulatory molecules are secreted not only by damaged myofibres but also by fibroblasts and infiltrating immune cells.

While the ECM plays a crucial role in normal muscle function and regeneration, its dysregulation can lead to pathological consequences, most notably muscle fibrosis[22]. Muscle fibrosis is a pathological condition characterized by excessive deposition of ECM, particularly collagen, in skeletal muscle tissue. This process is characteristic of several skeletal muscle disorders, including Duchenne muscular dystrophy.

1.4 Immune-Mediated Muscle Regeneration

While MuSCs are the predominant contributor to skeletal muscle regeneration, the inflammatory response is a critical mediator of skeletal muscle repair. This intricate phenomenon is characterized by a dynamic and temporally regulated interplay between innate and adaptive immune cells and the regenerating tissue. Following acute injury, damage-associated molecular patterns (DAMPs) and pro-inflammatory contents are released from the necrotic myofibres, serving as key mediators in the initiation and propagation of the inflammatory response.

Neutrophils are among the first immune cells to infiltrate the site of injury, appearing within one hour and remaining up to 96 hours, with peak infiltration occurring between 12-24 hours[23–25]. The primary function of neutrophils following muscle damage is to initiate and drive the early inflammatory response. As neutrophils transmigrate into the tissue, they facilitate the removal of necrotic fibres via phagocytosis while promoting further monocyte recruitment and repair by releasing a wide array of reactive oxygen species (ROS), cytokines, chemokines, and growth factors. These include but are not limited to tumour necrosis factor alpha (TNFα), interferon-gamma (IFNγ), interleukin 1 alpha/beta (IL-1α/β), IL-6, IL-8, monocyte chemotactic protein-1 or CC chemokine ligand (MCP-1/CCL2), TGFβ, FGF, insulin growth factor 1 (IGF1), platelet-derived growth factor (PDGF), and vascular endothelial growth factor (VEGF) (reviewed in 4–7).

Macrophages are the key innate effector cell during skeletal muscle regeneration. Skeletal muscle contains populations of tissue-resident macrophages ($CD45^+F4/80^+CD64^+$ $Ly6C^{low}$) that support muscle homeostasis, regeneration and

growth[26,30]. Wang et al. identified a CCR2^{-}MHCII^{low}Lyve1^{high} population as the predominant skeletal muscle resident macrophages, characterized by strong phagocytic activity based on gene expression and morphology, emphasizing their role in clearing damaged myofibres and cellular debris[26]. Moreover, macrophages residing in skeletal muscle, specifically within the diaphragm and quadriceps, exhibit distinct gene expression clusters. These differences are hypothesized to reflect functional diversity, likely driven by the unique characteristics and roles of each muscle type[26,31].

Infiltrating, inflammatory macrophages (Ly6C^{hi}), derived from circulating monocytes, are recruited to muscle injuries via the release of MCP-1 by damaged muscle tissue and previously infiltrated neutrophils[32–34]. Macrophage infiltrates begin to increase day one post-injury, and peak between day three and four before gradually declining for the remainder of regeneration[35,36]. Within the first one to three days after injury, inflammatory macrophages aid in the clearance of necrotic myofibres, promoting further immune cell recruitment and priming MuSCs for myoblast proliferation and muscle regeneration[37–41]. As debris is cleared and the myogenic program is initiated, the recruited macrophages begin to transition to an anti-inflammatory state (Ly6^{lo})[42,43]. Characterized by their secretion of anti-inflammatory cytokines (e.g., IL-4, IL-10, IL-13) and growth factors (e.g., TGFβ, FGF, IGF1, PDGF, VEGF), these macrophages promote myoblast differentiation, matrix remodeling and angiogenesis[44,45]. Several studies have shown that depleting macrophages or inhibiting their recruitment during acute injury impairs skeletal muscle regeneration, highlighting their importance in musculoskeletal health[23,46–50]. However, one study has shown that macrophage depletion prior to exhaustive exercise reduced the number of injured myofibres

and proinflammatory cytokines, and similar benefits are seen when targeting macrophage populations in chronic injury disease models[51–53].

In addition to macrophages, T-cells play a crucial role in skeletal muscle repair and regeneration following injury. Both conventional $CD4^+$ and $CD8^+$ T-cells contribute significantly to these processes; however, the precise mechanisms by which they promote muscle repair remain less clearly defined. For this study, the contributions of T-cells to skeletal muscle health were not examined as an emphasis was placed on infiltrating macrophages. However, the role of T-cells in muscle regeneration and repair, along with avenues for further investigation, will be detailed in the Discussion section.

In summary, immune cells are indispensable orchestrators of skeletal muscle regeneration, guiding the process from the initial inflammatory response through to the resolution of inflammation and the completion of muscle repair. Their diverse functions, including phagocytosis, cytokine and growth factor secretion, and interactions with muscle stem cells and other niche components, make them central to the successful regeneration of skeletal muscle in both mice and humans. Disruptions to this carefully coordinated process, such as a persistent pro-inflammatory phase or premature transition to the anti-inflammatory phase, can lead to impaired muscle regeneration, as observed in various muscle pathologies.

1.5 Duchenne Muscular Dystrophy: Overview

Duchenne muscular dystrophy is the most prevalent and severe form of muscular dystrophies[54,55]. This X-linked recessive genetic disorder affects approximately 1 in 5000 male births and has a median survival rate of 22 years[56]. However, median life expectancy

for individuals born after 1990 increases to approximately 28 years, likely attributable to improvements in both the management and treatment of the disease [57]. Children with DMD present signs of developmental and motor delay around two years old and most use a wheelchair by 12 years. By the age of 20, most DMD patients have respiratory complications and cardiomyopathy, which are the leading cause of fatality.

DMD arises from inherited (2/3 of cases) or spontaneous (1/3 of cases) frameshift or nonsense point mutations in the dystrophin gene[58,59]. Dystrophin is a cytoskeletal protein encoded by the DMD gene, the largest gene in the human genome, spanning over 2Mb which further complicates potential therapies[60]. Dystrophin forms part of the dystrophin-associated protein complex (DAPC), integral for maintaining muscle structure and function[61] (**Fig. 1**). Dystrophin binds to the F-actin cytoskeleton in the muscle sarcomere (contractile unit of the myofibre) and is anchored to the extracellular matrix via its interaction with the intracellular domain of dystroglycan[62,63]. The loss of this connection in DMD leads to weakening of the muscle sarcolemma (muscle cell membrane) by disrupting the mechanical and signalling components that maintain structural integrity and contractile activity. Consequently, the muscle becomes prone to contraction-induced damage giving rise to cycles of regeneration and degeneration. Loss of dystrophin in DMD patients presents as progressive muscle wasting and excessive fibrosis which leads to loss of skeletal muscle function [64].

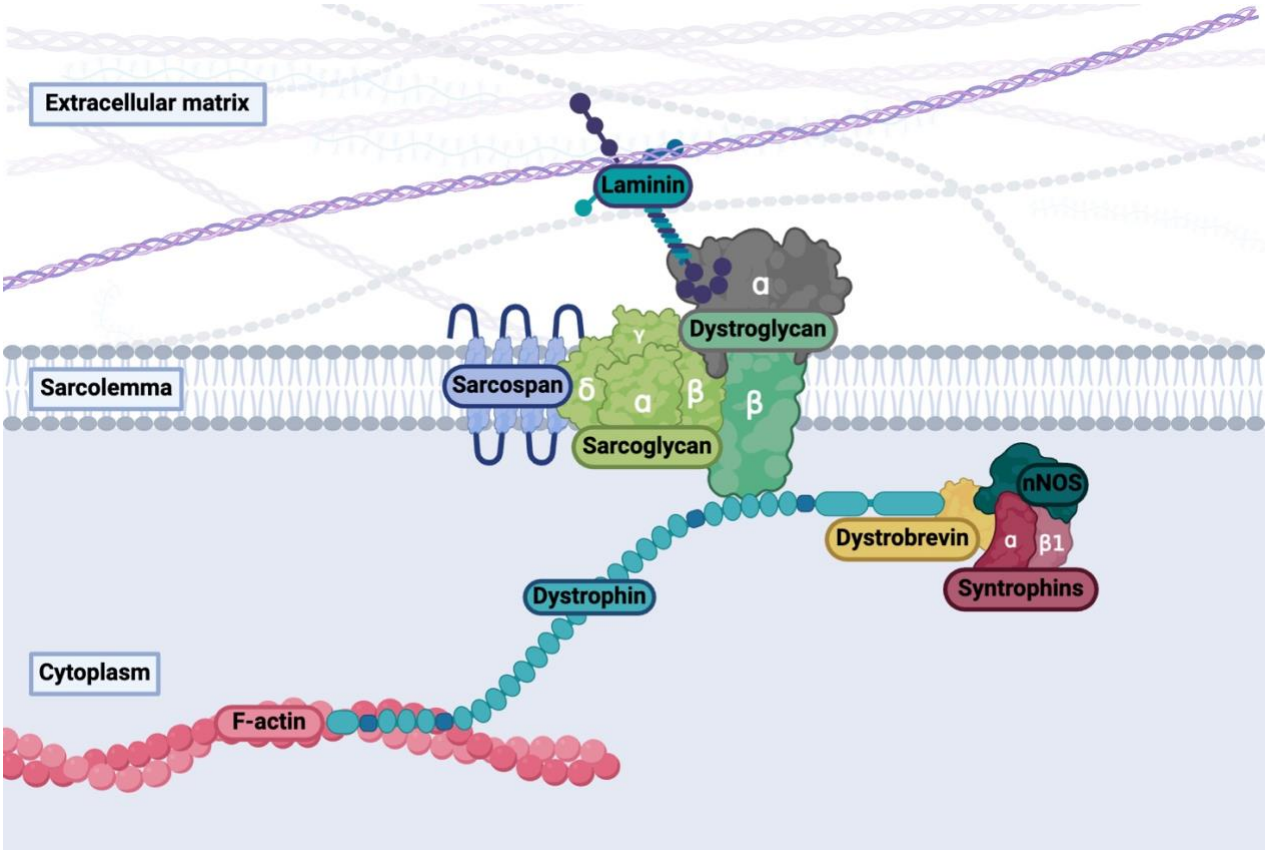

Figure 1. **The dystrophin-associated protein complex (DAPC).** The DAPC is a critical multi-protein assembly that links the intracellular cytoskeleton of skeletal muscle cells to the extracellular matrix, providing structural stability and protecting muscle fibres from contraction-induced damage. This diagram illustrates the key components of the DAPC and their organization within the sarcolemma (muscle cell membrane). **Laminin**: An extracellular matrix protein that interacts with dystroglycan to anchor the DAPC to the extracellular matrix**. Dystroglycan (α and β subunits):** A transmembrane protein complex that connects laminin in the extracellular matrix to dystrophin in the cytoplasm. The α-subunit binds laminin, while the β-subunit spans the membrane and interacts with dystrophin. **Sarcoglycan (α, β, δ, γ subunits):** A group of transmembrane proteins that stabilize the DAPC and contribute to its structural integrity. **Sarcospan:** A transmembrane protein that associates with sarcoglycans and helps maintain the stability of the DAPC. **Dystrophin**: A cytoskeletal protein that links the actin cytoskeleton (F-actin) to the DAPC, providing mechanical support and preventing muscle damage during contraction. **Dystrobrevin:** A cytoplasmic protein that interacts with dystrophin and syntrophins, contributing to signal transduction and structural stability. **Syntrophins (α and β1 subunits):** Adapter proteins that bind signalling molecules, such as neuronal nitric oxide synthase (nNOS), and mediate intracellular signalling. **nNOS:** An enzyme associated with the DAPC that produces nitric oxide, a signalling molecule involved in muscle function and blood flow regulation.

1.5.1 Mouse Models of DMD

Mouse models of Duchenne muscular dystrophy (DMD) play a crucial role in understanding the pathophysiology of this debilitating disease and developing potential therapies. The most extensively studied mouse model is the *mdx* mouse, first discovered by Bulfield et al. in a colony of inbred C57BL/10ScSn mice[65]. These mice harbour a point mutation in exon 23 on the dystrophin gene, resulting in the loss of dystrophin protein and reduced dystrophin RNA in skeletal muscle[66–68]. While the *mdx* mouse exhibits chronic degeneration and regeneration of myofibres with peak necrosis occurring at age 5-6 weeks, the progressive deterioration and development of fibrosis is primarily seen in the diaphragm[69]. In contrast, the hindlimb muscles of *mdx* mice fail to recapitulate the severity of the disease compared to human DMD patients. The hindlimb muscles display significant necrosis, immune cell infiltration, and reduced power and force outputs when normalized to cross-sectional area (CSA) and muscle mass[70–72]. However, the discrepancy between the disease progression in the *mdx* mice and humans is largely attributed to a robust regenerative capacity and partial compensation by the upregulation of utrophin in the mouse model[71–74]. These mice have a much milder phenotype, and their lifespan is reduced by up to 25% compared to controls whereas the lifespan of DMD patients is reduced by roughly 65%[75].

To address the limitations of the *mdx* model, researchers have developed several variations and additional models which are reviewed in depth elsewhere[76,77]. Of particular interest is the D2.B10-Dmd *mdx* /J model (herein referred to as D2.*mdx*), established by Fukada et al. in 2010[78]. The group demonstrated that in response to cardiotoxin (CTX; snake

venom utilized for contraction-induced damage and muscle cell lysis) injury, DBA/2J mice had decreased muscle weight, less myofibres, and impaired satellite cell renewal in comparison to BALB/c, C3H/HeN and C57BL/6 mice. By crossing the *mdx* mutation onto the DBA/2J background, many of the inherent limitations of the traditional *mdx* model were addressed. Consequently, D2.*mdx* mice exhibit a more severe pathology, with both the diaphragm and limb muscles undergoing progressive degeneration like that observed in DMD patients. Comparative studies between the *mdx* and D2.*mdx* models have shown that the latter experience more extensive muscle degeneration, which is attributable to diminished regenerative capacity, heightened inflammation, fibrosis, fat infiltration, and earlier onset of disease[78–81]. D2.*mdx* mice also exhibit cardiomyopathy, have lower respiratory rates, and perform poorer on hanging wire and grip strength tests[80,82] The severity of disease in the D2.*mdx* model and DMD patients is attributed to a Latent Transforming Growth Factor Beta Binding Protein 4 (LTBP4) polymorphism, a known genetic modifier [81,83]. LTBP4 plays a critical role in regulating TGFβ activity by sequestering it and thereby limiting its activity. The polymorphism seen in D2.*mdx* mice compromises the stability of LTBP4, resulting in increased activation of TGFβ and consequent tissue degeneration and fibrosis, further intensifying disease pathology [83,84].

While the D2.*mdx* better models the disease progression of DMD patients, it does not come without limitations. These mice develop calcifications that can impact the analysis of fibrosis and there are conflicting studies as to whether the DBA/2J background is a confounder in cardiac fibrosis and hypertrophic cardiomyopathy [85–88].

1.5.2 Satellite Cell Dysfunction in DMD

Direct defects in MuSCs have been observed in DMD. Asymmetric division is essential for the self-renewal and myogenic fates of MuSCs. In DMD-derived MuSCs, the absence of dystrophin and DAPC interactions has been shown to affect the polarity of MuSCs and their expression of myogenic transcription factors, effectively impairing their commitment and function[89,90]. Interestingly, MuSC depletion in limb-girdle muscular dystrophy and DMD models improved histopathology, potentially due to reduced MuSC activation and MyoD-driven myogenesis[91]. This challenges the conventional view that MuSCs are universally beneficial for repair and implies that persistent MuSC activation contributes to sarcolemmal fragility, potentially by generating new but structurally compromised myofibres that are more prone to degeneration. Conversely, MuSCs isolated from aged dystrophic muscle retain the same regenerative potential as those from young or aged wild-type mice when grafted into immunocompromised dystrophic mice[92]. This is further highlighted by environmental modifications, such as host muscle irradiation, use of immunodeficient mice, or even age, which enhance donor MuSC proliferation and self-renewal[93–95]. In summary, there are intrinsic defects in dystrophic MuSCs that appear to be exacerbated by the muscle microenvironment and in DMD this niche is strongly infiltrated by immune cells and fibro-adipogenic progenitors (FAPs).

1.5.3 Immune Cell-Mediated Fibrosis in DMD: Innate effector cells

Unlike acute injuries, frequent damage in DMD muscle leads to the persistence and accumulation of neutrophils and pro-inflammatory macrophages. This leads to elevated levels of pro-inflammatory cytokines and free radicals that increase oxidative stress, inhibit

myogenic differentiation and increase muscle cell lysis. For example, neutrophil depletion and the use of etanercept (a TNF-α inhibitor) in *mdx* mice reduced both spontaneous and exercise-induced muscle damage[96]. Similarly, IL-6 blockade in *mdx* mice led to reduced necrosis, improved treadmill performance, decreased classical NF-κB signalling (Nuclear factor kappa-light-chain-enhancer of activated B cells), and increased the expression of myogenic markers *Pax7*, *Myod1*, *Myog*, *Des* and *Il4*[97]. Myeloperoxidase (MPO) and inducible nitric oxide synthase (iNOS), primarily released by neutrophils and pro-inflammatory macrophages, respectively, catalyze the production of reactive oxygen species (ROS) and reactive nitrogen species (RNS)[98,99]. Evidence also suggests that MPO is capable of increasing the catalytic activity of iNOS in inflamed areas[100]. Knockout models for both MPO and iNOS in *mdx* mice have demonstrated reductions in muscle membrane lysis[101,102].

In the dysregulated inflammatory milieu, the balance between macrophage transition states is also affected. IFN$_\gamma$-signalling is a strong inducer of the pro-inflammatory phenotype and has been shown to inhibit C2C12 myoblast proliferation and differentiation *in vitro*, and promoted muscle damage and decreased MyoD expression in *mdx* mice[103]. In 12-week-old IFN-$\gamma^{-/-}$*mdx* mice, there was significantly less muscle damage consistent with reductions in macrophage infiltrate, necrotic myofibres and a shift towards anti-inflammatory macrophages[103]. Notably, no significant differences were noted in younger, 4-week-old mice where degeneration seems to outpace regenerative efforts[103]. Since distinct regions of the muscle may be in different states of damage and repair, macrophages can also exhibit a transitional state displaying both pro/anti-inflammatory effector functions resulting in an unresolving environment. For example, the anti-inflammatory macrophages are a key

source of TGFβ, which is elevated in D2.*mdx* mice and DMD patients[81,83,84,104]. TGFβ is a well-established driver of fibrosis and impairs myogenesis, contributing to disease severity[105–108]. The sustained levels of TGFβ are capable of converting fibroblasts to a myofibroblast phenotype resulting in increased collagen production and induces the differentiation of myogenic cells into fibrogenic cells[107,109,110]. As the disease progresses and TGFβ increases, it also competes with TNFα and outpaces the ability of macrophages to induce TNFα-dependent apoptosis in FAPs[111,112]. By promoting FAP differentiation into myofibroblasts, collagen production is further increased and contributes the replacement of muscle tissue with non-functional fibrotic deposits.

1.5.4 Current and Emerging Therapeutic Strategies for DMD: Challenges and Limitations:

Despite medical advances, all current treatments for DMD remain palliative. The gold standard of care includes glucocorticoid therapy (e.g., prednisone and deflazacort) combined with multidisciplinary management, encompassing physical therapy, respiratory care, nutritional support, and cardiac monitoring [113,114]. While these drugs can slow the progression of the disease through their anti-inflammatory effects, there are notable concerns regarding adverse events associated with long-term use of anti-inflammatory steroids such as excessive weight gain, short stature, behavioural changes, and bone health issues.

To address the unmet clinical need for alternatives, there has been progress in developing nonsteroidal therapies for DMD patients; however, they have not yet demonstrated consistent and substantial improvements in patient outcome. Antisense

oligonucleotide based drugs (ASOs) function at the RNA level, degrading, inhibiting, or modulating the splicing of messenger RNA (mRNA) or pre-mRNA[115]. In general, ASOs for DMD work by binding target exons or splice sites on the dystrophin gene to restore the reading frame and produce a shorter but functional dystrophin protein[116]. Currently, four ASOs have reached FDA approval (eteplirsen, golodirsen, viltolarsen and casimersen) for demonstrating increased production of dystrophin, which does not necessarily correlate with clinical improvement[117–121]. Although ASOs present a promising therapeutic option for some DMD patients, the majority of patients remain ineligible for ASO treatment due to advanced disease progression or mutations that are not addressed by current therapies[122,123]. Read-through compounds, which attempt to enhance ribosomal reads of premature stop-codons are also being explored to address nonsense mutations, which comprise 10-15% of DMD cases[124,125]. Ataluren has been shown to delay both ambulatory and respiratory decline in patients with nonsense mutations[126,127]. However, its approval is limited to a small number of countries.

More recently, givinostat, a histone deacetylase (HDAC) inhibitor, received FDA approval[128]. Givinostat works by blocking enzymes involved in gene regulation, potentially activating muscle repair mechanisms, reducing inflammation, and decreasing fibrosis, as demonstrated in the *mdx* mouse[129]. Recent clinical trials have provided encouraging results, where DMD boys receiving givinostat performed significantly better on the 4-stair climb (4SC) time than the placebo group[78,82,130,131]. However, both groups still experienced a decline in performance times. As research continues, givinostat's broad applicability and ability to stabilize disease progression make it a significant addition to the muscular dystrophy

treatment landscape. These findings underscore the importance of identifying additional therapeutics capable of restoring or maintaining healthy tissue, which is crucial for enhancing the efficacy of cell and gene therapies.

1.6 The NF-κB Pathway

The NF-κB pathway exhibits a basal level of activation across most cell types under normal physiological conditions and is rapidly inducible in response to a variety of stimuli. The NF-κB family of transcription factors include RelA (p65), RelB, c-Rel, NF-κB1 (p105/p50) and NF-κB2 (p100/p52). These proteins share a highly conserved 300-amino acid Rel homology domain (RHD) at their N-terminus, which facilitates subunit dimerization to produce an NF-κB transcription factor. Through their RHD, the dimers interact with the inhibitors of NF-κB (IκBα, IκBβ, IκBε, p100, and p105), which sequester the subunits in the cytoplasm. Only upon their phosphorylation, ubiquitination, and subsequent degradation can the NF-κB subunit translocate to the nucleus to act on target genes. The IκB kinase (IKK) complex, composed of IKKα, IKKβ, and IKKγ (NEMO; NF-κB essential modulator), plays a central role in the activation of the NF-κB pathway[132]. The differential phosphorylation of the IKK subunits can bias the signalling towards either the classical (canonical) or alternative (non-canonical) arms (**Fig.2**)[132–134]. Through both signalling cascades, NF-κB has been implicated in a wide array of biological processes including innate and adaptive immunity, cell cycle progression, apoptosis, and stress responses[135,136]. Given its central role, dysregulation of this pathway is frequently associated with a variety of pathological conditions[136].

1.6.1 The NF-κB Pathway in Skeletal Muscle Regeneration and Disease

Both classical and alternative NF-κB pathways have been implicated in regulating myogenesis (**Fig.2**). Guttridge et al. revealed that classical NF-κB activation inhibits differentiation through posttranscriptional regulation of MyoD expression and function, thereby preventing premature differentiation of myoblasts. This finding has been corroborated by other studies that demonstrate that pro-inflammatory cytokines (TNFα, IL-1β and TNF-like weak inducer of apoptosis (TWEAK)) activate classical NF-κB signalling and inhibit myogenic differentiation[137,138]. Furthermore, Mourkioti et al. demonstrated that muscle-specific deletion of IKKβ led to impaired regeneration following injury[139]. Similarly, inactivation of components of the classical pathway in MuSCs (TAK1, TRAF6 and IKKβ), impairs self-renewal, regenerative myogenesis, and leads to premature differentiation[140–142]. Together these studies demonstrate that classical pathway activation supports proliferating myoblasts during early muscle regeneration and inhibits differentiation[42,44,143,144]. For differentiation to occur, the activity of the classical pathway decreases, and the alternative pathway becomes increasingly active. A paper from Bakkar et al. demonstrated that both arms of the NF-κB are essential for the myogenic program and are temporally regulated[145]. Specifically, myogenesis and differentiation are enhanced in $p65^{-/-}$ mice and myoblasts, and alternative pathway components, IKKα , RelB, and p52 are induced late into myogenesis [145]. Alternative signalling is also essential to myoblast fusion and myotube homeostasis by regulating mitochondria and oxidative metabolism [146–148].

Given the integral role of NF-κB in myogenesis and regeneration, it is no surprise that aberrant signalling is characteristic of several muscle diseases including DMD [149–152]. Studies

have shown that NF-κB DNA binding activity was significantly higher in diaphragm muscles from *mdx* mice compared to controls and consequently levels of pro-inflammatory cytokines (TNFα, IL-1β) were also increased [153,154]. Furthermore, pharmacological inhibition of the IKK/NF-κB pathway using the NEMO-binding domain (NBD) peptide in *mdx* mice resulted in improved diaphragm muscle function, with significantly higher developed tetanic force compared to controls[153,155]. This treatment also reduced inflammation and enhanced regeneration in limb muscles. In a chronic injury model using a MuSC-specific knockout of NEMO and constitutively active IKKβ ($IKK2CA^{MuSC}$), persistent activation of classical NF-κB resulted in telomere shortening[156]. Similarly, this study showed crossing the $IKK2CA^{MuSC}$ mice with the *mdx* mice worsened the dystrophic phenotype[156]. Improvement to the dystrophic phenotype in both *mdx* mice and golden retriever muscular dystrophy models has been demonstrated by Hammers et al. using edasalonexent and CAT-1041, both potent inhibitors of classical NF-κB signalling. Notably, CAT-1041 showed enhancements in muscle function and reductions in inflammation, fibrosis, and muscle damage[157]. Despite having a promising safety profile and slowing disease progression in phase I and II clinical trials, the clinical program for edasalonexent in DMD was halted due to the failure to meet primary (North Star Ambulatory Assessment; NSAA) and secondary endpoints (time to stand, 10-meter walk/run, and 4-stair climb) in the Phase 3 PolarisDMD trial[158–160]. These findings underscore the therapeutic potential of targeting NF-κB signalling pathways to mitigate disease pathology in muscular dystrophy. However, they also highlight the need for alternative approaches to modulate NF-κB more effectively, as current methods may not fully address the complexity of the disease or its side effects. Further exploration of diverse NF-κB-

targeting strategies is essential to maximize therapeutic benefits and improve patient outcomes.

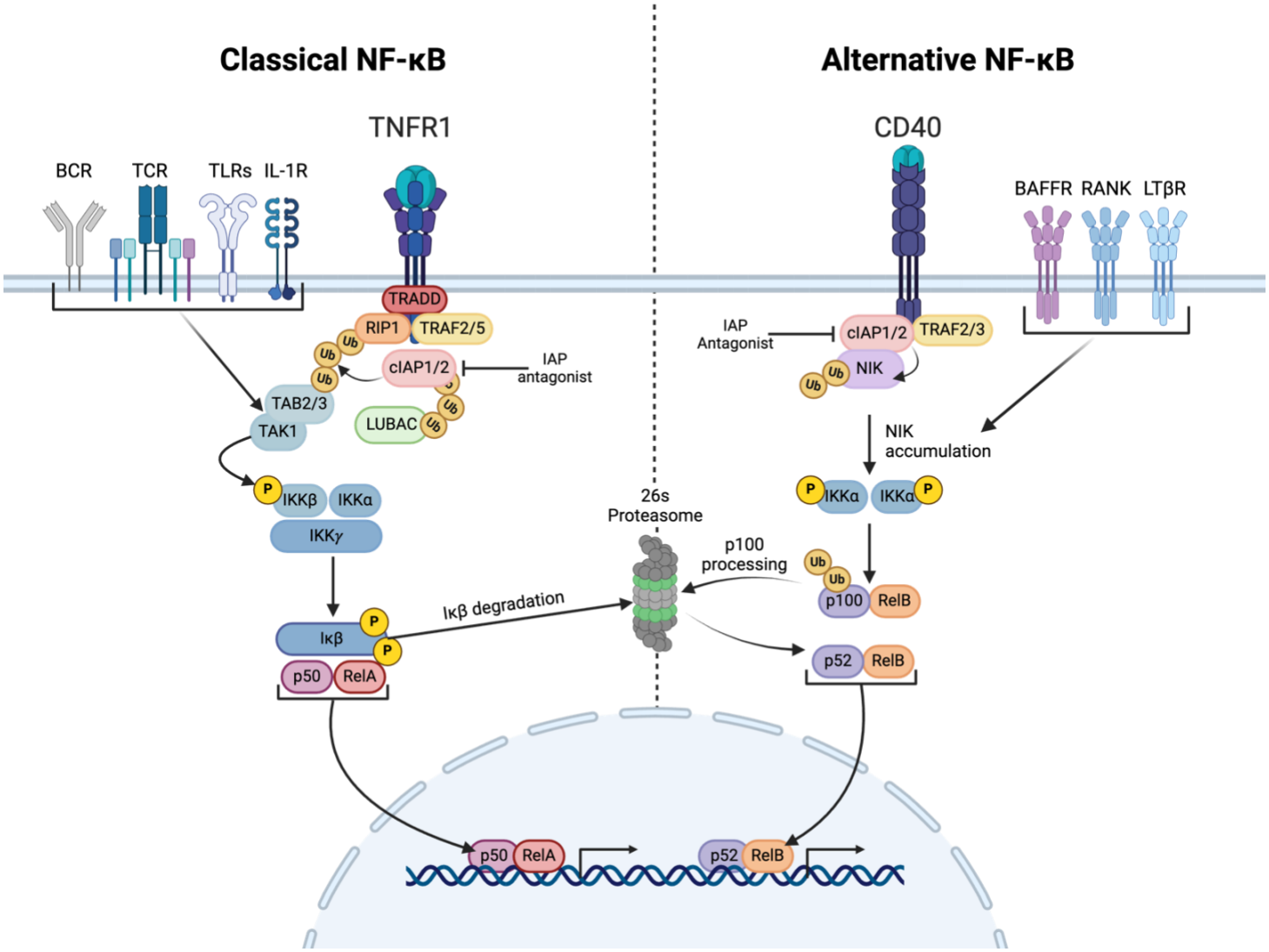

Figure 2. Classical and alternative NF-κB Signalling Pathways. The conventional mechanism of classical pathway activation involves ligand binding to various surface receptors, which subsequently converge on the IKK complex. Activation of classical signalling is achieved by the direct ubiquitination of receptor-interacting protein kinase 1 (RIPK1) by cIAP1/2, triggering the phosphorylation-dependent degradation of IκBα by the IKK complex. This relieves the inhibition on the NF-κB dimer to activate genes associated with regulating inflammation, immune responses, cell survival, proliferation, and stress responses. The alternative pathway is induced by ligand binding to TNF superfamily receptors leading to NIK accumulation, IKKα phosphorylation and the proteasomal processing of p100 into p52. The p52 unit dimerizes with RelB, and ultimately influences genes associated with B cell maturation, immune regulation, and tissue homeostasis. In the context of an IAP antagonist like a SMAC mimetic, cIAP1/2 degradation leads to NIK accumulation in a ligand-independent manner.

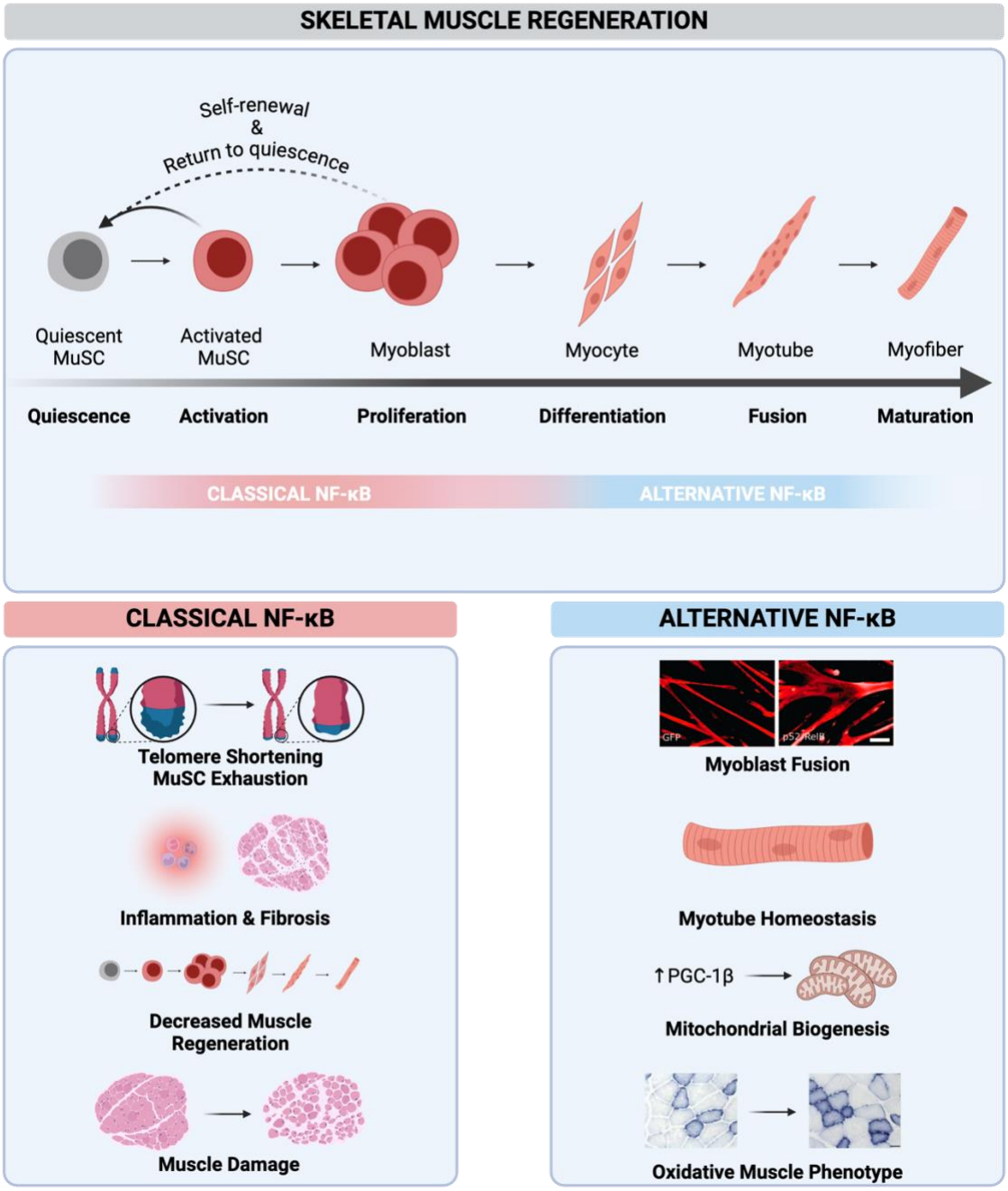

Figure 3. NF-κB Signalling Regulates Skeletal Muscle Regeneration and Diseases. (Top panel) Adapted from J. H. Nguyen et al. 2019; Byun, Lee, and Baek 2024. Schematic representation of skeletal muscle regeneration showing the progression from quiescent muscle stem cells (MuSCs) through activation, proliferation, differentiation, fusion, and maturation to form myofibres, with self-renewal capacity indicated. (**Bottom panel, left)** Classical NF-κB pathway activation in muscle disorders leads to telomere shortening and MuSC exhaustion, promotes inflammation and fibrosis, and results in decreased muscle regenerative capacity and muscle damage. **(Bottom panel, right)** Alternative NF-κB signalling supports healthy muscle function by promoting myoblast fusion, maintaining myotube homeostasis, enhancing mitochondrial biogenesis through PGC-1β upregulation, and establishing an oxidative muscle phenotype.

1.7 Inhibitors of Apoptosis Proteins

The inhibitors of apoptosis proteins (IAPs) are a family of antiapoptotic proteins that exert their function through the direct inhibition of caspase or via downstream signalling pathways. Within the human genome, eight IAPs are encoded by BIRC (baculoviral IAP repeat-containing) genes, of which the X-linked IAP (XIAP) and cellular IAP 1 and 2 (cIAP1, cIAP2) are the most widely studied (**Fig.4**). Shared amongst XIAP, cIAP1, and cIAP2 are three BIR domains, a ubiquitin-associated domain (UBA) and a Really Interesting New Gene (RING) domain which mediate protein-protein interactions, interact with ubiquitinated proteins and confer E3 ligase activity, respectively[161–163]. The cIAPs possess an additional conserved caspase recruitment domain (CARD) which has been implicated in protein-protein interactions and inhibits the E3 ligase activity of cIAP1 and subsequent RING dimerization[164,165].

While the IAPs are implicated in apoptosis and caspase inhibition, their roles extend beyond the regulation of cell death. Due to their intrinsic E3-ligase activity, the IAPs are capable of mediating ubiquitin-dependent signalling events in cell-cycle progression and signal transduction pathways. The diverse functions of the IAPs, specifically cIAP1/2, have been thoroughly reviewed elsewhere[166,167]. Of particular interest, are the roles of cIAP1 and cIAP2 in immune cells and inflammation through their regulation of classical and alternative NF-κB pathways (**Fig.2**) and their significance appears to be context-dependent, varying with infection or disease conditions.

1.7.1 cIAP1/2 in Skeletal Muscle Biology and Disease

As key intermediates of NF-κB signalling, the Korneluk lab has focused on the role of the IAPs in skeletal muscle biology. Research has focused on cIAP1 as it is the only cIAP expressed in skeletal muscle[168]. These studies have demonstrated that cIAP1 negatively regulates myoblast fusion and its expression is upregulated in dystrophic and denervated muscle[146,169,170]. Loss of cIAP1 appears to have positive impact on muscle histology and function in *mdx* mice[169–171]. In comparisons between macrophage infiltration of cIAP1$^{+/+}$ and cIAP1$^{-/-}$ *mdx* mice, Enwere et al. demonstrated that mice lacking cIAP1 had a greater population of M2 macrophages (CD163^{+}) compared to pro-inflammatory macrophages (CD68^{+}) in the soleus muscle[169]. They also showed a general reduction in inflammatory markers (*Il6*, *Tnfα*, and *Il10*) in cIAP1$^{-/-}$*mdx* mice compared to cIAP1$^{+/+}$*mdx* mice. To date, no studies have demonstrated a role for the IAPs in muscle fibrosis, despite their known roles in degenerative pathology and similarly, the underlying mechanism of attenuation of fibrosis and improved muscle histology remains unknown. Also, cIAP1-null macrophages have a diminished capacity to produce and release nitric oxide (NO), which promotes muscle damage *in vitro* and *in vivo*[172–174]. Unpublished data from our lab has shown that cIAP1-null mice had decreased MuSCs in the tibialis anterior and soleus after CTX injury and both cIAP2-null mice and conditional knockout of cIAP1 from PAX7^{+} cells results in smaller regenerated fibres[171]. Together these studies suggest that cIAP1/2 have roles in skeletal muscle repair by influencing both the tissue-resident cells and infiltrating immune cells.

1.7.2 Targeting the IAPs: SMAC Mimetics

SMAC mimetics (SMCs) are a class of small molecule drugs designed to mimic the activity of the endogenous Second Mitochondria-derived Activator of Caspases (SMAC) protein. Specifically, these compounds replicate the Ala-Val-Pro-Ile (AVPI) tetrapeptide binding motif of SMAC, which facilitates their interaction and subsequent inhibition or degradation of XIAP and cIAP1/2, respectively[175]. SMAC mimetics can be classified as monovalent or bivalent based on the presence of one or two AVPI domains, the latter of which has 100-1000 times greater potency based on *in vitro* studies[175]. Clinical and pre-clinical research of these compounds has focused on the treatment of cancers given that the IAPs are overexpressed in many solid and hematological cancers[176]. Through cIAP1/2 degradation, SMCs promote NF-κB signalling via NIK stabilization, shifting the pathway towards alternative signalling. As a secondary effect, they can also induce classical signalling through autocrine TNF-α production[177].

1.7.3 SMAC Mimetics Effects on Macrophages

In the context of immune responses, SMCs have been shown to mediate the induction of cytokines and chemokines, improving immune cell infiltration, increase TNFα and IFN_{γ} production in macrophages as well as revert their phenotype from anti-inflammatory to pro-inflammatory[177]. Unpublished data from the Robertson Lab at Dalhousie University also demonstrated that the monovalent SMC, LCL161, biased macrophages towards a pro-inflammatory phenotype and induces apoptosis in anti-inflammatory macrophages *in vivo*[178]. McComb et al., also demonstrate significant decreases in macrophage populations upon the administration of SM-164, a bivalent SMC,

but did not investigate whether there was preferential killing of specific phenotypes [179]. Interestingly, another study using LCL161 revealed cIAP2 is preferentially expressed in pro-inflammatory macrophages while cIAP1 appears to be expressed in anti-inflammatory macrophages, despite functional redundancies between the two IAPs[180]. Additionally, it has been demonstrated that apoptosis of human pro-inflammatory macrophages by LCL161 is dose-dependent and partially reliant on cIAP2 [181]. As potent IAP antagonists and modulators of NF-κB signalling, SMCs hold promise for drug repurposing in diseases characterized by dysregulated NF-κB activity.

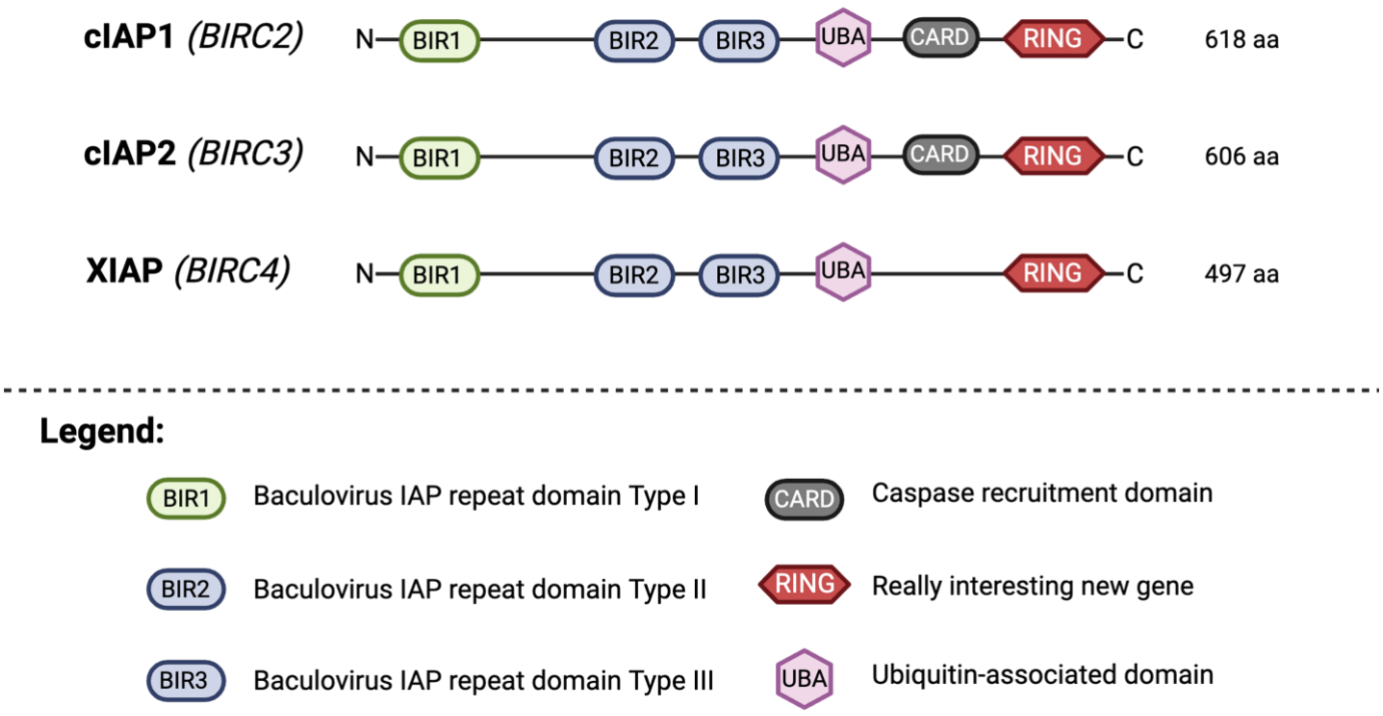

Figure 4. Schematic representation of selected human inhibitor of apoptosis domain structures. In the mammalian IAP family, BIR domains enable protein-protein interactions. Type I BIR domains (BIR1) primarily interact with tumour necrosis factor receptor-associated factor 1 and 2 (TRAF1, TRAF2) while type II BIR domains (BIR2, BIR3) interact with caspases, SMAC and IAP antagonists. The UBA domain binds ubiquitin and polyubiquitin. In cIAP1/2, CARD domain inhibits the E3 ligase activity of the RING domain.

1.8 Rationale and Hypothesis

Skeletal muscle atrophy and fibrosis are distinct but associated events characteristic of muscular dystrophies, myopathies, and chronic inflammation from multiple injuries. The role of cIAP1/2 in muscle fibrosis remains unknown as does the relative contribution of IAP expression in fibrotic tissue versus infiltrating immune cells. Since loss of cIAP1 reduces the profibrotic inflammatory response and macrophage infiltration in BL10-*mdx* mice and the IAP antagonist, LCL161, reduces diaphragm histopathology of BL-10-*mdx* mice (**Fig.5**), **I hypothesize that the loss of IAPs will attenuate muscle fibrosis**.

The specific aims of the study are to:

1. *Evaluate fibrosis and the inflammatory response in adult D2.mdx mice treated with LCL161*
2. *Evaluate fibrosis and the inflammatory response in juvenile D2.mdx mice treated with LCL161*

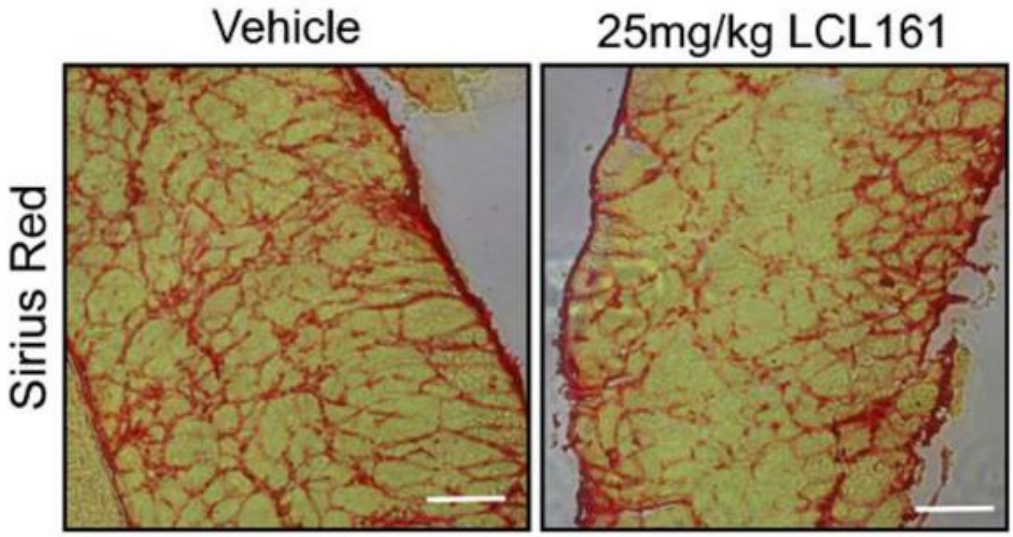

Figure 5. The IAP antagonist, LCL161, reduces fibrosis in the diaphragm of *mdx* mice. Picrosirius red staining of diaphragm muscle from BL10-*mdx* mice treated with vehicle (30% 0.1N HCl + 70% 100mM NaOAc) or 25 mg/kg LCL161. Scale bars= 50 μm. Unpublished data from Dr. Neena Lala-Tabbert.

CHAPTER TWO: MATERIALS AND METHODS

2.1 Animal Care and Experimental Design

Mice were handled as recommended by the guidelines established by the University of Ottawa Animal Care Veterinary Service and the Canadian Council on Animal Care. D2.*mdx* and the corresponding genotype control, DBA/2J (Wild type) were obtained from Jackson Laboratories at 5-8 weeks. All animals were housed in a controlled facility (22 °C with 30% relative humidity on a 12-hour light/dark cycle) and provided with food and water ad libitum.

To explore whether SMCs can reduce muscle fibrosis, mice were administered either a vehicle solution (30% 0.1N HCl and 70% 100 mM NaOAc) or LCL161 (25 mg/kg, Novartis) via oral gavage three times weekly for 4 to 8 weeks. Mice were categorized as adults if treatment began at 8 weeks of age and concluded at 16 weeks, and as juveniles if treatment began at 5 weeks and concluded at 9 weeks. Functional assessments (hanging wire and grip strength) were performed following the standardized protocol outlined in the TREAT-NMD SOPs: DMD_M.2.1.004 and DMD_M.2.2.001 [182,183] .

Mice were sacrificed 1 (juvenile) or 5 (adult) days after the final treatment. The left and right tibialis anterior (TA), gastrocnemius (Gas), soleus (Sol), and extensor digitorum longus (EDL) were collected along with the diaphragm and heart (adult only) and weighed. Tissue used for sectioning was either embedded in Tissue-Tek OCT compound or fixed in 10% neutral buffered formalin (NBF) for freezing in liquid nitrogen-cooled isopentane or paraffin embedding, respectively. Tissues used for biochemical analysis were flash frozen in liquid nitrogen. Treatments and functional tests were performed in a blinded manner.

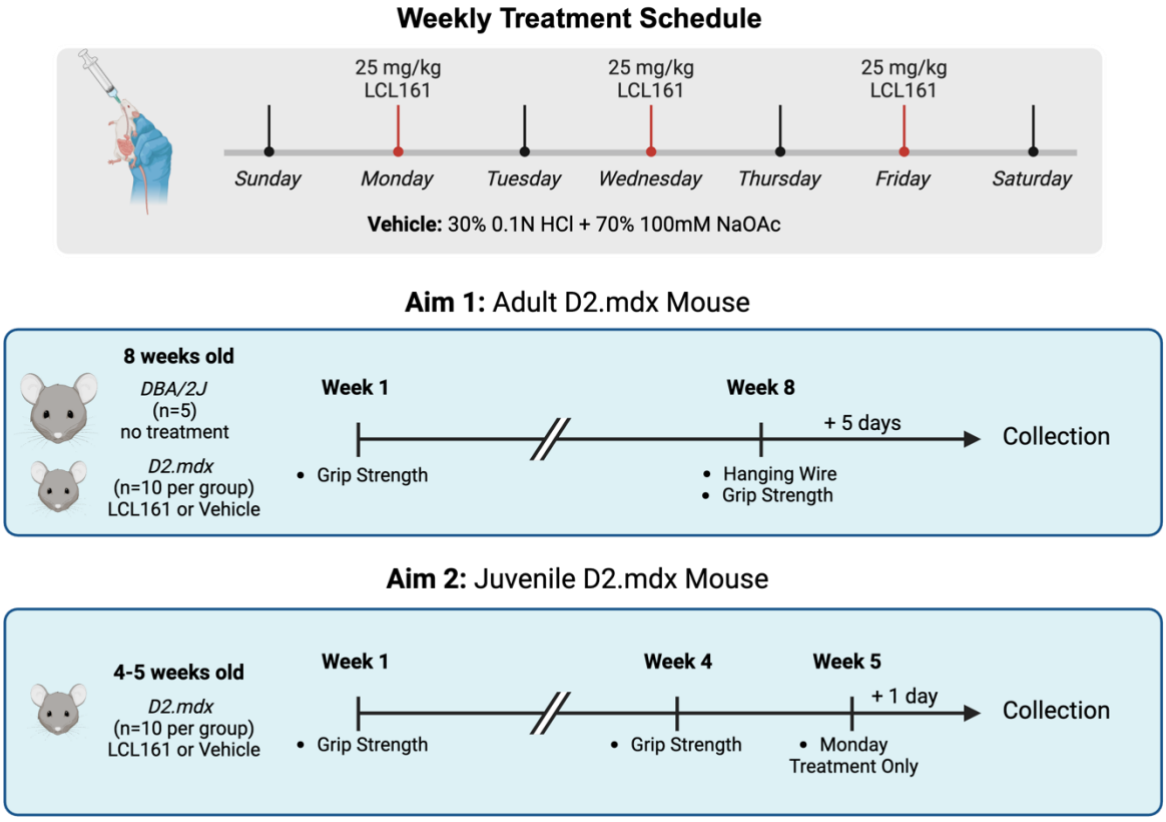

Figure 6. Schematic of treatment schedule for the adult and juvenile mice.

2.2 Creatine Kinase Assay:

Whole blood was collected from mice into Eppendorf tubes at endpoint via cardiac puncture. To isolate serum, tubes were left incubated for 30 minutes at room temperature, then centrifuged at 10 000 rpm for 10 minutes at 4°C. The serum was removed and transferred to fresh Eppendorf tubes and stored at −80°C. Quantitative analysis of creatine kinase (CK) activity in serum was conducted using the liquid creatine kinase reagent set (Pointe Scientific, 23-666-208), following the standardized protocol outlined in the TREAT-NMD SOP: MD_M2.2.001[184].

2.3 Histology:

Gastrocnemius and hemi-diaphragms from D2.*mdx* mice were collected and placed in 10% NBF at room temperature for 48 hours. Tissues were then placed in 70% EtOH and sent to the Louise Pelletier Histology Core Facility (LPHCF, University of Ottawa) for processing, paraffin-embedding, sectioning and H&E staining services. Muscle samples were sectioned into 4µm-thick cross-sections.

Prior to staining, slides were baked at 60°C for 1 hour and deparaffinized in a series of xylene washes (3 x 5 min). Xylene was then removed by two washes 100% EtOH (2 x 10 minutes) and rehydrated through a graded series of EtOH (95%, 70% 50%, 5 minutes each) and placed in double-distilled water (ddH2O) for 5 minutes.

2.4 Picrosirius Red Staining

To stain for collagen networks within the muscle tissue, sections were stained with picrosirius red. Once deparaffinized and rehydrated, slides were post-fixed in a pre-warmed

jar of Bouin's Solution (Sigma-Aldrich, HT10132) at 60°C for 1 hour and excess solution was rinsed under running tap water for 10 minutes followed by submersion in ddH2O for 2 minutes. The slides were then stained with picrosirius red (Abcam, ab150681) for 1 hour at room temperature, with gentle rocking and protected from light. The stain was removed using acetic acid solution, dehydrated in 100% EtOH, cleared with xylene and cover-slipped with DPX mountant (Sigma-Aldrich, 06522)

2.5 Multiplex Immunohistochemistry (mIHC)

Multiplex IHC was performed with Opal 6-Plex Manual Detection Kit (Akoya Biosciences, NEL811001KT) to detect total macrophage, pro-inflammatory macrophage and anti-inflammatory macrophage populations in D2.*mdx* gastrocnemius. See Table 1 for the Macrophage Panel, including a comprehensive list of antigen retrieval conditions, primary antibody dilutions, and fluorophore pairings. Deparaffinized and rehydrated slides were placed in the provided antigen retrieval buffer (Akoya Biosciences) and underwent heat-induced antigen retrieval (HIAR) using the 2100 Antigen Retriever (Prestige Medical, 210050). Slides were allowed to cool to room temperature prior to proceeding with staining. Cooled slides were briefly washed with 1X Tris-buffered saline with 0.1% Tween 20 (3x3min, TBST) and placed in ddH2O. Autofluorescence was quenched with TrueBlack Lipofuscin Quencher (Biotium,23007) for 1 minute, washed with 1xTBST (3x3 min) and then blocked with Ab diluent/block (Akoya, ARD1001EA) for 10 minutes. All primary antibodies were diluted in the provided blocking buffer and incubated overnight at 4°C. Subsequently, slides were washed with 1X TBST and incubated with 1x Opal Anti Ms+Rb HRP (Akoya, ARH1001EA) for 10 minutes. Slides were washed again in 1X TBST and then incubated for 30 minutes with Opal

520, 570, 650, or 690) diluted in 1X Plus Manual Amplification diluent (1:100, Akoya, FP1609) for primary antibody detection. Fluorophore staining was quenched using HIAR in the buffer optimized for the next primary antibody. Blocking, primary incubation and fluorophore signal generation were repeated until all targets were stained. Slides were counterstained with DAPI (PerkinElmer, 0.5ug/mL) and cover-slipped using Dako Fluorescence mounting medium (Agilent, S3023). Antigen retrieval buffer, primary antibody dilution and staining order were all optimized prior final staining and imaging.

2.6 Embryonic Myosin Heavy Chain (eMyHC) Staining:

Immunofluorescence staining was performed as previously described for paraffin-sections [185]. Deparaffinized and rehydrated slides underwent HIAR in IHC-Tek Epitope Retrieval Solution (IHCWorld, 1W-1100-1L). Slides were permeabilized with 0.1M Glycine, 0.1% Triton X-100 in PBS for 10 minutes. Autofluorescence was quenched with TrueBlack, and sections were blocked with 5% normal goat serum and 2% bovine serum albumin (BSA) in PBS. When staining with mouse antibodies, mouse-on-mouse IgG blocking solution was added at 1:40 (Invitrogen, R37621). Sections were probed overnight at 4°C, with MYH3/eMyHC (Developmental Studies Hybridoma Bank, F1.652) and laminin (Abcam, ab11575) at 1:2 and 1:200, respectively. Signal was generated using goat anti-mouse IgG1 AlexaFluor 594 (1:250) and goat anti-rabbit IgG AlexaFluor 488 (1:250) and slides were cover-slipped using Dako Fluorescence mounting medium.

2.7 Image Acquisition and Analysis:

All microscopy images were acquired using the 10X objective on the Zeiss AxioImager Z2 widefield microscope with Colibri 5/7. Entire cross-sections were imaged and stitched using Zen Blue 2.3 (Zeiss). LED intensity and exposure time were consistent across all samples within the same experiments and imaging techniques, ensuring uniform imaging conditions. Cross-sectional area and minimum Feret diameter were determined using full muscle-cross sections stained with laminin and analyzed with MIRAVision AI (MIRA Vision Microscopy GmbH, Wangen, Germany).

2.7.1 Quantification of Fibrosis

Percent fibrosis of gastrocnemius was quantified using FIJI software by first converting the picrosirius red stained tissue images to an RGB stack. This process allowed for the separation of colour channels, enabling precise identification of the red-stained collagen areas indicative of fibrosis. The green channel was selected for further analysis, as it provided the optimal contrast for thresholding the red-stained regions. To account for variability in staining intensity across samples, the baseline threshold value was set using the image that displayed the highest sensitivity to red staining. This threshold was then applied consistently across all images to ensure accurate and comparable quantification of the red-stained regions. The area of the thresholded regions was measured to determine the extent of fibrosis in each sample.

2.7.2 mIHC Analysis

mIHC samples were spectrally unmixed using the single-stain spectral library compiled for the macrophage panel in skeletal muscle tissue. Images were imported and analyzed using QuPath 0.5.0., following the documentation for multiplexed analysis [186,187]. Briefly, cell detection was performed using DAPI as the detection channel using the default parameters. A training dataset was created by selecting a random subset of images and duplicating them into their individual channels. The Random Trees object classifier was then trained using manually annotated samples, allowing it to learn and differentiate between multiple cell types based on the individual staining intensity of Opal 520 (CD86+), Opal570 (F480+), and Opal650 (CD206+). For each trained classifier, artifacts and non-specific staining were also considered by annotating them under the "Ignore*" class. Three classifiers were defined for the identification of macrophages: Total macrophages (F480+), Pro-inflammatory macrophages (F480+CD86+), and Anti-inflammatory macrophages (F480+CD206+). These classifiers were subsequently applied to the entire dataset to quantify macrophage populations across the entire tissue section. The results were defined as number of macrophages per mm^2 of tissue to account for variations in overall cellularity between samples.

2.8 Total Collagen Assay:

Total collagen content in the gastrocnemius of adult and juvenile D2.*mdx* mice was quantified using the Perchlorate-Free Total Collagen Assay Kit (Abcam, ab222942), following the manufacturer's instructions. Briefly, 10 mg of adult D2.*mdx* tissue or 50mg of juvenile D2.*mdx* tissue was pulverized into a powder and further homogenized using a Bio-Gen

PRO200 tissue homogenizer (Pro Scientific, 01-01200). Samples were then hydrolyzed in 10N concentrated NaOH at 120°C for 1 hour and neutralized with an equal volume of 10N concentrated HCl. Hydrolyzed samples were centrifuged at 10 000 x g for 5 minutes and the hydrolysate (supernatant) was transferred to a new tube. To a 96-well plate, 10uL of each sample was added in triplicate, evaporated at 65°C and incubated the Chloramine-T reagent for 20 minutes at room temperature. Subsequently, the samples were incubated with the developer solution and DMAB concentrate for 5 minutes at 37°C and 45 minutes at 65°C, respectively. Absorbance was measured at 560 nm using the Biotek Synergy HTX microplate reader. A standard curve was generated using the provided collagen standard, and the collagen content in each sample was calculated accordingly.

2.9 Cytokine and Chemokine Array

Cytokine and chemokine expression in adult D2.*mdx* gastrocnemius samples were analyzed using the Proteome Profiler Mouse XL Cytokine Array Kit (R&D Systems, ARY028). Frozen gastrocnemius from 16-week-old D2.*mdx* mice were digested using gentleMACS M-tubes (Miltenyi Biotec,130-096-335) in 1% Triton X-100 in phosphate buffered-saline (PBS) with protease and phosphatase inhibitors. Tissue lysate was quantified using a standard curve and 200 µg of protein was used for the assay, according to the manufacturer's protocol for LI-COR Detection and scanned on the LI-COR Odyssey CLx imaging system. For the first trial, membranes were scanned at the same settings but individually, while subsequent trials were scanned as one to minimize any differences in pixel intensity. It should be noted that the observed global shift in treatments was not affected by the scanning technique. Blots

were analyzed using QuickSpots software (IdealEyes, Bountiful, United States) and data were expressed as pixel intensity and fold-changed, normalized to the vehicle group.

2.10 Gene Expression Analysis:

Total RNA was extracted from the hemi-diaphragms of adult and juvenile D2.*mdx* mice using standard RNAzol isolation and 1µg was reversed transcribed using iScript gDNA Clear cDNA Synthesis kits (BioRad). Synthesized cDNA was diluted 1:2 *Il6* only) or 1:5 in ddH_2O prior to being added to a total reaction volume of 10 µL using SsoAdvanced SYBR Green SuperMix (BioRad). Real-time quantitative PCR (RT-qPCR) was performed on Applied Biosystems' QuantStudio 6 Pro Real-Time PCR System. Primers for RT-qPCR were synthesized by IDT and full sequences can be found in Table 2. Cycling parameters were set under the FAST run mode. Initial denaturation was 95°C for 30 seconds followed by 40 cycles of 95°C for 15 seconds and the optimized primer temperature for 30 seconds. Gene expression was normalized to the geometric mean of the housekeeping genes *RPL13A, AP3D1 and CSNK2A2*, as previously described[188,189]. Results were expressed as fold-induction compared to wild-type (DBA/2J) for adult D2.*mdx* mice or vehicle-treated for juvenile D2.*mdx* mice.

2.11 Western Blot Analysis:

Protein lysates were collected from three gastrocnemii of vehicle or LCL161-treated juvenile D2.*mdx* muscle with modified RIPA-SDS (0.1%) including protease and phosphatase inhibitors. Protein was quantified using the Bio-Rad Protein Assay (500-0006) and protein loading was normalized to 25µg per well. The proteins were resolved on an 8 or

10% SDS-PAGE gel and transferred to a nitrocellulose membrane. Total protein staining was performed using REVERT™ total protein stain (LI-COR, 926-11011) following the manufacturer's protocol to normalize the protein levels. Membranes were then probed with specific antibodies: cIAP1/2 (Cyclex, CY-P1041), p100/p52 (Santa Cruz Biotech, sc-7386), RelB (Cell Signaling, 10544S), P105/p50 (Cell Signaling, 13586S) and GAPDH (Advanced ImmunoChemical Inc., 2-RGM2). Alexa Fluor 680 (Invitrogen, A21109) or IRDye® 800 (LI-COR, 926-32210) were used to detect the primary antibodies, and fluorescent signals were detected using the Odyssey CLx Imaging System (LI-COR). Signals were determined using the Image Studio software (LI-COR) and normalized using the lane normalization factor from total protein stain with the highest signal.

2.12 Statistical Analyses:

The statistical analyses were determined using GraphPad Prism 10 software (San Diego, CA). Data from experiments evaluating the differences between the vehicle- and LCL161-treated D2.*mdx* mice were analyzed using the Mann–Whitney *U* test. When comparing D2.*mdx* with the wild-type, the Kruskal-Wallis with Dunn's post-hoc test for multiple comparisons was performed. For data comparing time and treatment related differences a two-way repeated measures ANOVA was performed. Where relevant, data are presented as mean ± SEM. All p values <0.05 were statistically significant and are represented as follows: *$p < 0.05$, ** $p < 0.01$, ***$p < 0.001$, and ****$p < 0.0001$.

Table 1. Optimized Antibody Order, Antigen Retrieval Conditions and Fluorophore Pairing for Multiplex Immunohistochemistry Panel of Macrophage Markers

Staining Position	Antibody	Product ID	Concentration	Antigen Retrieval	Opal Fluorophore Pairing
1	CD86	Cell Signaling, #19589	1.1 µg/mL	AR9, pH=9	Opal520
2	CD206	Cell Signaling, #24595	0.2325 µg/mL	AR9, pH=9	Opal650
3	F4/80	Cell Signaling, #70076	1.45 µg/mL	AR9, pH=9	Opal570
4	Laminin	Abcam, ab11575	7.2 µg/mL	AR9, pH=9	Opal690

Table 2. List of primer sequences used for RT-qPCR

Gene	Primer Sequences
Col1a1	Forward: 5'-AGACCTGTGTGTTCCCTACT-3'
	Reverse: 5'-GAATCCATCGGTCATGCTCTC-3'
Fn1	Forward: 5'-TTCAAGTGTGATCCCCATGAAG-3'
	Reverse: 5'-CAGGTCTACGGCAGTTGTCA-3'
Timp1	Forward: 5'-CGAGACCACCTTATACCAGCG-3'
	Reverse: 5'-ATGACTGGGGTGTAGGCGTA-3'
Tgfb1	Forward5'-AACAACGCCATCTATGAGAAAACC-3'
	Reverse: 5'-CCGAATGTCTGACGTATTGAAGAA-3'
Ctgf	Forward: 5'-GGGCCTCTTCTGCGATTTC-3'
	Reverse: 5'-ATCCAGGCAAGTGCATTGGTA-3'
Il6	Forward: 5'-TAGTCCTTCCTACCCCAATTTCC-3'
	Reverse: 5'-TTGGTCCTTAGCCACTCCTTC-3'
Tnfα	Forward: 5'-GGTGCCTATGTCTCAGCCTCTT-3'
	Reverse: 5'-GCCATAGAACTGATGAGAGGGAG-3'
Pax7	Forward: 5'-GACGACGAGGAAGGAGACAA-3'
	Reverse: 5'-CGGGTTCTGATTCCACATCT-3'
Myod1	Forward 5'-TGGCATGATGGATTACAGCG-3'
	Reverse: 5'-CCACTATGCTGGACAGGCAGT-3'
Myog	Forward: 5'-ATCGCGCTCCTCCTGGTTGA-3'
	Reverse: 5'-CTGGGGACCCCTGAGCATTG-3'
Csnk2a2	Forward: 5'-AAAGCTCTGGATTACTGCCAC-3'
	Reverse: 5'-AGACCCCAATCAATCAGTCGG-3'
Ap3d1	Forward: 5'-CGACCGCATGTTCGATAAGAA-3'
	Reverse: 5'-GCTTGATCTCGTCAATGCACTG-3'
Rpl13a	Forward: 5'-CCTGCTGCTCTCAAGGTTGTT-3'
	Reverse: 5'-CGATAGTGCATCTTGGCCTTT-3'

CHAPTER THREE: RESULTS

3.1 Aim 1: Evaluation of fibrosis and the inflammatory response in adult D2.*mdx* mice treated with LCL161

LCL161 treatment induces splenomegaly and shows marginal effects on muscle damage and strength.

Since DMD is characterized by progressive muscle degeneration, tracking body weight changes can reflect the overall physical health of the mice. A lack of weight gain or weight loss may indicate muscle wasting, disease severity, or compromised health due to the disease or therapy. Therefore, to determine whether LCL161 treatment helped maintain muscle mass or slowed muscle degeneration, D2.*mdx* body weights were tracked over the course of 9 weeks (8 weeks of treatment) and compared to age-matched wild-type (DBA/2J) mice. There was no significant difference between the vehicle group compared to the LCL161 group when final body weights were measured (**Fig.7A**). However, only the LCL161-treated mice were significantly smaller than the wild-type at endpoint (17 weeks of age) while surprisingly the vehicle-treated D2.*mdx* were not. Given the differences in starting weights among the mice, the percent change in body weight from the initiation of treatment was also evaluated. A similar pattern was observed, with wild-type mice showing a 16.8% increase in body weight, while D2.*mdx* mice exhibited increases of 11.6% in the vehicle group and 5.8% in the LCL161-treated group. When comparing collected muscle weights of the diaphragm, heart and hindlimbs, again, the diaphragm and heart of LCL161-treated mice were not significantly different from wild-type levels (**Fig. 7B**). The gastrocnemius muscle weights in both D2.*mdx* groups were significantly lower than those of the wild-type controls, with no significant difference between the two D2.*mdx* groups. In contrast, the soleus and extensor

digitorum longus (EDL) muscles showed no significant differences across all groups. Spleen weights, however, were significantly larger in the LCL161 group. Notably, muscle/body weight ratios did not impact the observed results to a significant degree.

While body weight may give some insight into muscle degeneration, I also performed a creatine kinase (CK) assay and functional tests (hanging wire and grip strength) to evaluate the therapeutic efficacy of LCL161 on muscle damage, strength, coordination and endurance (**Fig.8**). As a biomarker of reduced muscle damage and increased muscle integrity, CK levels were measured from the serum of wild-type and D2.*mdx* mice. LCL161-treated D2.*mdx* mice exhibited lower CK levels, averaging ~101 U/L, whereas vehicle-treated D2.*mdx* mice had significantly elevated CK levels compared to the wild-type mice, at ~212 U/L (**Fig.8A**). After 8 weeks of treatment, the max hang time of mice treated with LCL61 was not significantly better than the vehicle treated mice, however, it was marginally greater (~230 sec vs 180 sec, **Fig.8B**). During grip strength assessments, both groups exhibited a decline in force from week 1 to week 8; however, the LCL161-treated mice showed a slightly smaller reduction in strength compared to the vehicle group (**Fig.8C**). Conversely, while both groups of mice demonstrated an increase in muscular endurance, as assessed by fatigue grip strength, the LCL161-treated group exhibited a significantly greater improvement compared to the initial measurement (**Fig.8D**). These tests were initially conducted across all groups (DBA/2J, D2.*mdx*-Vehicle, and D2.*mdx*-LCL161) during the first round of treatment. However, the wild-type DBA/2J mice appeared to adapt to the testing procedures, and their performance did not surpass that of the D2.*mdx* mice, likely due to the development of a learned avoidance behaviour.

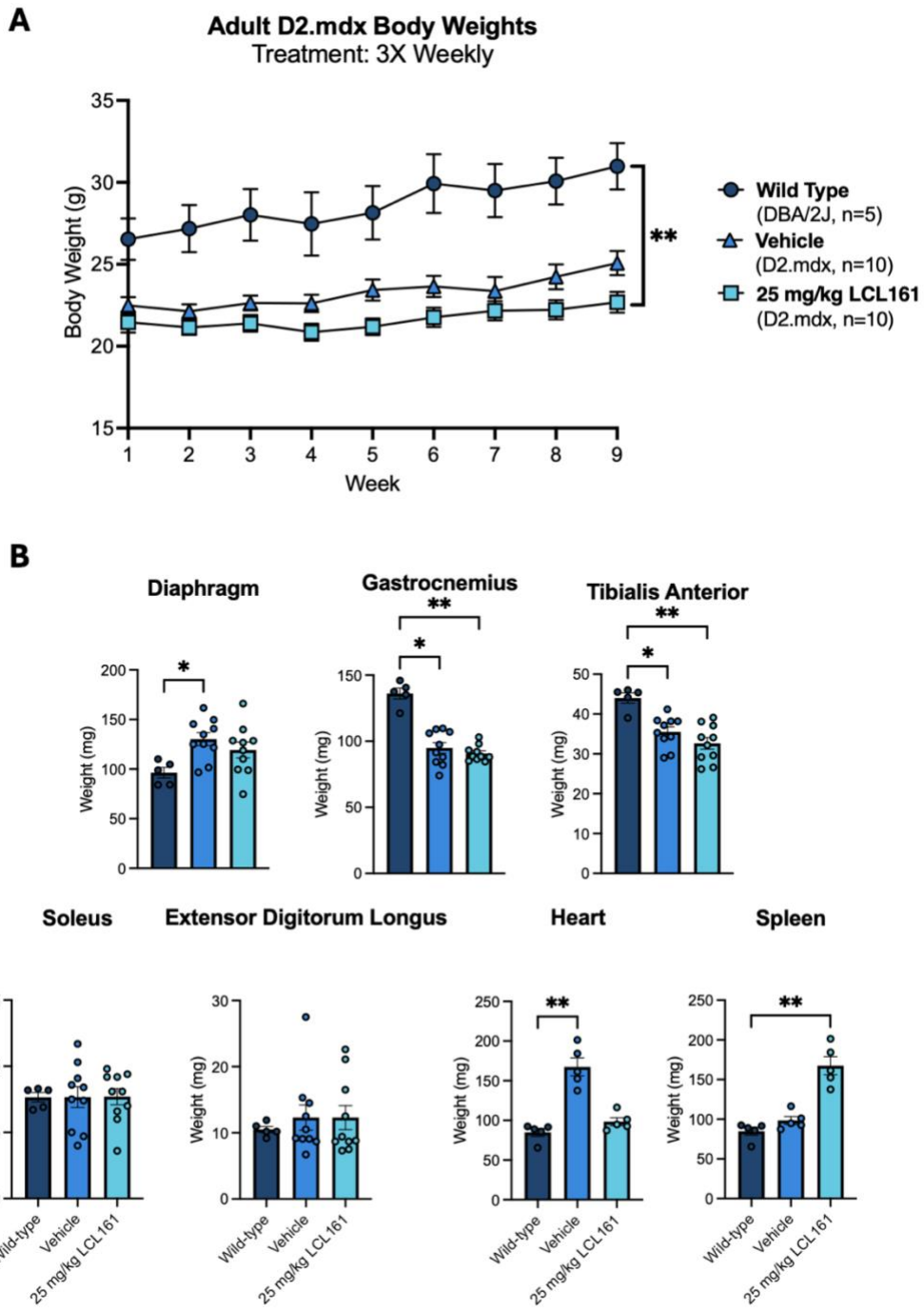

Figure 7. LCL161 treatment does not significantly affect body weight or muscle mass in adult D2.*mdx* mice but induces splenomegaly. (A) Body weight trajectories of adult D2.*mdx* mice treated with 25 mg/kg LCL161 three times per week for 8 weeks compared to vehicle-treated D2.*mdx* mice and wild-type (DBA/2J) controls. Data were collected weekly, and weights were recorded up to the collection date (8 weeks treatment + 5 days). at which point mice were 16-weeks of age **(B)** Weights of diaphragm, gastrocnemius, tibialis anterior, soleus, extensor digitorum longus (EDL), heart, and spleen collected at the end of the study (5 days post-final treatment). Data represent the mean ± SEM (n=5-10 per group).

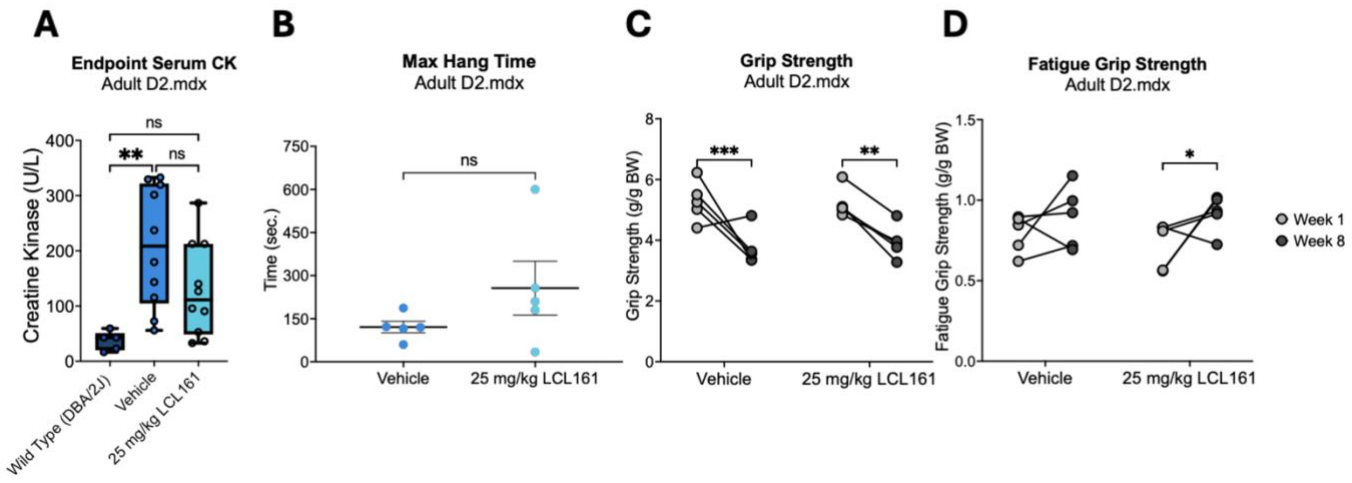

Figure 8. LCL161 treatment shows marginal effects on muscle damage and strength but significantly improves resistance to fatigue in adult D2.*mdx* mice. Baseline serum creatine kinase (CK) levels of adult wild-type and D2.*mdx* mice were measured from blood collected at endpoint. Indices of muscle function were assessed by **(B)** max hang time at week 8, **(C)** grip strength and **(D)** fatigue grip strength at weeks 1 and 8. Data represent mean ± SEM (n=5-10 per group).

LCL161 affects gastrocnemius and diaphragm histopathology of adult D2.mdx mice.

Previous reports demonstrated that genetic and pharmacological ablation of cIAP1 in *mdx* and C57BL/6 reduces muscle atrophy and results in larger fibres with the same trend observed seen in cIAP2-null C57BL/6 mice[169–171]. Since LCL161 is a potent inhibitor of cIAP1/2, fibre sizes were also analyzed to determine if this was still consistent in the D2.*mdx* model. Though not significant, the gastrocnemius from LCL161-treated mice appears to have a greater distribution of larger fibres (>1000 um^2) and increased mean fibre size compared to the vehicle-treated mice (**Fig.9A**). Notably, only the vehicle-treated mice had significantly smaller mean fibre sizes when compared to the wild-type mice. The cross-sectional area of the diaphragm does not follow the same trend as the gastrocnemius with D2.*mdx* populations being skewed towards smaller fibres (**Fig.9B**). Additionally, the mean fibre sizes measured in the diaphragm of each group were significantly smaller than the wild-type diaphragms. Despite the observed differences, our treatment with LCL161 was not sufficient to produce a statistically measurable change in fibre sizes, which has been consistent with the observations in the functional assessment.

As a hallmark of muscular dystrophy, I next aimed to quantify fibrosis in the D2.*mdx* mice compared to the wild type (**Fig.10**). The development of fibrosis in the gastrocnemius is more progressive over a 12-month period while the diaphragm becomes hyper-fibrotic as early as 4 months [79]. Given the advanced disease state in the diaphragm and the lack of shift towards larger fibre size distributions, attention was directed to the gastrocnemius to assess the extent to which LCL161 treatment mitigates this pathological process. Fibrosis quantification in the gastrocnemius muscle showed a moderate reduction in collagen

deposition in LCL161-treated mice compared to vehicle-treated controls (7.29% vs 8.25%, **Fig.10B**) however this did not reach statistical significance ($p<0.05$). To support this observation, a biochemical assay for total collagen content was also performed (**Fig.10C**). Despite using a homogenized fraction of the gastrocnemius, the general trend was still observed and only the vehicle-treated mice had significantly more collagen per mg of tissue compared to the wild-type.

To assess the regenerative response induced by LCL161 administration, embryonic myosin heavy chain (eMyHC) was detected via immunofluorescence, serving as a well-established marker of nascent myofibre formation (**Fig.11**). An increase in the number of eMyHC+ fibres can be seen in both the gastrocnemius (approx. 128 vs 79) and diaphragm (approx. 93 vs 84) of the LCL161-treated mice, although this difference is not statistically significant (**Fig.11B**). When expressed as a percent of total fibres, there is an absolute difference of 2% in the gastrocnemius and 1% in the diaphragm (**Fig.11C**). In both muscle tissues, the total number of fibres analyzed between groups was not significantly different.

The balance between a pro-inflammatory and anti-inflammatory (pro-regenerative) muscle microenvironment is essential for the effective resolution of inflammation and the repair of muscle tissue. Given the critical role of macrophages in orchestrating the shift from inflammation to regeneration, I used the pan-macrophage marker F4/80 along with pro-inflammatory and anti-inflammatory markers, CD86 and CD206 to delineate macrophage phenotypes within the D2.*mdx* gastrocnemius (**Fig.12A**). Since the spontaneous injury of D2.*mdx* muscle is unevenly distributed throughout the muscle, I investigated whether the proportions and identities of macrophages shift in areas exhibiting significant damage

(regions with necrosis and/or centrally located nuclei, cross-referenced with H&E-stained images). As adult D2.*mdx* mice tend to exhibit less muscle damage compared to juvenile D2.*mdx* mice, the boundaries of damage were not as clearly established and, in some instances, could not be reliably drawn. Analysis of these damage areas revealed virtually no differences compared to whole tissue analysis (i.e., macrophage infiltrate and phenotypes were not significantly different) and was therefore omitted. Examining the tissue as a whole, reveals that there is a slight reduction in total macrophages detected in the LCL161-treated mice. Within treatment groups, the proportions of pro-inflammatory ($F480^{+}CD86^{+}CD206^{-}$) and anti-inflammatory ($F480^{+}CD86^{-}CD206^{+}$) macrophages were not significantly different from one another and between groups, this is also observed. While not significant, there are fractionally more pro-inflammatory macrophages and a decrease in anti-inflammatory macrophage in the LCL161-treated mice compared to those that received the vehicle.

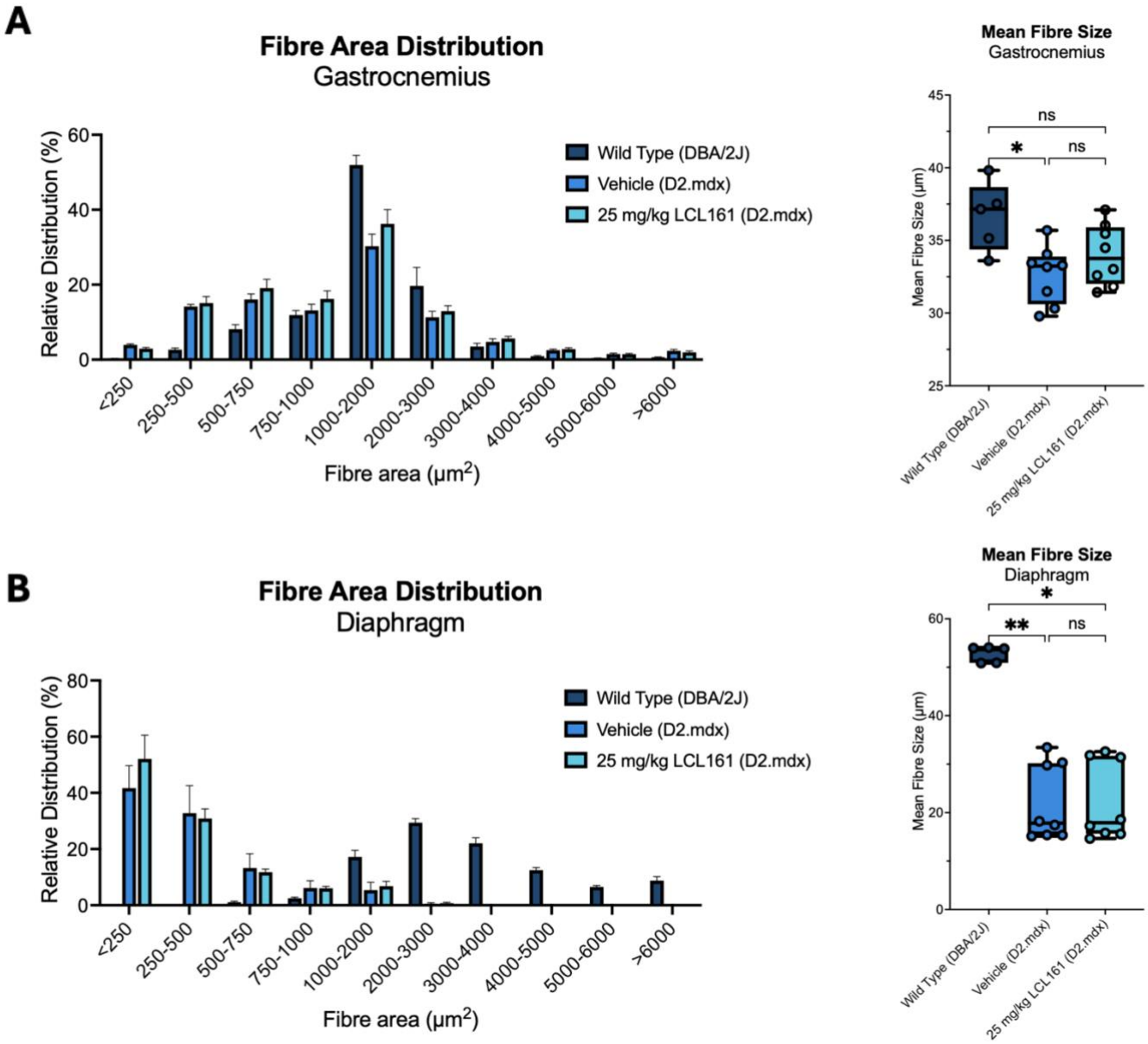

Figure 9. Gastrocnemius muscle from LCL161-treated adult D2.*mdx* mice demonstrates a more notable presence of larger fibres. Cross-sectional area and mean fibre size (min. Feret diameter) for adult wild-type and D2.*mdx* mice were determined using whole muscle sections with MIRAVision AI-Assisted Image Analysis. **(A)** Relative fibre area distribution (%) and distribution of fibre size for gastrocnemius muscle. **(B)** Relative fibre area distribution and distribution of fibre size for the diaphragm muscle. Relative fibre area distribution is presented as mean ± SEM (n=5-8 per group)

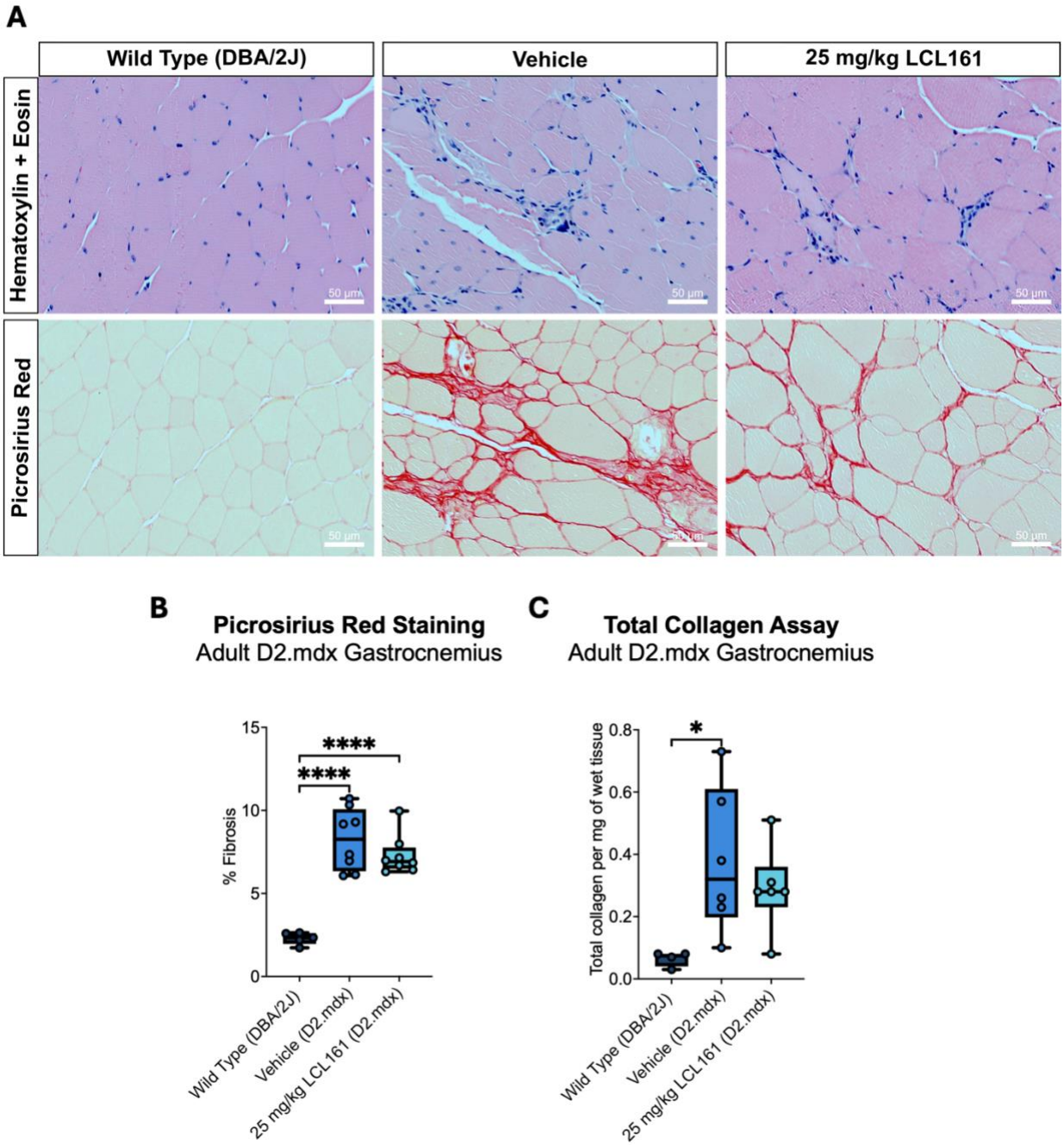

Figure 10. LCL161 treatment trends towards reduced fibrosis in the gastrocnemius of adult D2.*mdx* mice. **(A)** Hematoxylin and eosin (H&E; top panel) stained sections of the gastrocnemius from wild type, vehicle- and LCL161-treated adult D2.*mdx* and the corresponding picrosirius red stain (bottom panel). **(B)** Quantification of fibrosis in the gastrocnemius, measured as a percent of red stained area to total area from the picrosirius red stain using Fiji (n=5-8 per group). **(C)** Total collagen content (µg/mg wet tissue) in gastrocnemius muscle lysates determined via colorimetric detection (n=4-6 per group).

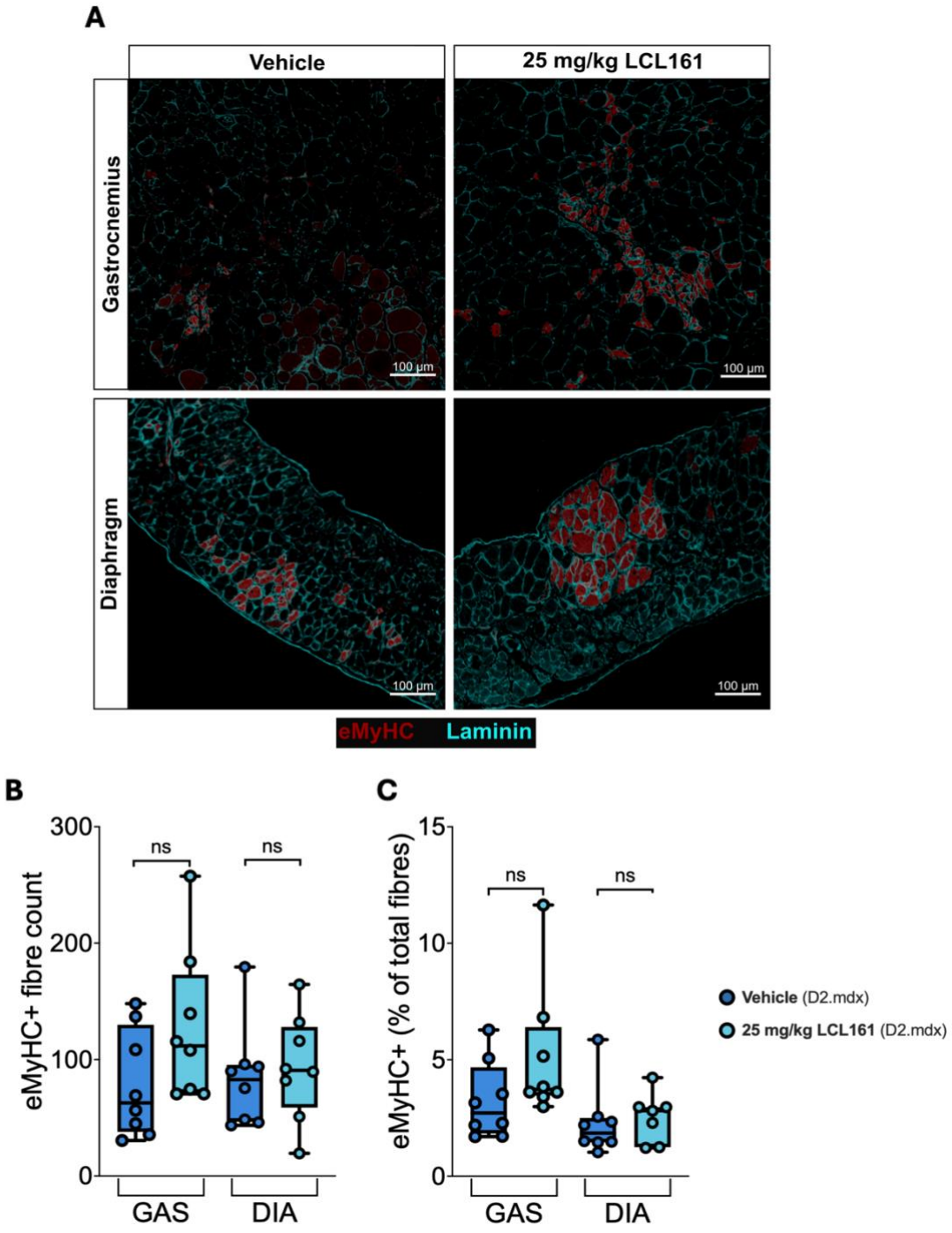

Figure 11. LCL161 treatment trends towards increased regeneration in the gastrocnemius and diaphragm of adult D2.*mdx* mice. **(A)** eMyHC expression assessed in the gastrocnemius (top panel) and diaphragm (bottom panel) of vehicle- and LCL161-treated adult D2.*mdx* mice. Representative images show the size and distribution of eMyHC$^+$ myofibres (red), co-stained with laminin (turquoise) in the respective muscle types. **(B)** Quantification of eMyHC$^+$ myofibres in the gastrocnemius and diaphragm (n=8 per group). **(C)** eMyHC$^+$ myofibres expressed as a percent of total fibres detected in the gastrocnemius and diaphragm (n=8 per group).

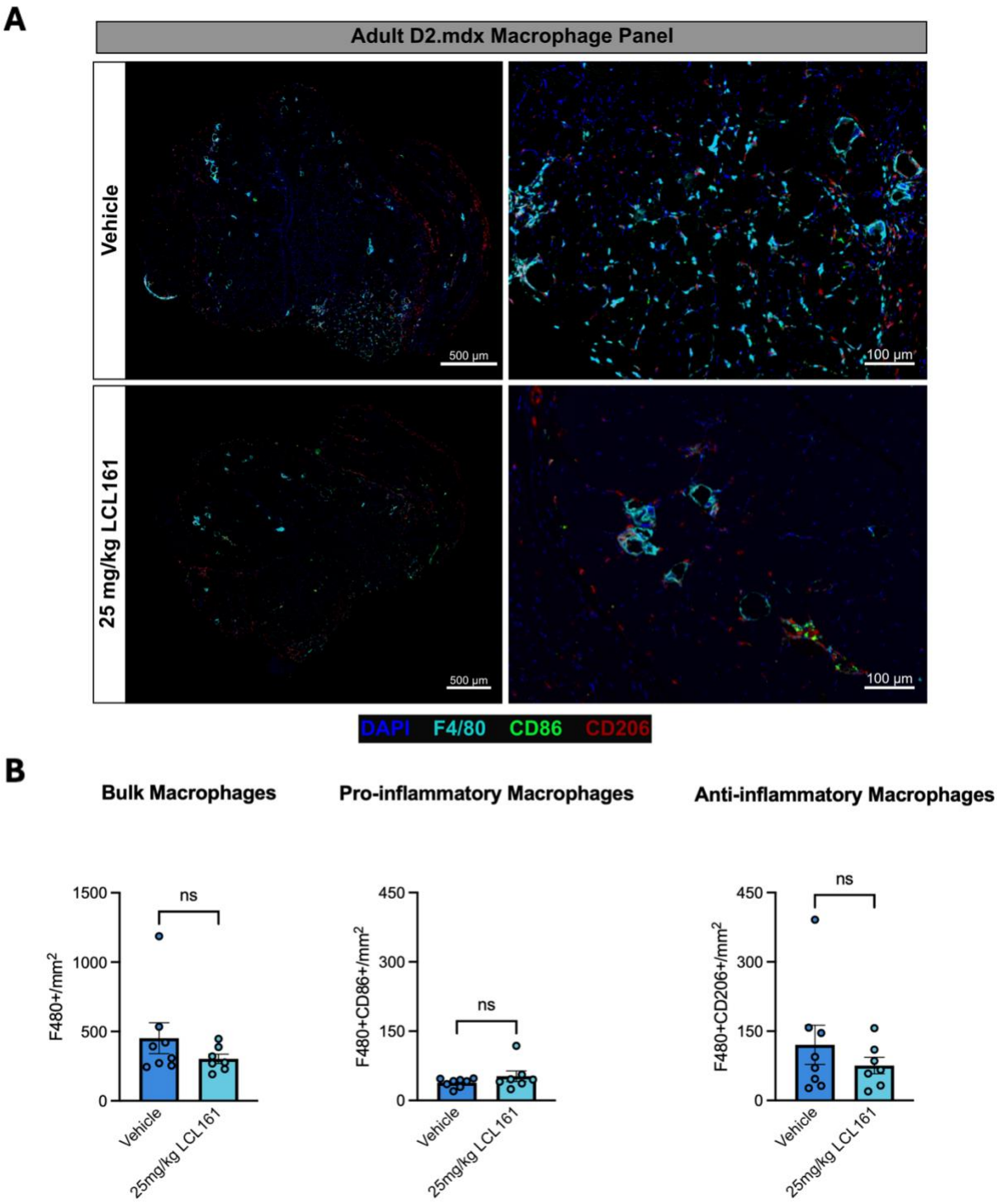

Figure 12. LCL161 has no apparent impact on macrophage infiltrate or phenotype in adult D2.*mdx* gastrocnemius. (A) Representative images showing entire gastrocnemius cross-sections and regions of interest with increased macrophage ($F4/80^+$) density from vehicle- (top panel) and LCL161-treated (bottom panel) D2.*mdx* mice. **(B)** Quantification of total macrophage infiltrate ($F4/80^+$), pro-inflammatory ($F4/80^+CD86^+CD206^-$) and anti-inflammatory phenotypes ($F4/80^+CD86^-CD206^+$) per unit area (mm^2). Data represent mean ± SEM (n=7-8 per group).

LCL161 changes the expression profile of inflammatory, fibrotic and myogenic markers in the gastrocnemius and diaphragm of adult D2.mdx mice.

Given the critical role of the immune response in muscle repair, regeneration, and fibrosis, and the immunomodulatory properties of LCL161, cytokine and chemokine profiling of the D2.*mdx* gastrocnemius muscle was performed (**Fig.13**). This analysis aimed to determine whether LCL161 elicited a significant effect on the muscle microenvironment and to assess how it may influence the recruitment of immune cells and modulate inflammatory responses. It is important to note that three biological replicates were used from both the LCL161 and vehicle-treated groups. However, data from the third replicate were excluded when thresholding due to the presence of non-positive pixel density values for certain markers. Despite this, the raw pixel density data from all replicates showed a clear shift in the LCL161-treated gastrocnemius. Using just the remaining replicates, 71.17% of the markers were elevated compared to the vehicle group (70.27 and 72.07% vs 29.73 and 27.93%, **Fig.13A**). When applying thresholds of 0.5-fold and 1.5-fold changes, 25 proteins were upregulated in Trial 1, and 27 in Trial 2, while just 3 proteins were downregulated in Trial 1 and 2 proteins in Trial 2 of the 111 proteins analyzed (**Fig.13B**).

As previously mentioned, the diaphragm displays advanced disease progression including fibrosis before the hindlimb muscles. Due to difficulties accurately quantifying the fibrosis in the diaphragm and tissue availability, I looked at the expression of genes associated with fibrosis, inflammation and myogenesis (**Fig.14**). *Col1a1, Tgfb1* and *Timp1* levels are all significantly higher in the D2.*mdx* mice compared to the wild-type mice while *Fn1* and *Ctgf* expression is not-significantly different across all cohorts. Again, although

there is no significance between the vehicle and LCL161-treated mice, the gene expression of these fibrotic markers is decreased to varying degrees. *TIMP1* is markedly increased compared to the other fibrosis-associated genes in the D2.*mdx* mice, highlighting that the development of fibrosis is strongly driven by failed ECM remodeling, outpacing the degradation of these components. When looking at the genes associated with inflammation, *TNFα* expression is significantly increased in the LCL161-treated mice even 5 days post-final treatment while no significant differences are seen between the wild-type and vehicle D2.*mdx*. This lack of significance is seen across cohorts for *Il6*, however there does appear to be slightly less *Il6* transcripts in the LCL161-treated mice which follows the trend from the gastrocnemius cytokine and chemokine array. Analysis of the myogenic markers (*Pax7, Myod1 and Myog*), showed that *Myog* was significantly higher in the LCL161-treated mice when compared to the wild-type and moderately increased compared to the vehicle D2.*mdx* mice. The lack of significance between vehicle and LCL161-treated mice in *Myod1* transcripts is consistent with similarities in the diaphragm's regenerative response (**Fig.11**).

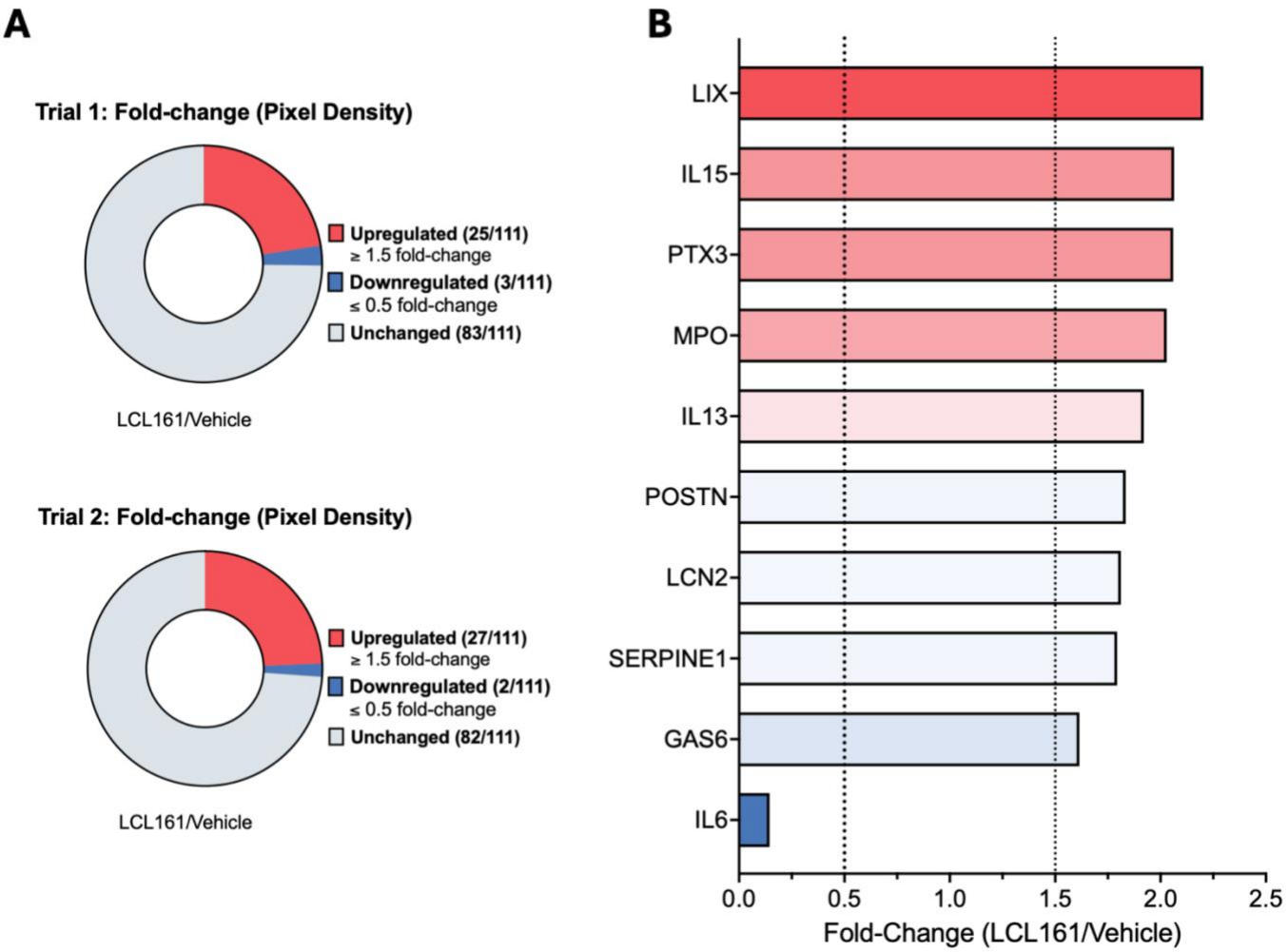

Figure 13. Difference in immune response modulation by LCL161 in the gastrocnemius muscle of D2.*mdx* mice through cytokine and chemokine profiling. (A) Fold-change (LCL161/Vehicle) of 111 cytokines and chemokines measured from the protein lysates of D2.*mdx* gastrocnemius. A fold-change of ≤0.5 or ≥1.5 was defined as the threshold to determine the effect of LCL161. Data represent 2 individual trials (n=1 per group, per trial). **(B)** List of proteins that exhibited similar changes across trials, based on fold change thresholds.

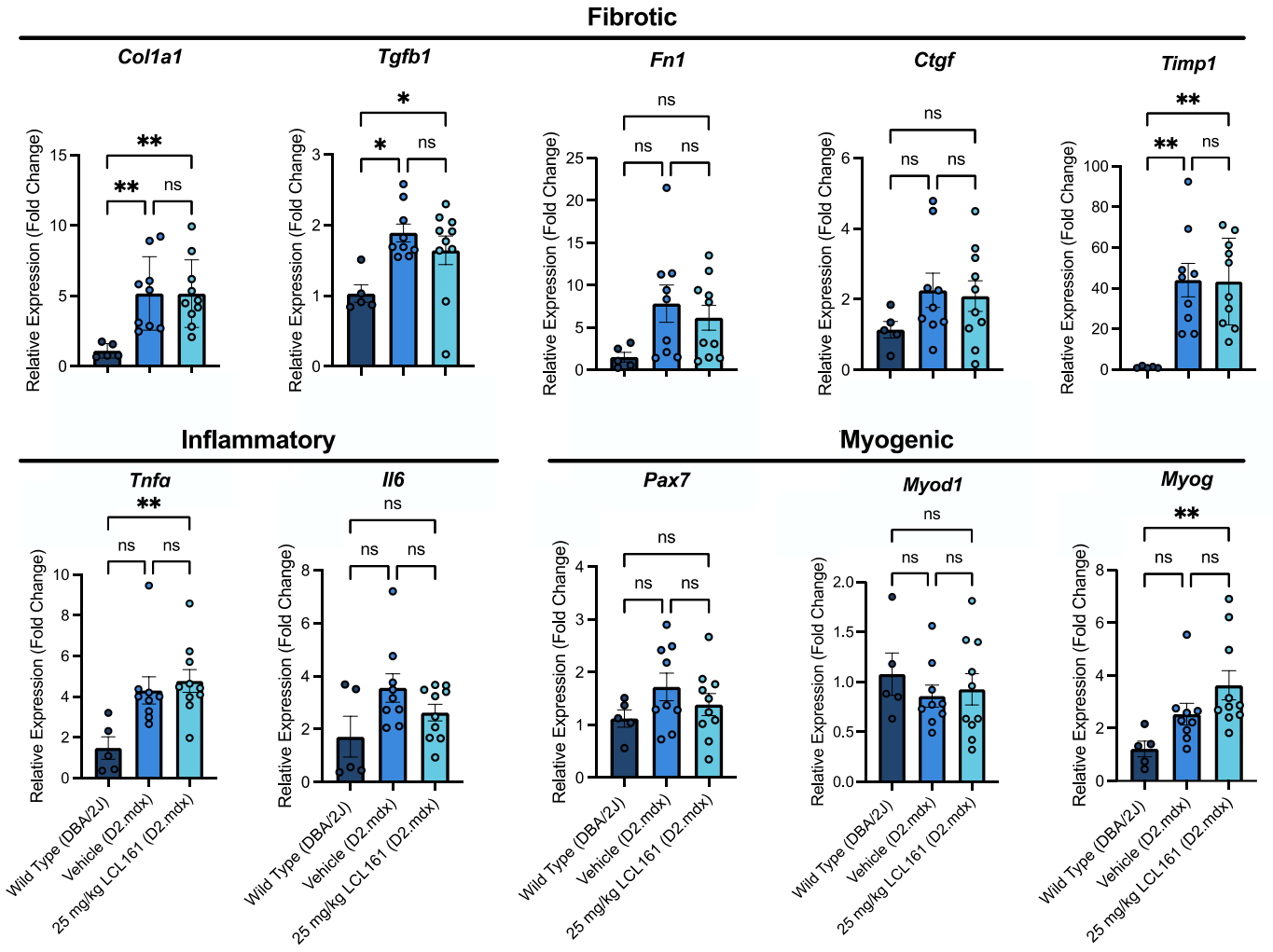

Figure 14. Expression of fibrotic, inflammatory, and myogenic markers in the diaphragm of LCL161-treated adult D2.*mdx* mice. Genes associated with fibrosis (*Col1a1, Tgfb1, Fn1, Ctgf, Timp1*), inflammation (*Tnf/Tnfα, Il6*) and myogenesis (*Pax7, Myod/Myod1, Myog*). Relative mRNA expression levels were measured via qPCR in diaphragm muscle tissue from wild-type, vehicle- and LCL161-treated adult D2.*mdx* mice. Data represent mean ± SEM (n=5-10 per group).

3.2 Aim 2: Evaluation of fibrosis and the inflammatory response in juvenile D2.*mdx* mice treated with LCL161

In comparison to the adult D2.*mdx* mice, juvenile D2.*mdx* mice exhibit an enhanced inflammatory response that fails to resolve efficiently and have a poor regenerative capacity leading to increased damage. Thus, I examined whether earlier intervention with LCL161 could improve these observed trends by modulating the muscle microenvironment during heightened inflammation. To address this question, juvenile D2.*mdx* mice (4-5 weeks) were administered 25 mg/kg LCL161 for 4 weeks (+1 final dose 24 hours prior to collection). To capture transient effects of the drug, these mice were also collected 1-day post-final treatment as opposed previously where adult mice were sacrificed 5 days after.

LCL161 treatment increases soleus weight, reduces muscle damage, but has no effect on muscle strength.

Although D2.*mdx* mice generally weigh less than their wild-type counterparts, they still experience age-dependent weight gain, which may be partially attributed to the accumulation of fat and fibrotic tissue as muscle degeneration progresses. Over a 5-week period, I aimed to evaluate whether LCL161 treatment could promote the preservation of muscle mass and enhance body weight maintenance, potentially mitigating the negative impact of muscle wasting in the younger D2.*mdx* mice. Both the vehicle- and LCL161-treated mice exhibited a significant increase in body weight from week 1 to week 5 ($P<0.0001$), with weight changes of 38% and 28.9%, respectively (**Fig. 15A**). However, no significant difference was observed between the two groups during this period. Upon examination of

the muscle weights, on average, the diaphragm, gastrocnemius and heart were smaller in the LCL161-treated mice although only the gastrocnemius exhibited a significant decrease in muscle weights (**Fig.15B**). The TA, soleus and EDL of the LCL161-treated mice tend to be larger, but only the soleus was significantly heavier than the vehicle-treated mice. Consistent with the adult D2.*mdx* mice and existing data on LCL161 treatment in mice, the spleen was significantly larger.

To assess functional improvements, I again looked at CK levels and grip strengths at the start and end of treatments. Analysis of the serum CK levels revealed that CK levels in LCL161-treated mice were 50.6% lower than the vehicle-treated mice (**Fig.16A)**. Importantly, this significant reduction in muscle damage does not appear to correlate with any improvements to grip strength (**Fig.16B**), suggesting the damage may be affecting other muscle groups more than those recruited for the test. While both vehicle- and LCL161-treated mice experienced a significant decline in grip-strength, LCL161-treated mice appear to have had a greater decline from week 1. There was no significant difference between groups at week 1 and week 4 and the fatigue grip strengths were virtually unchanged (**Fig. 16C**).

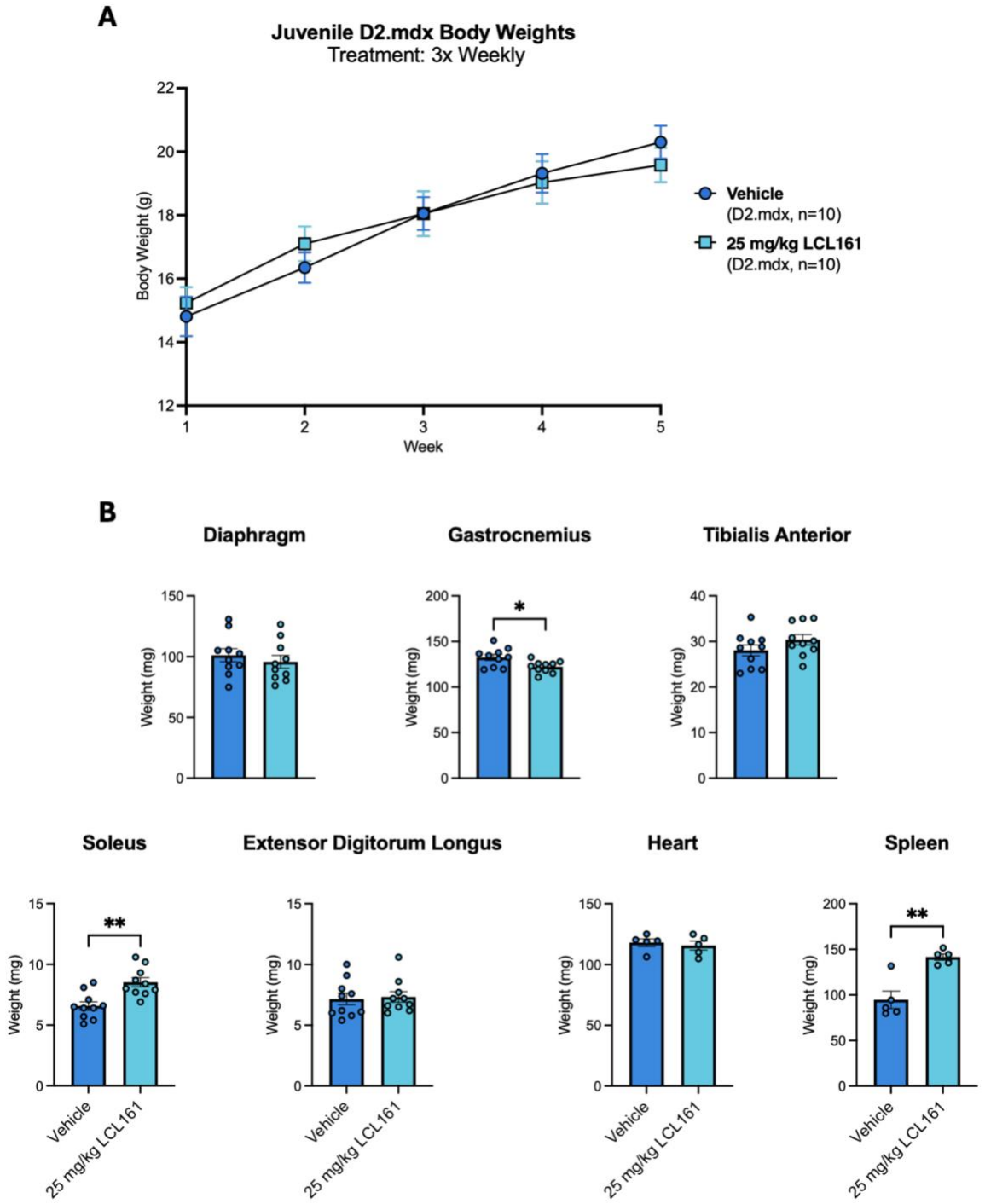

Figure 15. LCL161 treatment alters select muscle weights and induces splenomegaly without affecting body weight in juvenile D2.*mdx* mice. **(A)** Body weight trajectories of juvenile D2.*mdx* mice treated with 25 mg/kg LCL161 three times per week for 4 weeks compared to vehicle-treated D2.*mdx* mice. Data were collected weekly, and weights were recorded up to the collection date (4 weeks treatment + 1 day). at which point mice were 9-weeks of age **(B)** Weights of diaphragm, gastrocnemius, tibialis anterior, soleus, extensor digitorum longus (EDL), heart, and spleen collected at the end of the study (1-day post-final treatment). Data represent the mean ± SEM (n=5-10 per group).

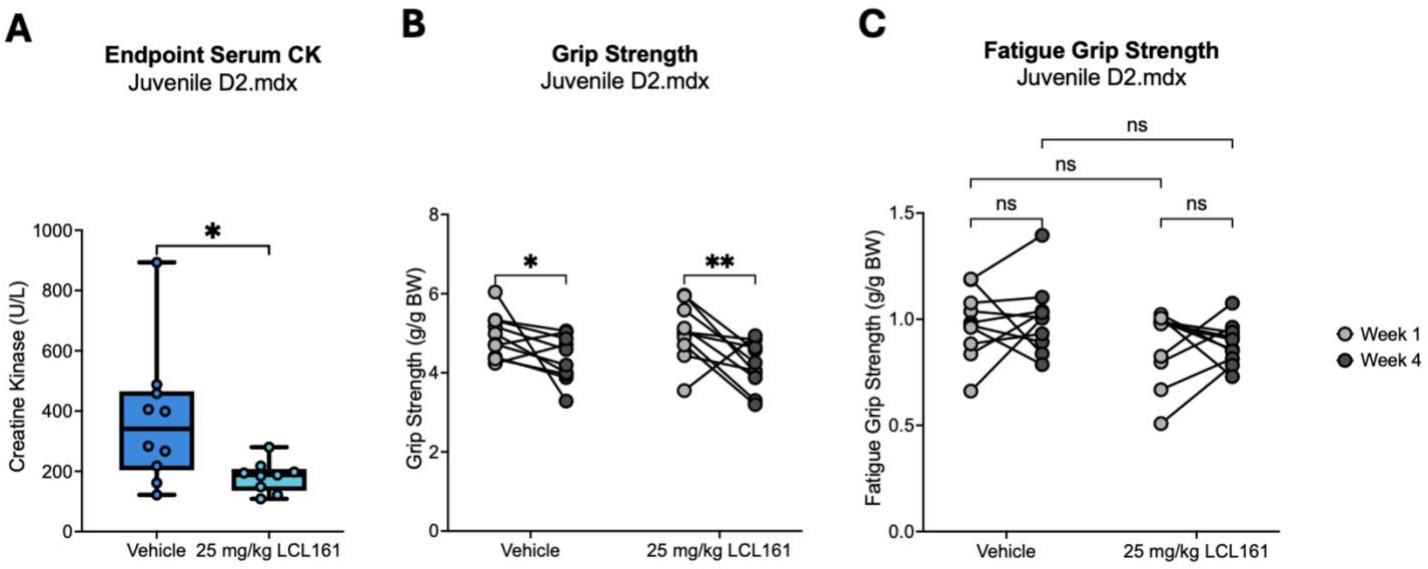

Figure 16. Functional assessments reveal reduced muscle damage in LCL161-Treated juvenile D2.*mdx* mice despite no improvement in grip strength. (A) Baseline serum creatine kinase (CK) levels of vehicle- and LCL161-treated D2.*mdx* mice were measured from blood collected at endpoint. Indices of muscle function were assessed by **(B)** grip strength and **(C)** fatigue grip strength at weeks 1 and 4. Data represent mean ± SEM (n=10 per group).

LCL161 increases necrosis and macrophage infiltrate in the gastrocnemius of D2.mdx mice.

In line with the rationale used for adult D2.*mdx* mice, I also examined fibre sizes in the gastrocnemius and diaphragm muscles of juvenile mice (**Fig.17**). I also wanted to determine whether the significant reduction in muscle damage observed with LCL161 treatment corresponded to fibre preservation, with potential changes in fibre area and size. The distribution of fibre cross-sectional areas between treatment groups showed no distinct shift, with both groups displaying a similar pattern and balance without marked asymmetry (**Fig.17A, B; left panels**). Interestingly, there was an upward trend in larger fibres within the diaphragm muscle of LCL161-treated mice, though this did not reach statistical significance. In examining mean fibre sizes for both muscle groups (**Fig.17A, B; right panels**), a slight increase in median fibre size was observed in vehicle-treated mice compared to LCL161-treated mice, though this difference was not statistically significant. This minor trend could suggest a slight enlargement of individual fibres in the vehicle group, even though the overall distribution pattern remained largely consistent across treatments

I evaluated muscle morphology in juvenile gastrocnemius muscles from LCL161-treated mice to assess necrosis, fibrosis, and collagen content (**Fig.18**). Examination of H&E-stained sections revealed extensive tissue damage in the LCL161-treated samples, which contrasted with the overall decrease in muscle damage suggested by lower CK levels (**Fig.18A; top panel**). To clarify, I quantified necrotic regions characterized by myofibre damage and dense immune cell infiltration. The results showed that LCL161-treated gastrocnemii exhibited 10.5% necrotic tissue area, significantly higher than the 6.1% necrotic area observed in vehicle-treated controls (**Fig.18B**). Further analysis focused on

fibrosis. Histochemical and biochemical assays revealed no significant differences in fibrosis levels between treatment groups, with no consistent pattern emerging between the two methods (**Fig.18C, D**). This suggests that while LCL161 treatment may impact gastrocnemius muscle integrity, its effects on fibrosis and collagen deposition in juvenile D2.*mdx* gastrocnemius are inconclusive.

Juvenile D2.*mdx* mice exhibit impaired regeneration and an amplified inflammatory response, characterized by extensive macrophage infiltration. Given the complex inflammatory environment in these mice and LCL161's ability to modulate NF-κB pathways—affecting cytokine and chemokine production as well as macrophage polarization—the specific effects of LCL161 in this heightened inflammatory context are difficult to predict. My aim was to determine whether LCL161's influence on macrophage infiltration would be more pronounced under these conditions (**Fig.19**). Consistent with the extensive necrosis observed in H&E-stained gastrocnemius sections, LCL161-treated mice displayed significantly higher macrophage infiltration (F4/80+), likely due to tissue damage (**Fig.19B**). Notably, this significance is lost upon removal of an outlier, which corresponds to the same sample showing severe necrosis in H&E-stained sections (**Fig.18**). The outlier remains significant in the pro-inflammatory macrophage count but not in the anti-inflammatory subset and does not affect the significance of either population. Both pro-inflammatory and anti-inflammatory macrophages increased in parallel with the total macrophage count, suggesting that the rise in both subsets may be attributed to the overall increase in macrophages rather than a direct effect of LCL161 treatment.

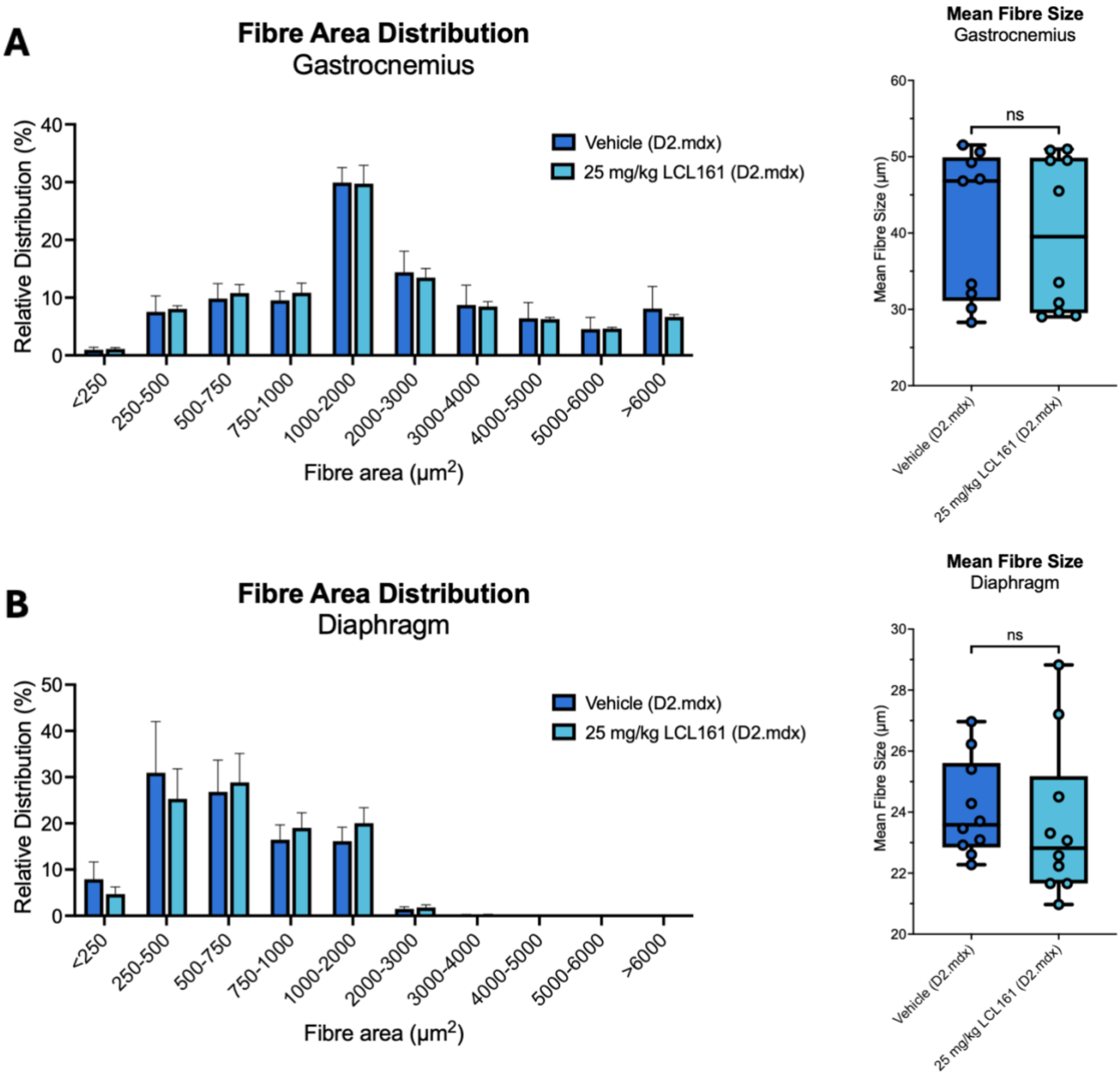

Figure 17. LCL161 has no effect on fibre size distribution in the gastrocnemius and diaphragm of D2.*mdx* mice. Cross-sectional area and mean fibre size (min. Feret diameter) for vehicle- and LCL161-treated D2.*mdx* mice were determined using whole muscle sections with MIRAVision AI-Assisted Image Analysis. **(A)** Relative fibre area distribution (%) and distribution of fibre size for gastrocnemius muscle. **(B)** Relative fibre area distribution and distribution of fibre size for the diaphragm muscle. Relative fibre area distribution is presented as mean ± SEM (n=10 per group).

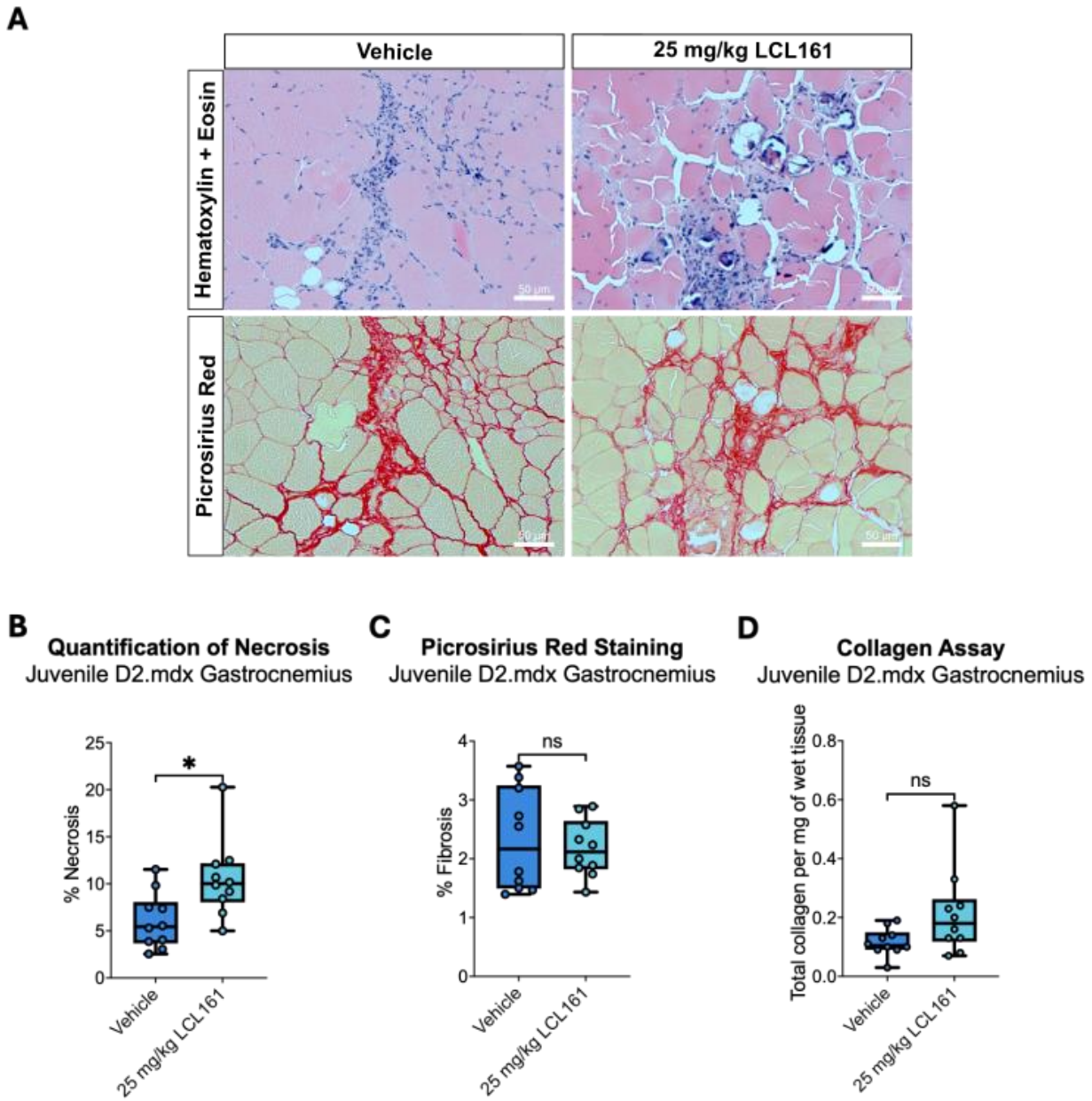

Figure 18. LCL161 has no effect on fibrosis but significantly increases necrosis in the gastrocnemius of D2.*mdx* mice. (A) Hematoxylin and eosin (H&E; top panel) stained sections of the gastrocnemius from vehicle- and LCL161-treated juvenile D2.*mdx* and the corresponding picrosirius red stain (bottom panel). **(B)** Quantification of necrosis in the gastrocnemius, defined as regions with dead/damaged myofibres, loss of muscle structure and presence of inflammatory infiltrate, expressed as a percent of total tissue area. **(C)** Quantification of fibrosis in the gastrocnemius, measured as a percent of red stained area to total area from the picrosirius red stain using Fiji. **(D)** Total collagen content (µg/mg wet tissue) in gastrocnemius muscle lysates determined via colorimetric detection. (n=10 per group).

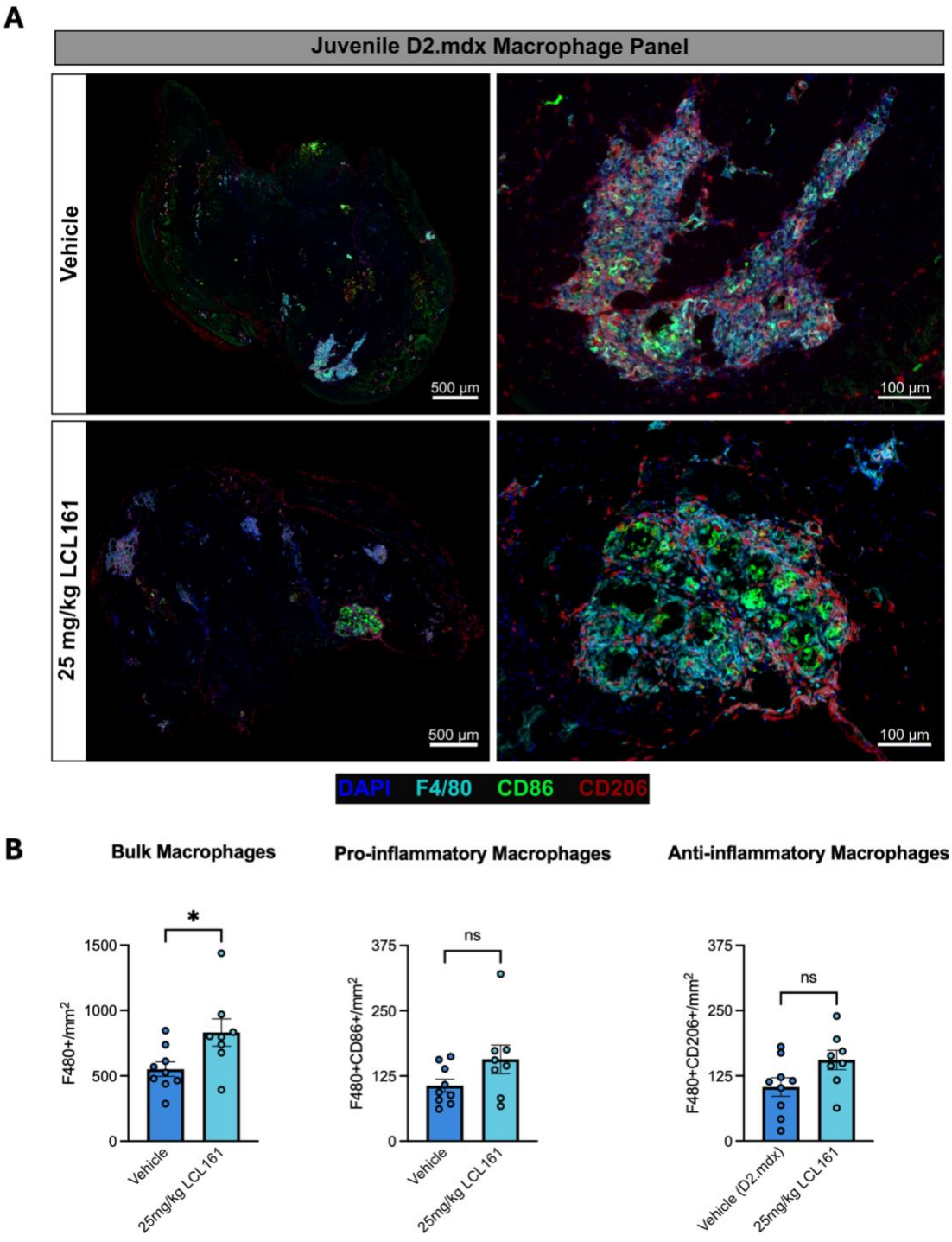

Figure 19. LCL161 treatment increases macrophage infiltrate in juvenile D2.*mdx* mice but has no effect on macrophage polarization. (A) Representative images showing entire gastrocnemius cross-sections and regions of interest with increased macrophage ($F4/80^+$) density from vehicle- (top panel) and LCL161-treated (bottom panel) D2.*mdx* mice. **(B)** Quantification of total macrophage infiltrate ($F4/80^+$), pro-inflammatory ($F4/80^+CD86^+CD206^-$) and anti-inflammatory phenotypes ($F4/80^+CD86^-CD206^+$) per unit area (mm^2). Data represent mean ± SEM (n=8-9 per group).

LCL161 reduces Tnfa and Pax7 mRNA levels and cIAP1/2 protein levels in the diaphragm and gastrocnemius muscle, respectively, of juvenile D2.mdx mice.

Phase I clinical trials in patients with advanced solid tumors reported that LCL161 reaches peak plasma concentrations within 30 minutes to 2 hours, followed by a decline over 4-16 hours[190]. Given its rapid absorption, the effects on gene expression may be more pronounced 24 hours after treatment rather than after 5 days (as examined in the adult D2.*mdx* mice). To explore this further, I again examined the expression of fibrotic, inflammatory, and myogenic genes in the juvenile D2.*mdx* mice (**Fig.20**). Among the five fibrotic genes analyzed (*Col1a1, Tgfb1, Fn1, Ctgf, and Timp1*), LCL161 induced modest, non-significant reductions in transcript levels. Notably, *TNFα* levels were significantly decreased following treatment, while *Il6* remained unaffected. Regarding myogenic markers, *Pax7* expression was significantly reduced, while *Myod1* and *Myog* showed a decrease, though not significantly.

To determine the effects of LCL161 on NF-κB signalling 24 hours after treatment, western blots were performed on the protein lysates from the juvenile D2.*mdx* mice (**Fig.21**). Although only modest degradation of the cIAPs was observed, the significant enlargement of the spleen in LCL161-treated mice suggests that the drug is engaging its target and modulating immune responses (**Fig.15B**) (**Fig.21A**).While spleen enlargement alone is not definitive evidence of IAP degradation, its occurrence alongside even partial IAP depletion aligns with previous findings from our lab in mouse models of cancer, muscular dystrophy, and muscle atrophy treated with LCL161. Notably, the difference is cIAP2 degradation is approximately 2.21-fold while cIAP1 is degraded to a lesser extent at 1.41-fold. This was

accompanied by insignificant downwards trends in both p50/p105 ratios in the classical pathway, and in the p52/p100 ratio in the alternative pathway (**Fig.21B, C**).

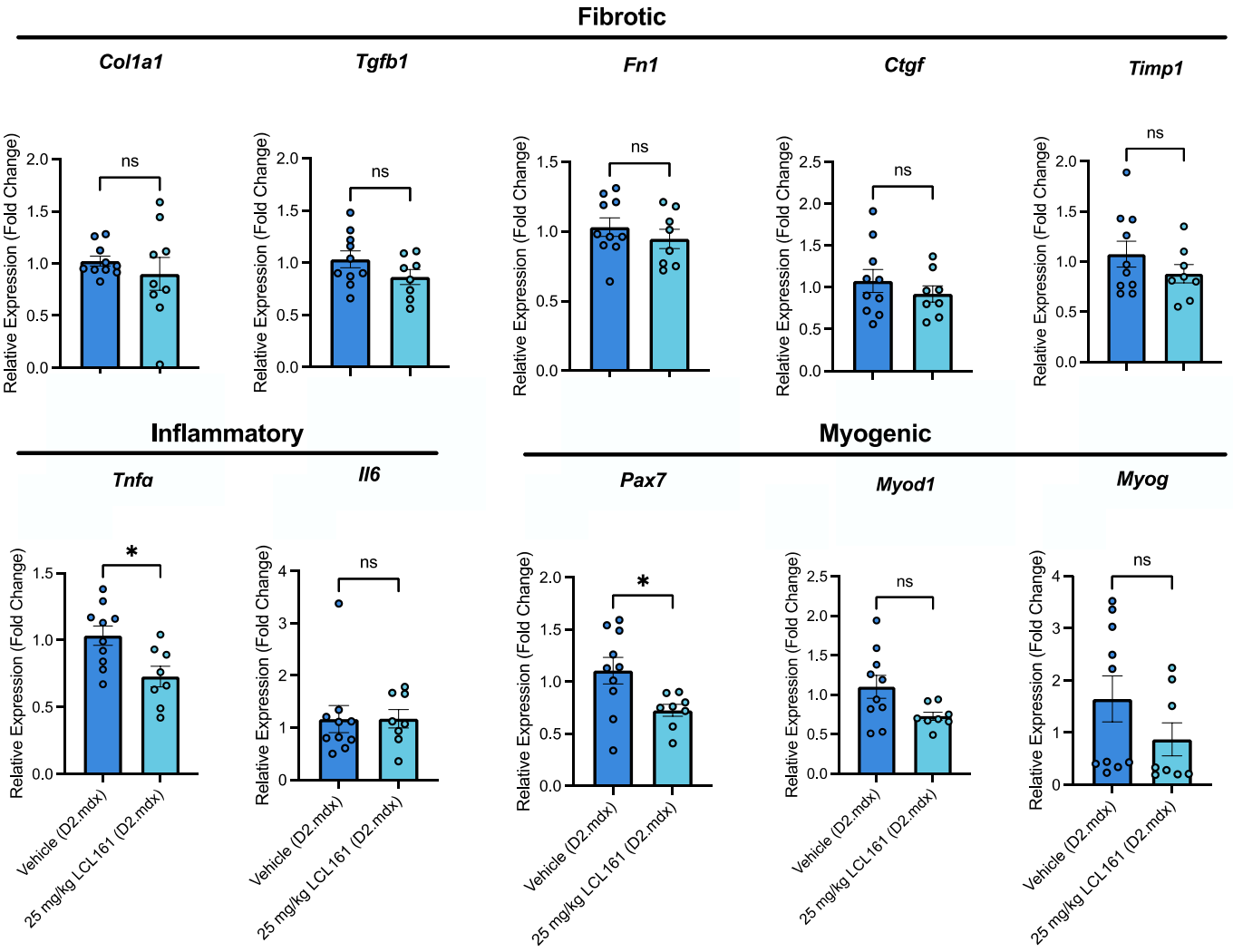

Figure 20. LCL161 treatment reduces *Tnfa* and *Pax7* levels in the gastrocnemius muscle of juvenile D2.*mdx* mice. Genes associated with fibrosis (*Col1a1, Tgfb1, Fn1, Ctgf, Timp1*), inflammation (*Tnf/Tnfα, Il6*) and myogenesis (*Pax7, Myod1, Myog*). Relative mRNA expression levels were measured via qPCR in diaphragm muscle tissue from vehicle- and LCL161-treated juvenile D2.*mdx* mice. Data represent mean ± SEM (n=8-10 per group).

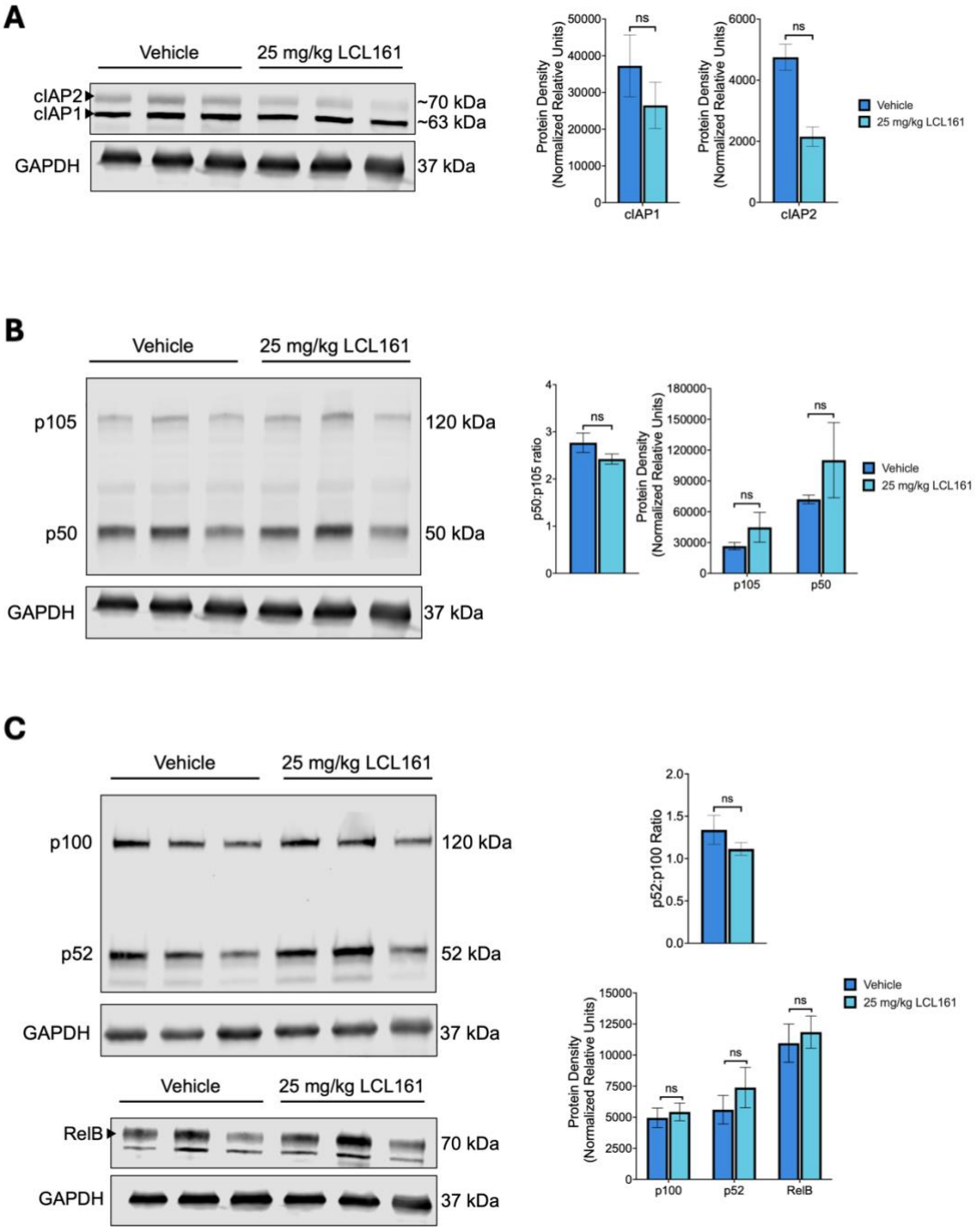

Figure 21. LCL161 leads to degradation of cIAP1 and cIAP2 in juvenile D2.*mdx* gastrocnemius muscle. Representative western blots of **(A)** cIAP1/2, **(B)** classical NF-κB (p105, p50) and **(C)** alternative NF-κB (RelB, p100, p52) signalling with their corresponding densitometric quantitation. Data represent mean ± SEM (n=3 per group).

CHAPTER FOUR: DISCUSSION

Overview:

This thesis investigated the therapeutic potential of LCL161, an IAP antagonist and SMAC mimetic targeting cIAP1/2, in both adult and juvenile D2.*mdx* mice as a model for Duchenne Muscular Dystrophy (DMD). The study revealed age-dependent effects of LCL161 treatment, with adult mice showing trends towards reduced fibrosis and modulated cytokine profiles, while juvenile mice exhibited reduced muscle damage but increased necrosis and altered gene expression. These findings underscore the broader importance of aligning therapeutic strategies with the timing and severity of disease progression, with IAP inhibition serving as a compelling example. The age-dependent effects of LCL161 observed in this study highlight the complex interplay between muscle regeneration, inflammation, and fibrosis in DMD progression. Further investigation is necessary to elucidate the precise mechanisms by which LCL161 modulates these processes across different disease stages.

4.1 Muscle Preservation and Functional Outcomes.

In both adult and juvenile mice treated with LCL161, there was no significant decline in body weight compared to the vehicle group. Although the percent change in body weight from the start of treatment to collection was higher in the untreated mice, it is unlikely that this reflects a biologically beneficial outcome. D2.*mdx* mice typically exhibit age-dependent increases in body weight, often driven by pathological factors such as increased fibrosis, fat infiltration, or edema-induced muscular enlargement[79,80,88]. These factors contribute to weight gain both directly and indirectly through reduced mobility and functional impairment. However, the current treatment regimen using LCL161 does not have a clear effect on these variables. On the contrary, this study does demonstrate that both the dose, frequency, and

length of treatment using LCL161 is well tolerated in this mouse model. Work from our lab has demonstrated that acute doses of 75 mg/kg LCL161 reduce muscle atrophy, whereas chronic dosing can have detrimental effects on muscle health[2, unpublished data]. Despite this, LCL161 has shown a favorable safety profile in cancer research, where it is generally well tolerated and reports 5-10% loss in body weight recovered when treatment was discontinued[190–192]. The effects of LCL161 are context-dependant and modifications to dosing and frequency should be determined for each model. Further emphasizing what we have seen in muscle, LCL161 has been less favourable in a MYC-driven lymphoma model where 75 mg/kg twice weekly exacerbated cytokine storm and reduced survival[193]. A similar effect was reported in 3 out of 53 patients during a Phase I clinical trial using LCL161 in patients with advanced solid tumors[190]. In contrast, a mouse xenograft model of human melanoma tolerated daily doses of 100 mg/kg for four weeks without significant adverse effects[194].

While this study focused on the diaphragm and gastrocnemius muscles, there is some evidence for a more pronounced effect on certain muscles compared to others. This is potentially due to variations in muscle composition, regeneration capacity, or disease severity across different muscle groups. In the adult D2.*mdx* mice, LCL161 treatment does not contribute to detectable weight differences in the diaphragm and hindlimb weights however the weight of the heart remained at wild-type levels. Although there's no apparent significant difference when compared to the vehicle, it's possible that a real effect exists but the sample size is too small. Most DMD patients develop dilated cardiomyopathy (DCM), whereby the left ventricle stretches, becomes weaker and leads to heart enlargement [195,196].

Similarly, D2.*mdx* have significantly larger hearts than wild-type controls due to fibrosis and calcification of the epicardium by 16-weeks and reduced cardiac functioning by 28-weeks[82,197]. Future studies should look to determine the biological significance of this trend by increasing the sample size. Assuming the observation is biologically relevant, analysis of cardiac structure function should be performed, similar to the methods seen by Hayes et al. [198]. Classical NF-κB signalling in cardiomyocytes has been linked to adverse remodeling, fibrosis, myocyte atrophy and endoplasmic reticulum-induced apoptosis in heart failure models [199–201]. Notably, Maier et al., able to reduce inflammatory DCM and heart failure by turning off IKKβ in their transgenic mouse model[199]. LCL161's capacity to activate alternative NF-κB signalling presents a potential avenue for further investigation of cardiomyocytes.

In the juvenile D2.*mdx* mice, LCL161 treatment resulted in increased soleus weight and decreased gastrocnemius weight. The soleus muscle is predominantly composed of slow-twitch (type I) fibres, which are reportedly less susceptible to dystrophic processes[202–206]. This was first demonstrated by Webster et al. in 1988, where fast-twitch fibres (particularly type IIb) were shown to degenerate earlier[202] . Another study confirmed that despite their larger mean diameter, type II fibres were significantly reduced in number, suggesting greater vulnerability to degeneration[203]. This aligns with my findings of no significant difference in soleus weight between adult D2.mdx and wild-type mice, as well as with mdx models, where the soleus exhibits resilience to eccentric contraction-induced damage and benefits from low-intensity eccentric training[204,205]. Additionally, in *mdx* mice, the loss of cIAP1 reduced macrophage infiltration and centronucleation in the soleus, while enhancing its contractile properties[169]. The reason for the increase in soleus weight in

LCL161-treated juvenile D2.*mdx* mice remain unclear, although the observed decrease in CK levels suggests that LCL161 is reducing overall muscle damage and potentially promoting muscle growth or maintenance. This is entirely speculatory and must be confirmed in future analyses to rule out LCL161-induced pseudohypertrophy, which is commonly seen in DMD muscles and may explain the weight increase. The discrepancy between the juvenile and adult D2.*mdx* solei response to LCL161 should also be clarified.

The observed decrease in gastrocnemius weight is more difficult to explain. When examining the H&E images, it appeared that the gastrocnemius of LCL161 treated juvenile D2.*mdx* mice had larger regions of necrosis. As this conflicted with the CK assay, I quantified the necrotic area and found that there was significantly more necrosis following LCL161 treatment. While necrosis results in a loss of muscle continuity and atrophy, analysis of the juvenile gastrocnemius fibre sizes and numbers does not reflect this increase. Additionally, there are no considerable differences in fibrotic deposits that may have contributed to weight changes.

4.2 LCL161's impact on muscle regeneration may be dependent on disease severity and regulation of MuSCs.

In the adult D2.*mdx* gastrocnemius, LCL161 treatment appeared to modestly increase the number of regenerating myofibres and the mean fibre size, though the total fibre count showed fewer notable changes. These promising trends are less distinct in the more severely affected diaphragm. However, *Myog* expression was slightly elevated compared to the vehicle group, and significantly higher than in wild-type controls. While LCL161 may exert mild effects on muscle regeneration, it seems insufficient to counteract the extensive

muscle damage seen in this model, preventing substantial improvements. This is further supported by the significant decrease in *Pax7* and modest reductions in *Myod1* and *Myog* in juvenile diaphragms, where inflammation and damage are more pronounced. The severity of damage in D2.*mdx* muscle could also explain the discrepancy between these findings and previous studies, where LCL161 or cIAP1 loss reduced atrophy and promoted myoblast fusion in acute injury models and in the less severe *mdx* mouse[146,169,170].

A common finding between the juvenile and adult D2.*mdx* diaphragms was the reduction in *Pax7* expression. While this decrease was not significant in the adult mice, it may be attributed to the unexpected improvement in regenerative capacity with age, despite only a 7-week difference compared to the younger mice [207]. The exact mechanism by which LCL161 reduces *Pax7* expression in the juvenile diaphragm remains unclear. Excessive inflammation and poor ECM remodeling contribute to MuSC dysfunction; however, LCL161 does not significantly elevate fibrotic or proinflammatory gene expression. A possible explanation may lie in LCL161's modulation of classical NF-κB signalling. A study using $BaCl_2$ to induce acute injury in the TA demonstrated an increase in classical NF-κB signalling in MuSCs[208]. It also highlighted the crucial role of IKKβ in MuSCs, as MuSC-specific deletion of IKKβ led to reduced MuSC numbers in injured muscle, impaired proliferation, and increased apoptosis[208]. These findings build on previous work from this group, showing that classical NF-κB is essential for MuSC survival, proliferation, and self-renewal. This was demonstrated through the deletion of upstream regulators, TAK1 and TRAF6, in mice or by using TWEAK, a known degrader of IAPs[140,141,209]. Interestingly, the TWEAK study showed a decrease in $PAX7^+$ cells cultured on myofibres and an increase of binding to a NF-κB consensus sequence

without distinguishing between the pathways[209]. Notably, the dose they used (10ng/mL) has been shown to preferentially upregulate alternative signalling[141,146]. Together, these studies highlight the possibility that LCL161 is affecting MuSCs by promoting alternative NF-κB signalling. Future studies should explore the impact of LCL161 on MuSC activation, proliferation, and differentiation in both acutely injured wild-type mice and the D2.*mdx* model. Furthermore, investigating the dose-dependent effects of LCL161 on the expression of key MRFs, including *Pax7, Myod1*, and *Myog*, could help identify optimal therapeutic windows based on age and disease severity, particularly in the context of MuSC dysfunction.

Based on these data and existing literature, future studies should investigate the direct effects of LCL161 on the regenerative capacity of dystrophic muscle. The observed trends may stem from its influence on muscle regeneration rather than from preventing fibrosis or modulating inflammation. Muscle sections should be examined for the number of proliferating (Pax7+/MyoD+), differentiating (Myogenin+) and self-renewing (Pax7+/MyoD-) cells to evaluate MuSC function. This could be more easily studied using acute injury models to reduce the complexity and confounding factors present in the D2.*mdx* model. However, it would also be of interest to explore any age-dependent differences in D2.*mdx* mice. Importantly, the treatment regimen should be refined to enable more direct comparisons.

4.3 Is fibrosis secondary to the regenerative benefits of LCL161?

I aimed to determine whether fibrosis was attenuated upon LCL161 administration. Encouragingly, there was a general trend toward reduced collagen deposition in the gastrocnemius of adult D2.*mdx* mice, and slightly lower expression of fibrotic genes (*Col1a1, Tgfb1, Fn1, Ctgf, Timp1*) in both adult and juvenile diaphragms compared to vehicle-treated

controls. Activation of both NF-κB pathways has been shown to regulate the expression of *Col1a1, FN1, Tgfb1* in lung fibroblasts, bronchiolar epithelial cells and in fibroblastic cells isolated from a model of pulmonary fibrosis and classical NF-κB regulated *TIMP1* expression[210,211]. Since NF-κB activation can regulate both the transition to myofibroblasts and direct regulation of pro-fibrotic genes, its modulation by LCL161 and the underlying effects should be further explored. While this presents a possible explanation for the slight reductions in collagen deposition and fibrotic gene expression but does not elicit enough of an effect to overcome other mechanisms and cell-types driving pro-fibrotic genes. Periostin (POSTN) and plasminogen activator inhibitor-1 (PAI-1/SERPINE1) were also elevated in the gastrocnemius of LCL161-treated mice and have previously been implicated in fibrosis for their roles in extracellular matrix and tissue remodelling[212–214]. Their elevation may be explained by a potential rebound/withdrawal effect from LCL161 and restoration of classical NF-κB[215–217].

Unfortunately, as with many of the other findings in this study, true conclusions cannot be drawn due to lack of statistical significance. However, aside from the necrosis observed in the juvenile gastrocnemius, LCL161 does not appear to significantly worsen the phenotype either. The observed trends instead highlight the potential for optimizing treatment timing and dosing to maximize its benefits. I attempted to address this by utilizing the juvenile model; however, treatment and collection occurred within a period when inflammation and regenerative deficits had begun to subside, with fibrosis becoming increasingly predominant[79]. Positive effects of LCL161 may become more apparent with extended treatment duration, as suggested by the modestly improved outcomes observed

after the 8-week treatment period in adult mice, where the benefits of sustained alternative NF-κB signalling can begin to emerge. To facilitate clearer comparisons in future studies, maintaining treatment lengths when examining mice at two distinct time points would help minimize confounding variables and allow for more direct assessment of treatment impact.

To more effectively assess the impact of LCL161 on regeneration, acute injury studies could be performed in the wild-type strain, reducing the complexity introduced by disease-related damage based on the methods used by Mázala et al. [207]. Specifically, the MuSC and macrophage dynamics within the early days of injury, along with the tracking of nascent myofibre formation and fibre regeneration and maturation over the month following injury, are crucial areas of investigation. Pre-treatment and post-treatment assessments with LCL161 can also provide insights into its potential to limit muscle damage and enhance the regenerative capacity of muscle tissue. While extensive data exist on the influence of cIAP1 in these processes, much of this research has been conducted using knockout models. Variations in tissue and target specificity, drug kinetics, and dosage effects can significantly impact the observed outcomes, despite targeting the same mechanism. The results from these studies may also inform which muscle groups should be prioritized for analysis in testing the disease model.

Another interesting avenue is exploring the effects of LCL161 on FAPs. The replacement of the functional muscle tissue with fibrotic tissue and fat infiltrate is a hallmark of DMD and multipotent ability of FAPs to differentiate into fibrotic and adipogenic lineages is problematic[218]. Human muscle-derived FAPs (PDGFRα+) have been shown to accumulate in dystrophic tissue and colocalize with areas of fatty and fibrous degeneration and can

express Peroxisome proliferator-activated receptor gamma (PPARγ), a master regulator of adipose cell development or secrete high levels of TGFβ[218]. Importantly, these high levels of TGFβ limit FAP apoptosis from macrophage-secreted TNFα[52]. Therefore, in vitro studies can be designed to address how LCL161 impacts the expansion of FAPs and influences the differentiation potential of adipogenic or fibrogenic fates. Through dose-dependent experiments, one can determine whether LCL161 is cytotoxic to these populations and if certain doses preferentially direct the differentiation program. It would also be valuable to culture FAPs in the presence of TNFα or macrophage conditioned media to better model the inflammatory environment of dystrophic muscle. While TNFα alone does not induce FAP apoptosis, does LCL161 also sensitize these cells to apoptosis when exposed to inflammatory stimuli. In vivo, using flow cytometry or mIHC, FAPs, adipocytes and fibroblast populations can be tracked, and their relative ratios can be compared between treatment groups. Multiplex IHC could provide the added layer of spatial resolution to identify interactions with macrophages and distribution through the tissue and injured regions.

4.4 LCL161 influences inflammation in D2.*mdx* mice.

In various mouse models utilized in our laboratory, administration of LCL161 has often resulted in splenomegaly. Although literature on this phenomenon is limited and conflicting, a study conducted in 2014 demonstrated that full-body knockouts of cIAP1, cIAP2, and XIAP—targets of LCL161—lead to severe sterile inflammation and subsequent splenomegaly[193,219–221]. This observation suggests that LCL161 treatment induces a systemic inflammatory response in both juvenile and adult D2.*mdx* mice, with the observed enlargement of the spleen likely attributable to the expansion of splenic immune cells.

Despite these observable alterations, the actual effect on inflammation in juvenile and adult D2.*mdx* muscles revealed no consistent patterns. For instance, in the cytokine and chemokine array performed on the adult D2.*mdx* gastrocnemius, IL-15 protein expression was higher in LCL161 treated mice. In the *mdx* mouse model, IL-15 administration increased diaphragm strength, cross-sectional area and decreased collagen content [219]. Additionally, IL-15 promotes myofibre regeneration and reduces fat infiltration, though it is also positively associated with the severity of fibrosis and the fate of fibroblasts derived from FAPs [222].

Furthermore, IL-13, a well-established driver of tissue fibrosis, is elevated in the gastrocnemius of LCL161-treated adult D2.*mdx* mice[223–225]. In partial agreement with the published findings, the mildly positive trends in strength and cross-sectional area, collagen deposition and regenerating fibres, may result from changes in IL-15, while being blunted by the elevated IL-13 levels. However, the fact that these measurements were taken five days post-final dose from just 2 trials complicates the assessment of LCL161's true effects. LCL161. The association between these findings should be interpreted with caution, as they involve different models, distinct muscle types, and are based on data with a low sample size. Repeating the array could help identify consistent changes induced by LCL161, which could then be validated through a secondary approach, such as ELISA.

As inflammatory markers, LIX (CXCL5/6), Pentraxin 3 (PTX3) and MPO were all elevated in the adult D2.*mdx* gastrocnemius following LCL161 treatment. Broadly, research has implicated each of these proteins in the coordination of the initial immune response and recruitment of immune cells to injured tissue. For instance, in models of pulmonary disease, LIX has been shown to promote both neutrophil and macrophage chemotaxis and activation

of classical NF-κB resulting in excessive inflammation and development of fibrosis[226–229]. Additionally, LIX appears to be involved in adipogenesis, insulin resistance, and oxidative stress although its role is not entirely clear. In CXCL5-treated soleus muscles, insulin-stimulated glucose transport was diminished, whereas inhibition of CXCL5 or its receptor, CXCR2, improved insulin sensitivity in obese, insulin-resistant mice[226]. Conversely, CXCL5 $^{-/-}$ mice developed insulin resistance and showed impaired ROS clearance, leading to oxidative stress[227]. PTX3 is positively associated with myocardial damage and fibrosis in DMD patients and influences parenchymal, stromal, and immune cell activity; *in vitro* studies show it promotes TGFβ activation, anti-inflammatory responses in macrophages, and fibrocyte differentiation[230–234]. As previously discussed, MPO plays a role in promoting oxidative stress, inflammation and necrosis. Since temporal dynamics of these proteins are intricately linked to muscle damage and regeneration, their elevation alone does not allow us to definitively determine whether LCL161 is beneficial or detrimental to the tissue.

Consistent between the mRNA of the diaphragm and the protein expression in the adult D2.*mdx* gastrocnemius was the reduction of IL-6. IL-6 is significantly upregulated in DMD patients and *mdx* mice and contributes to myofibre damage through sustained inflammation and MuSC exhaustion[235–237]. Blockade of IL-6 have had differing effects; a 2012 study demonstrated that anti-IL-6R antibody administration in *mdx* mice increased immune cell infiltrate and IL-10 expression (but not TNFα) but did not worsen muscle pathology while IL-6R antibody therapy in dystrophin-utrophin deficient mice decreased creatine kinase levels, fibrosis and improved MuSC function and regeneration [238,239]. Reduction of IL-6 may be one of the mechanisms driving the positive trends seen considering both protein from the

gastrocnemius and RNA from the diaphragm followed similar patterns. This was not observed in the RNA from the diaphragm of the juvenile D2.*mdx* perhaps because the effects of the drug cannot surmount the highly inflammatory environment. The fact that LCL161 has immunomodulatory properties complicate the very nature of these findings. Due to biological variability in disease progression and how the pathological processes of DMD manifest over time. This is further exemplified by the significant decrease in TNFα seen in the juvenile diaphragms, seemingly opposite from the adult diaphragms.

Despite examining two distinct age cohorts and time points, LCL161 administration did not elicit significant alterations in macrophage phenotypes within the gastrocnemius muscle of either adult or juvenile D2.*mdx* mice. Notably, the increase in total macrophage infiltration in LCL161-treated juvenile D2.*mdx* gastrocnemii is likely associated with the substantial necrosis detected. Conversely, the reduced macrophage infiltration in LCL161-treated adult D2.*mdx* gastrocnemii lacked biological significance. Given that chronic inflammation and persistent macrophage infiltration are detrimental to muscle homeostasis, further investigation is warranted to elucidate whether LCL161 actively promotes macrophage clearance in adult D2.*mdx* mice. Additionally, the underlying mechanisms responsible for the increased necrosis and macrophage infiltration in juvenile D2.*mdx* mice require further exploration. Considering the temporal dynamics of immune cell infiltration and the cycles of regeneration and degeneration in DMD, studying macrophage populations over a time course following LCL161 withdrawal could offer deeper insights into transient and age-related changes.

4.5 Investigating T-Cell dynamics in response to LCL161.

While macrophages have long been regarded as the primary immune mediators of skeletal muscle regeneration, the role of T-cells in orchestrating immune responses and influencing muscle repair mechanisms necessitates additional research. Recent findings underscore the multifaceted contributions of T-cells, not only in acute injury models but also in chronic pathological contexts.

In a CTX model, $CD8^{-/-}$ mice had poorer regeneration, smaller myofibres and increased ECM deposition[240]. This phenotype was rescued upon $CD8^{+}$ T-Cell transplantation[240]. $CD8^{+}$ T-Cells also secrete MCP-1, and their absence decreased the recruitment of protein gamma response 1 (Gr1)-expressing macrophages that contribute to the stemness and proliferation of MuSCs[240]. Additionally, Castiglioni et al. demonstrated a myogenic deficit, as evidenced by reduced *Pax*7 expression, decreased MuSC populations and smaller myofibre size in CTX-injured mice that lack lymphocytes ($Rag2^{-/-}$ γ-$chain^{-/-}$). Similarly, delayed muscle regeneration in $RAG1^{-/-}$-mice (lack mature T-cells and B-cells) was reversed with activated $CD3^{+}$ T-cell transplantation[241]. This study also demonstrated that T-cell-derived cytokines such as IL-1α, IL-13, TNF-α, and IFNγ stimulated MuSCs in injured muscle and enhanced their proliferation *in vitro*[241]. This supported previous co-culture experiments with MuSCs and T-Cells that demonstrated enhanced MuSC migration and proliferation[242].

Most notably, work from Burzyn et al. has shown the significance of T_{regs} in muscle regeneration. The group demonstrated that T_{regs} that direct the pro-inflammatory to anti-inflammatory macrophage transition and influence MuSC function[243]. As the muscle

microenvironment shifts to the anti-inflammatory/pro-regenerative state, T_{regs} accumulate and represent roughly half of all $CD4^+$ T-Cells by day 14 post-CTX injury. These T_{regs} have unique T-Cell receptors (TCRs) and distinct transcriptomes from lymphoid-derived T_{regs} suggesting they are clonally expanded during regeneration of injured muscle[243]. Ablation of T_{regs} in mice compromised the accrual and polarization towards the anti-inflammatory phenotype of muscle macrophages in vivo, prolonged inflammation, impaired regeneration and promoted fibrosis[243]. Additionally, $Rag1^{-/-}$ mice had milder fibrosis and more efficient repair than the T_{reg}-depleted mice, emphasizing the importance of T_{regs} in controlling the infiltrating immune populations[243]. T_{regs} appear to exert a dual effect on MuSCs by both modulating the secretion of cytokines, chemokines, and growth factors from other immune cells that influence MuSC activity, and through the overexpression of amphiregulin (AREG), an epidermal growth factor (EGFR) ligand, which has been shown to enhance MuSC proliferation and differentiation *in vitro*, as well as promote repair *in vivo*[244,245].

In immunocompromised *mdx* mice (*mdx*-nu/nu, scid/*mdx*), markers of fibrosis, including TGFβ1 were reduced when compared to immunocompetent *mdx* mice[11,246]. Similarly, antibody-depletion of $CD4^+$ and $CD8^+$ T-cells significantly reduced the histopathology and TGFβ1 levels in *mdx* mice compared to normal C57BL/10 mice[247]. In a study by Villalta et al., DMD patients and *mdx* mice had elevated T_{reg} populations and in *mdx* mice treated with IL-2c to expand T_{regs}, mice had reduced muscle damage due to the suppression of proinflammatory macrophage phenotypes [248]. Similarly, partial depletion of T_{regs} with an anti-CD25 antibody increased serum creatine kinase levels in young *mdx* mice whereas a marked reduction in creatine kinase was seen upon IL-2c expansion[245].

Furthermore, the study revealed that the distinct population of muscle-specific Tregs, previously identified in healthy muscle following acute injury, was also expanded in dystrophic muscle[245]. However, the chronic nature of muscle damage in dystrophic conditions may overshadow the reparative functions typically associated with these cells in acute injury scenarios. The role of T-cells in fibrosis development is more extensively documented in other tissues, such as the kidney, liver and lungs, suggesting there may be similar trends in modulating immune responses and tissue-resident cells in skeletal muscle[249].

Together these studies emphasize the role of T-cells in maintaining skeletal muscle health, and extensive research has focused on the regulation of T-cell activation, proliferation, and survival through the NF-κB pathways[250–252]. Given this context, it is important to explore how IAP antagonists, such as SMAC mimetics, may influence T-cell effector functions, either directly or indirectly by modulating T-cell recruitment mechanisms. However, the existing literature on the effects of SMCs on T-cell function presents mixed results, with variations observed among different compounds within this family and based on the model used.

LCL161 has been shown to enhance antigen-specific expansion of human T-cells, promote IL-2 production in both mice and humans, and increase TNFα production in humans but reduces T_{reg} differentiation in a model of multiple sclerosis[253–255]. Additionally, LCL161 has demonstrated the ability to reinvigorate $CD8^+$ T-cells by targeting pro-inflammatory macrophages[256]. However, findings by Burton et al. indicate that treating human peripheral blood mononuclear cells and purified T-cells with LCL161 did not

enhance IL-2, IFN-γ, or TNFα production and reduced T-cell proliferation, consistent with another study that found minimal effects on CD4 and CD8 proliferation and survival[253,257]. These discrepancies between *in vitro* and *in vivo* models highlight the complexity of immune modulation and raises the question of whether SMCs can influence T-cells within skeletal muscle. Future studies should investigate the effects of LCL161 on T-cells in injured and diseased skeletal muscle, focusing on potential shifts in activation, proliferation, and T-cell subsets through modulation of the immune environment to provide a more holistic view.

4.6 Conclusion

The investigation into the therapeutic potential of the IAP antagonist LCL161 in Duchenne muscular dystrophy (DMD) has revealed complex and stage-dependent effects that contribute to our understanding of IAP inhibition as a therapeutic strategy. Through careful examination of both adult and juvenile D2.*mdx* mice, this study has suggested that the efficacy of LCL161 is intrinsically linked to the stage of disease progression, presenting both opportunities and challenges for therapeutic intervention.

In adult D2.*mdx* mice, the effects of LCL161 were modest but noteworthy, particularly in reducing fibrosis in the gastrocnemius muscle and altering the cytokine and chemokine profile. However, the most striking results came from the juvenile mice, where the treatment significantly reduced muscle damage, though it did not translate to measurable improvements in functional strength. Interestingly, while muscle damage decreased, the gastrocnemius muscle of juvenile mice showed an increase in necrotic regions, alongside significant reductions in TNFα and PAX7 expression—suggesting a complex relationship between IAP inhibition and the muscle's ability to regenerate.

These findings provide valuable insights into DMD treatment strategies but also underline the need for further exploration. Key questions remain about how IAP inhibition influences muscle repair, inflammation, and fibrosis at different stages of the disease. A deeper understanding of the NF-κB pathway and the role of IAP degradation is particularly important. While this study touched on these mechanisms in juvenile D2.*mdx* mice, further research is needed to refine the dosing strategy and determine whether the lack of certain therapeutic outcomes might be due to insufficient cIAP1/2 degradation or suboptimal activation of alternative NF-κB signalling.

To build on these findings, time-course studies will be crucial to track how quickly and effectively cIAP1/2 is degraded after administering 25 mg/kg LCL161, how long the effects persist, and whether they result in meaningful biological changes in NF-κB pathways. Moreover, future studies should include multiple muscle types to uncover any muscle-specific differences in response to the treatment. Understanding these mechanisms will be crucial for optimizing the therapeutic potential of LCL161 and similar IAP antagonists.

REFERENCES:

1. Seale, P. *et al.* Pax7 is required for the specification of myogenic satellite cells. *Cell* **102**, 777–786 (2000).
2. Hernández-Hernández, J. M., García-González, E. G., Brun, C. E. & Rudnicki, M. A. The myogenic regulatory factors, determinants of muscle development, cell identity and regeneration. *Semin. Cell Dev. Biol.* **72**, 10–18 (2017).
3. Von Maltzahn, J. *et al.* Characteristics of Satellite Cells and Multipotent Adult Stem Cells in the Skeletal Muscle. *Stem Cells Cancer Stem Cells* **12**, 63–73 (2014).
4. Braun, T., Buschhausen-Denker, G., Bober, E., Tannich, E. & Arnold, H. H. A novel human muscle factor related to but distinct from MyoD1 induces myogenic conversion in 10T1/2 fibroblasts. *EMBO J.* **8**, 701–709 (1989).
5. Zammit, P. S. Function of the myogenic regulatory factors Myf5, MyoD, Myogenin and MRF4 in skeletal muscle, satellite cells and regenerative myogenesis. *Semin. Cell Dev. Biol.* **72**, 19–32 (2017).
6. Davis, R. L., Weintraub, H. & Lassar, A. B. Expression of a single transfected cDNA converts fibroblasts to myoblasts. *Cell* **51**, 987–1000 (1987).
7. Chen, J. C. J. & Goldhamer, D. J. Transcriptional mechanisms regulating MyoD expression in the mouse. *Cell Tissue Res.* **296**, 213–219 (1999).
8. Rhodes, S. J. & Konieczny, S. F. Identification of MRF4: a new member of the muscle regulatory factor gene family. *Genes Dev.* **3**, 2050–2061 (1989).
9. Wright, W. E., Sassoon, D. A. & Lin, V. K. Myogenin, a factor regulating myogenesis, has a domain homologous to MyoD. *Cell* **56**, 607–617 (1989).
10. Hasty, P. *et al.* Muscle deficiency and neonatal death in mice with a targeted mutation in the myogenin gene. *Nat. 1993 3646437* **364**, 501–506 (1993).
11. Farini, A. *et al.* T and B lymphocyte depletion has a marked effect on the fibrosis of dystrophic skeletal muscles in the scid/mdx mouse. *J. Pathol.* **213**, 229–238 (2007).
12. Takala, T. E. & Virtanen, P. Biochemical composition of muscle extracellular matrix: the effect of loading. *Scand. J. Med. Sci. Sports* **10**, 321–325 (2000).
13. Halper, J. & Kjaer, M. Basic components of connective tissues and extracellular matrix: elastin, fibrillin, fibulins, fibrinogen, fibronectin, laminin, tenascins and thrombospondins. *Adv. Exp. Med. Biol.* **802**, 31–47 (2014).
14. Mukund, K. & Subramaniam, S. Skeletal muscle: A review of molecular structure and function, in health and disease. *Wiley Interdiscip. Rev. Syst. Biol. Med.* **12**, (2020).
15. Hody, S., Croisier, J. L., Bury, T., Rogister, B. & Leprince, P. Eccentric muscle contractions: Risks and benefits. *Front. Physiol.* **10**, 442082 (2019).

16. Mann, C. J. *et al.* Aberrant repair and fibrosis development in skeletal muscle. *Skelet. Muscle* **1**, 21 (2011).

17. Osses, N. & Brandan, E. ECM is required for skeletal muscle differentiation independently of muscle regulatory factor expression. *Am. J. Physiol. - Cell Physiol.* **282**, (2002).

18. Lynch, S. E., Nixon, J. C., Colvin, R. B. & Antoniades, H. N. Role of platelet-derived growth factor in wound healing: synergistic effects with other growth factors. *Proc. Natl. Acad. Sci. U. S. A.* **84**, 7696 (1987).

19. Ihn, H. Pathogenesis of fibrosis: role of TGF-beta and CTGF. *Curr. Opin. Rheumatol.* **14**, 681–685 (2002).

20. Schultz, G. S. & Wysocki, A. Interactions between extracellular matrix and growth factors in wound healing. *Wound Repair Regen.* **17**, 153–162 (2009).

21. Cabral-Pacheco, G. A. *et al.* The Roles of Matrix Metalloproteinases and Their Inhibitors in Human Diseases. *Int. J. Mol. Sci.* **21**, 1–53 (2020).

22. Mahdy, M. A. A. Skeletal muscle fibrosis: an overview. *Cell Tissue Res.* **375**, 575–588 (2019).

23. Lu, H., Huang, D., Ransohoff, R. M. & Zhou, L. Acute skeletal muscle injury: CCL2 expression by both monocytes and injured muscle is required for repair. *FASEB J.* **25**, 3344 (2011).

24. Belcastro, A. N., Arthur, G. D., Albisser, T. A. & Raj, D. A. Heart, liver, and skeletal muscle myeloperoxidase activity during exercise. *https://doi.org/10.1152/jappl.1996.80.4.1331* **80**, 1331–1335 (1996).

25. Fielding, R. A. *et al.* Acute phase response in exercise. III. Neutrophil and IL-1 beta accumulation in skeletal muscle. *https://doi.org/10.1152/ajpregu.1993.265.1.R166* **265**, (1993).

26. Wang, X. *et al.* Heterogeneous origins and functions of mouse skeletal muscle-resident macrophages. *Proc. Natl. Acad. Sci. U. S. A.* **117**, 20729–20740 (2020).

27. Torres-Ruiz, J., Alcalá-Carmona, B., Alejandre-Aguilar, R. & Gómez-Martín, D. Inflammatory myopathies and beyond: The dual role of neutrophils in muscle damage and regeneration. *Front. Immunol.* **14**, 1113214 (2023).

28. Yang, W. & Hu, P. Skeletal muscle regeneration is modulated by inflammation. *J. Orthop. Transl.* **13**, 25–32 (2018).

29. Shu, L. Z., Zhang, X. L., Ding, Y. D. & Lin, H. From inflammation to bone formation: the intricate role of neutrophils in skeletal muscle injury and traumatic heterotopic ossification. *Exp. Mol. Med. 2024 567* **56**, 1523–1530 (2024).

30. Davies, L. C., Jenkins, S. J., Allen, J. E. & Taylor, P. R. Tissue-resident macrophages.

Nat. Immunol. **14**, 986 (2013).

31. Sánchez Riera, C. *et al.* Muscle Diversity, Heterogeneity, and Gradients: Learning from Sarcoglycanopathies. *Int. J. Mol. Sci.* **22**, 1–15 (2021).

32. Shireman, P. K. *et al.* MCP-1 deficiency causes altered inflammation with impaired skeletal muscle regeneration. *J. Leukoc. Biol.* **81**, 775–785 (2007).

33. Contreras-Shannon, V. *et al.* Fat accumulation with altered inflammation and regeneration in skeletal muscle of CCR2-/- mice following ischemic injury. *Am. J. Physiol. - Cell Physiol.* **292**, 953–967 (2007).

34. Lu, H., Huang, D., Ransohoff, R. M. & Zhou, L. Acute skeletal muscle injury: CCL2 expression by both monocytes and injured muscle is required for repair. *FASEB J.* **25**, 3344 (2011).

35. Wang, H. *et al.* Altered Macrophage Phenotype Transition Impairs Skeletal Muscle Regeneration. *Am. J. Pathol.* **184**, 1167–1184 (2014).

36. Wang, X., Zhao, W., Ransohoff, R. M. & Zhou, L. Infiltrating macrophages are broadly activated at the early stage to support acute skeletal muscle injury repair. *J. Neuroimmunol.* **317**, 55 (2018).

37. Tidball, J. G. & Villalta, S. A. Regulatory interactions between muscle and the immune system during muscle regeneration. *Am. J. Physiol. - Regul. Integr. Comp. Physiol.* **298**, 1173–1187 (2010).

38. Shirakawa, T. *et al.* Tumor necrosis factor alpha regulates myogenesis to inhibit differentiation and promote proliferation in satellite cells. *Biochem. Biophys. Res. Commun.* **580**, 35–40 (2021).

39. Shang, M. *et al.* Macrophage-derived glutamine boosts satellite cells and muscle regeneration. *Nat. 2020 5877835* **587**, 626–631 (2020).

40. Tonkin, J. *et al.* Monocyte/macrophage-derived IGF-1 orchestrates murine skeletal muscle regeneration and modulates autocrine polarization. *Mol. Ther.* **23**, 1189–1200 (2015).

41. Dort, J., Fabre, P., Molina, T. & Dumont, N. A. Macrophages Are Key Regulators of Stem Cells during Skeletal Muscle Regeneration and Diseases. *Stem Cells Int.* **2019**, (2019).

42. Arnold, L. *et al.* Inflammatory monocytes recruited after skeletal muscle injury switch into antiinflammatory macrophages to support myogenesis. *J. Exp. Med.* **204**, 1057–1069 (2007).

43. Saclier, M. *et al.* Differentially activated macrophages orchestrate myogenic precursor cell fate during human skeletal muscle regeneration. *Stem Cells* **31**, 384–396 (2013).

44. Saclier, M. *et al.* Differentially Activated Macrophages Orchestrate Myogenic Precursor Cell Fate During Human Skeletal Muscle Regeneration. *Stem Cells* **31**, 384–396 (2013).

45. Wynn, T. A. & Vannella, K. M. Macrophages in Tissue Repair, Regeneration, and Fibrosis. *Immunity* **44**, 450–462 (2016).

46. Liu, X. *et al.* Macrophage depletion impairs skeletal muscle regeneration: The roles of regulatory factors for muscle regeneration. *Cell Biol. Int.* **41**, 228–238 (2017).

47. Summan, M. *et al.* Macrophages and skeletal muscle regeneration: A clodronate-containing liposome depletion study. *Am. J. Physiol. - Regul. Integr. Comp. Physiol.* **290**, 1488–1495 (2006).

48. Bencze, M. *et al.* Proinflammatory Macrophages Enhance the Regenerative Capacity of Human Myoblasts by Modifying Their Kinetics of Proliferation and Differentiation. *YMTHE* **20**, 2168–2179 (2012).

49. DiPasquale, D. M. *et al.* Urokinase-type plasminogen activator and macrophages are required for skeletal muscle hypertrophy in mice. *Am. J. Physiol. - Cell Physiol.* **293**, 1278–1285 (2007).

50. Dumont, N. & Frenette, J. Macrophages Protect against Muscle Atrophy and Promote Muscle Recovery in Vivo and in Vitro: A Mechanism Partly Dependent on the Insulin-Like Growth Factor-1 Signaling Molecule. *Am. J. Pathol.* **176**, 2228–2235 (2010).

51. Nawaz, A. *et al.* Depletion of CD206+ M2-like macrophages induces fibro-adipogenic progenitors activation and muscle regeneration. *Nat. Commun. 2022 131* **13**, 1–12 (2022).

52. Lemos, D. R. *et al.* Nilotinib reduces muscle fibrosis in chronic muscle injury by promoting TNF-mediated apoptosis of fibro/adipogenic progenitors. *Nat. Med. 2015 217* **21**, 786–794 (2015).

53. Kawanishi, N., Mizokami, T., Niihara, H., Yada, K. & Suzuki, K. Macrophage depletion by clodronate liposome attenuates muscle injury and inflammation following exhaustive exercise. *Biochem. Biophys. Reports* **5**, 146 (2016).

54. Theadom, A. *et al.* Prevalence of muscular dystrophies: a systematic literature review. *Neuroepidemiology* **43**, 259–268 (2014).

55. Salari, N. *et al.* Global prevalence of Duchenne and Becker muscular dystrophy: a systematic review and meta-analysis. *J. Orthop. Surg. Res.* **17**, 96 (2022).

56. Mercuri, E., Pane, M., Cicala, G., Brogna, C. & Ciafaloni, E. Detecting early signs in Duchenne muscular dystrophy: comprehensive review and diagnostic implications. *Front. Pediatr.* **11**, (2023).

57. Broomfield, J., Hill, M., Guglieri, M., Crowther, M. & Abrams, K. Life Expectancy in Duchenne Muscular Dystrophy: Reproduced Individual Patient Data Meta-analysis.

Neurology **97**, e2304 (2021).

58. Lee, T. *et al.* Differences in carrier frequency between mothers of Duchenne and Becker muscular dystrophy patients. *J. Hum. Genet.* **59**, 46 (2014).

59. Aartsma-Rus, A., Ginjaar, I. B. & Bushby, K. The importance of genetic diagnosis for Duchenne muscular dystrophy. *J. Med. Genet.* **53**, 145 (2016).

60. Koenig, M. *et al.* Complete cloning of the duchenne muscular dystrophy (DMD) cDNA and preliminary genomic organization of the DMD gene in normal and affected individuals. *Cell* **50**, 509–517 (1987).

61. Morton, A. B. *et al.* Barium chloride injures myofibers through calcium-induced proteolysis with fragmentation of motor nerves and microvessels. *Skelet. Muscle* **9**, 1–10 (2019).

62. Ibraghimov-Beskrovnaya, O. *et al.* Primary structure of dystrophin-associated glycoproteins linking dystrophin to the extracellular matrix. *Nature* **355**, 696–702 (1992).

63. Levine, B. A., Moir, A. J. G., Patchell, V. B. & Perry, S. V. The interaction of actin with dystrophin. *FEBS Lett.* **263**, 159–162 (1990).

64. Desguerre, I. *et al.* Endomysial Fibrosis in Duchenne Muscular Dystrophy: A Marker of Poor Outcome Associated With Macrophage Alternative Activation. *J. Neuropathol. Exp. Neurol.* **68**, 762–773 (2009).

65. Bulfield, G., Siller, W. G., Wight, P. A. L. & Moore, K. J. X chromosome-linked muscular dystrophy (mdx) in the mouse. *Proc. Natl. Acad. Sci.* **81**, 1189–1192 (1984).

66. Sicinski, P. *et al.* The Molecular Basis of Muscular Dystrophy in the mdx Mouse: A Point Mutation. *New Ser.* **244**, 1578–1580 (1989).

67. Hoffman, E. P., Brown, R. H. & Kunkel, L. M. Dystrophin: The protein product of the duchenne muscular dystrophy locus. *Cell* **51**, 919–928 (1987).

68. Chamberlain, J. S. *et al.* Expression of the Murine Duchenne Muscular Dystrophy Gene in Muscle and Brain. *Science (80-.).* **239**, 1416–1418 (1988).

69. Stedman, H. H. *et al.* The mdx mouse diaphragm reproduces the degenerative changes of Duchenne muscular dystrophy. *Nat. 1991 3526335* **352**, 536–539 (1991).

70. Lynch, G. S., Hinkle, R. T., Chamberlain, J. S., Brooks, S. V. & Faulkner, J. A. Force and power output of fast and slow skeletal muscles from mdx mice 6-28 months old. *J. Physiol.* **535**, 591–600 (2001).

71. COULTON, G. R., MORGAN, J. E., PARTRIDGE, T. A. & SLOPER, J. C. THE mdx MOUSE SKELETAL MUSCLE MYOPATHY: I. A HISTOLOGICAL, MORPHOMETRIC AND BIOCHEMICAL INVESTIGATION. *Neuropathol. Appl. Neurobiol.* **14**, 53–70 (1988).

72. Torres, L. F. B. & Duchen, L. W. THE MUTANT mdx: INHERITED MYOPATHY IN THE

MOUSE MORPHOLOGICAL STUDIES OF NERVES, MUSCLES AND END-PLATES. *Brain* **110**, 269–299 (1987).

73. Banks, G. B., Combs, A. C., Odom, G. L., Bloch, R. J. & Chamberlain, J. S. Muscle Structure Influences Utrophin Expression in mdx Mice. *PLOS Genet.* **10**, e1004431 (2014).

74. Amenta, A. R. *et al.* Biglycan recruits utrophin to the sarcolemma and counters dystrophic pathology in mdx mice. *Proc. Natl. Acad. Sci. U. S. A.* **108**, 762–767 (2011).

75. Chamberlain, J. S., Metzger, J., Reyes, M., Townsend, D. & Faulkner, J. A. Dystrophin-deficient mdx mice display a reduced life span and are susceptible to spontaneous rhabdomyosarcoma. doi:10.1096/fj.06-7353com.

76. Swiderski, K. & Lynch, G. S. Murine models of Duchenne muscular dystrophy: is there a best model? *Am. J. Physiol. - Cell Physiol.* **321**, C409–C412 (2021).

77. McGreevy, J. W., Hakim, C. H., McIntosh, M. A. & Duan, D. Animal models of Duchenne muscular dystrophy: From basic mechanisms to gene therapy. *DMM Dis. Model. Mech.* **8**, 195–213 (2015).

78. Fukada, S. I. *et al.* Genetic background affects properties of satellite cells and mdx phenotypes. *Am. J. Pathol.* **176**, 2414–2424 (2010).

79. Hammers, D. W. *et al.* The D2.mdx mouse as a preclinical model of the skeletal muscle pathology associated with Duchenne muscular dystrophy. *Sci. Reports 2020 101* **10**, 1–12 (2020).

80. van Putten, M. *et al.* Natural disease history of the D2-mdx mouse model for Duchenne muscular dystrophy. *FASEB J.* **33**, 8110 (2019).

81. Coley, W. D. *et al.* Effect of genetic background on the dystrophic phenotype in mdx mice. (2015) doi:10.1093/hmg/ddv460.

82. Coley, W. D. *et al.* Effect of genetic background on the dystrophic phenotype in mdx mice. *Hum. Mol. Genet.* **25**, 130–145 (2016).

83. Flanigan, K. M. *et al.* LTBP4 genotype predicts age of ambulatory loss in duchenne muscular dystrophy. *Ann. Neurol.* **73**, 481–488 (2013).

84. Van Den Bergen, J. C. *et al.* Validation of genetic modifiers for Duchenne muscular dystrophy: a multicentre study assessing SPP1 and LTBP4 variants. *J. Neurol. Neurosurg. Psychiatry* **86**, 1060–1065 (2015).

85. Zhao, W. *et al.* A Murine Hypertrophic Cardiomyopathy Model: The DBA/2J Strain. *PLoS One* **10**, e0133132 (2015).

86. Roberts, N. W., Holley-Cuthrell, J., Gonzalez-Vega, M., Mull, A. J. & Heydemann, A. Biochemical and Functional Comparisons of mdx and Sgcg−/− Muscular Dystrophy

Mouse Models. *Biomed Res. Int.* **2015**, (2015).

87. Nabors, C. E. & Ball, C. R. Spontaneous calcification in hearts of DBA mice. *Anat. Rec.* **164**, 153–161 (1969).

88. Hart, C. C., Lee, Y. il, Hammers, D. W. & Sweeney, H. L. Evaluation of the DBA/2J mouse as a potential background strain for genetic models of cardiomyopathy. *J. Mol. Cell. Cardiol. plus* **1**, 100012 (2022).

89. Chang, N. C. *et al.* The Dystrophin Glycoprotein Complex Regulates the Epigenetic Activation of Muscle Stem Cell Commitment. *Cell Stem Cell* **22**, 755-768.e6 (2018).

90. Dumont, N. A. *et al.* Dystrophin expression in muscle stem cells regulates their polarity and asymmetric division. *Nat. Med.* **21**, 1455–1463 (2015).

91. Boyer, J. G. *et al.* Depletion of skeletal muscle satellite cells attenuates pathology in muscular dystrophy. *Nat. Commun. 2022 131* **13**, 1–10 (2022).

92. Boldrin, L., Zammit, P. S. & Morgan, J. E. Satellite cells from dystrophic muscle retain regenerative capacity. *Stem Cell Res.* **14**, 20 (2015).

93. Collins, C. A. *et al.* Stem cell function, self-renewal, and behavioral heterogeneity of cells from the adult muscle satellite cell niche. *Cell* **122**, 289–301 (2005).

94. Boldrin, L., Neal, A., Zammit, P. S., Muntoni, F. & Morgan, J. E. Donor Satellite Cell Engraftment Is SignificantlyAugmented When the Host Niche Is Preserved and Endogenous Satellite Cells Are Incapacitated. *Stem Cells* **30**, 1971–1984 (2012).

95. Boldrin, L., Zammit, P. S., Muntoni, F. & Morgan, J. E. Mature Adult Dystrophic Mouse Muscle Environment Does Not Impede Efficient Engrafted Satellite Cell Regeneration and Self-Renewal. *Stem Cells* **27**, 2478–2487 (2009).

96. Hodgetts, S., Radley, H., Davies, M. & Grounds, M. D. Reduced necrosis of dystrophic muscle by depletion of host neutrophils, or blocking TNFα function with Etanercept in mdx mice. *Neuromuscul. Disord.* **16**, 591–602 (2006).

97. Pelosi, L. *et al.* Functional and Morphological Improvement of Dystrophic Muscle by Interleukin 6 Receptor Blockade. *EBioMedicine* **2**, 285 (2015).

98. Laskin, D. L. *et al.* Macrophages, reactive nitrogen species, and lung injury. *Ann. N. Y. Acad. Sci.* **1203**, 60 (2010).

99. Aratani, Y. Myeloperoxidase: Its role for host defense, inflammation, and neutrophil function. *Arch. Biochem. Biophys.* **640**, 47–52 (2018).

100. Galijasevic, S., Saed, G. M., Diamond, M. P. & Abu-Soud, H. M. Myeloperoxidase up-regulates the catalytic activity of inducible nitric oxide synthase by preventing nitric oxide feedback inhibition. *Proc. Natl. Acad. Sci. U. S. A.* **100**, 14766 (2003).

101. Nguyen, H. X., Lusis, A. J. & Tidball, J. G. Null mutation of myeloperoxidase in mice prevents mechanical activation of neutrophil lysis of muscle cell membranes in vitro

and in vivo. *J. Physiol.* **565**, 403 (2005).

102. Villalta, S. A., Nguyen, H. X., Deng, B., Gotoh, T. & Tidbal, J. G. Shifts in macrophage phenotypes and macrophage competition for arginine metabolism affect the severity of muscle pathology in muscular dystrophy. *Hum. Mol. Genet.* **18**, 482–496 (2009).

103. Villalta, S. A., Deng, B., Rinaldi, C., Wehling-Henricks, M. & Tidball, J. G. IFN-γ Promotes Muscle Damage in the mdx Mouse Model of Duchenne Muscular Dystrophy by Suppressing M2 Macrophage Activation and Inhibiting Muscle Cell Proliferation. *J. Immunol.* **187**, 5419–5428 (2011).

104. Gong, D. *et al.* TGFβ signaling plays a critical role in promoting alternative macrophage activation. *BMC Immunol.* **13**, 1–10 (2012).

105. Chen, Y. W. *et al.* Early onset of inflammation and later involvement of TGFβ in Duchenne muscular dystrophy. *Neurology* **65**, 826–834 (2005).

106. Allen, R. E. & Boxhorn, L. K. Inhibition of skeletal muscle satellite cell differentiation by transforming growth factor-beta. *J. Cell. Physiol.* **133**, 567–572 (1987).

107. Li, Y. *et al.* Transforming growth factor-beta1 induces the differentiation of myogenic cells into fibrotic cells in injured skeletal muscle: a key event in muscle fibrogenesis. *Am. J. Pathol.* **164**, 1007–1019 (2004).

108. Burks, T. N. & Cohn, R. D. Role of TGF-β signaling in inherited and acquired myopathies. *Skelet. Muscle* **1**, 1–13 (2011).

109. Chen, X. & Thibeault, S. L. Response of Fibroblasts to Transforming Growth Factor-β1 on Two-Dimensional and in Three-Dimensional Hyaluronan Hydrogels. *Tissue Eng. Part A* **18**, 2528 (2012).

110. Contreras, O., Rebolledo, D. L., Oyarzún, J. E., Olguín, H. C. & Brandan, E. Connective tissue cells expressing fibro/adipogenic progenitor markers increase under chronic damage: relevance in fibroblast-myofibroblast differentiation and skeletal muscle fibrosis. *Cell Tissue Res.* **364**, 647–660 (2016).

111. Lemos, D. R. *et al.* Nilotinib reduces muscle fibrosis in chronic muscle injury by promoting TNF-mediated apoptosis of fibro/adipogenic progenitors. *Nat. Med. 2015 217* **21**, 786–794 (2015).

112. Davies, M. R. *et al.* TGF-β Small Molecule Inhibitor SB431542 Reduces Rotator Cuff Muscle Fibrosis and Fatty Infiltration By Promoting Fibro/Adipogenic Progenitor Apoptosis. *PLoS One* **11**, (2016).

113. Birnkrant, D. J. *et al.* Diagnosis and management of Duchenne muscular dystrophy, part 1: diagnosis, and neuromuscular, rehabilitation, endocrine, and gastrointestinal and nutritional management. *Lancet. Neurol.* **17**, 251 (2018).

114. Birnkrant, D. J. *et al.* Diagnosis and management of Duchenne muscular dystrophy,

part 2: respiratory, cardiac, bone health, and orthopaedic management. *Lancet. Neurol.* **17**, 347 (2018).

115. Dhuri, K. *et al.* Antisense Oligonucleotides: An Emerging Area in Drug Discovery and Development. *J. Clin. Med.* **9**, 1–24 (2020).

116. Shimizu-Motohashi, Y. *et al.* Restoring Dystrophin Expression in Duchenne Muscular Dystrophy: Current Status of Therapeutic Approaches. *J. Pers. Med.* **9**, (2019).

117. Aartsma-Rus, A. & Krieg, A. M. FDA Approves Eteplirsen for Duchenne Muscular Dystrophy: The Next Chapter in the Eteplirsen Saga. *Nucleic Acid Ther.* **27**, 1 (2017).

118. Sabrina Haque, U., Kohut, M. & Yokota, T. Comprehensive review of adverse reactions and toxicology in ASO-based therapies for Duchenne Muscular Dystrophy: From FDA-approved drugs to peptide-conjugated ASO. *Curr. Res. Toxicol.* **7**, 100182 (2024).

119. Assefa, M., Gepfert, A., Zaheer, M., Hum, J. M. & Skinner, B. W. Casimersen (AMONDYS 45™): An Antisense Oligonucleotide for Duchenne Muscular Dystrophy. *Biomedicines* **12**, (2024).

120. Roshmi, R. R. & Yokota, T. Viltolarsen: From Preclinical Studies to FDA Approval. *Methods Mol. Biol.* **2587**, 31–41 (2023).

121. Aartsma-Rus, A. & Corey, D. R. The 10th Oligonucleotide Therapy Approved: Golodirsen for Duchenne Muscular Dystrophy. *Nucleic Acid Ther.* **30**, 67 (2020).

122. Dhillon, S. Viltolarsen: First Approval. *Drugs* **80**, 1027–1031 (2020).

123. Antisense Oligonucleotide-Mediated Exon-skipping Therapies: Precision Medicine Spreading from Duchenne Muscular Dystrophy. *JMA J.* **4**, 232–240 (2021).

124. Bello, L. & Pegoraro, E. Genetic diagnosis as a tool for personalizedtreatment of Duchenne muscular dystrophy. *Acta Myol.* **35**, 122 (2016).

125. Spelier, S., van Doorn, E. P. M., van der Ent, C. K., Beekman, J. M. & Koppens, M. A. J. Readthrough compounds for nonsense mutations: bridging the translational gap. *Trends Mol. Med.* **29**, 297–314 (2023).

126. McDonald, C. M. *et al.* Ataluren delays loss of ambulation and respiratory decline in nonsense mutation Duchenne muscular dystrophy patients. *J. Comp. Eff. Res.* **11**, 139–155 (2022).

127. Mercuri, E. *et al.* Safety and effectiveness of ataluren in patients with nonsense mutation DMD in the STRIDE Registry compared with the CINRG Duchenne Natural History Study (2015–2022): 2022 interim analysis. *J. Neurol.* **270**, 3896 (2023).

128. Mullard, A. FDA approves an HDAC inhibitor for Duchenne muscular dystrophy. *Nat. Rev. Drug Discov.* **23**, 329 (2024).

129. Consalvi, S. *et al.* Preclinical Studies in the mdx Mouse Model of Duchenne Muscular

Dystrophy with the Histone Deacetylase Inhibitor Givinostat. *Mol. Med.* **19**, 79 (2013).

130. Ito, T. *et al.* Imatinib attenuates severe mouse dystrophy and inhibits proliferation and fibrosis-marker expression in muscle mesenchymal progenitors. *Neuromuscul. Disord.* **23**, 349–356 (2013).

131. Mercuri, E. *et al.* Safety and efficacy of givinostat in boys with Duchenne muscular dystrophy (EPIDYS): a multicentre, randomised, double-blind, placebo-controlled, phase 3 trial. *Lancet. Neurol.* **23**, 393–403 (2024).

132. Pasparakis, M., Luedde, T. & Schmidt-Supprian, M. Dissection of the NF-κB signalling cascade in transgenic and knockout mice. *Cell Death Differ. 2006 135* **13**, 861–872 (2006).

133. Sen, R. & Baltimore, D. Multiple nuclear factors interact with the immunoglobulin enhancer sequences. *Cell* **46**, 705–716 (1986).

134. Xiao, G., Harhaj, E. W. & Sun, S. C. NF-κB-inducing kinase regulates the processing of NF-κB2 p100. *Mol. Cell* **7**, 401–409 (2001).

135. Capece, D. *et al.* NF-κB: blending metabolism, immunity, and inflammation. *Trends Immunol.* **43**, 757–775 (2022).

136. Taniguchi, K. & Karin, M. NF-κB, inflammation, immunity and cancer: coming of age. *Nat. Rev. Immunol. 2018 185* **18**, 309–324 (2018).

137. Dogra, C., Changotra, H., Mohan, S. & Kumar, A. Tumor necrosis factor-like weak inducer of apoptosis inhibits skeletal myogenesis through sustained activation of nuclear factor-κB and degradation of MyoD protein. *J. Biol. Chem.* **281**, 10327–10336 (2006).

138. LANGEN, R. C. J., SCHOLS, A. M. W. J., KELDERS, M. C. J. M., WOUTERS, E. F. M. & JANSSEN-HEININGER, Y. M. W. Inflammatory cytokines inhibit myogenic differentiation through activation of nuclear factor-κB. *FASEB J.* **15**, 1169–1180 (2001).

139. Mourkioti, F. *et al.* Targeted ablation of IKK2 improves skeletal muscle strength, maintains mass, and promotes regeneration. *J. Clin. Invest.* **116**, 2945–2954 (2006).

140. Ogura, Y. *et al.* TAK1 modulates satellite stem cell homeostasis and skeletal muscle repair. *Nat. Commun.* **6**, (2015).

141. Hindi, S. M. & Kumar, A. TRAF6 regulates satellite stem cell self-renewal and function during regenerative myogenesis. *J. Clin. Invest.* **126**, 151–168 (2016).

142. Straughn, A. R., Hindi, S. M., Xiong, G. & Kumar, A. Canonical NF-κB signaling regulates satellite stem cell homeostasis and function during regenerative myogenesis. *J. Mol. Cell Biol.* **11**, 53–66 (2019).

143. Collins, R. A. & Grounds, M. D. The Role of Tumor Necrosis Factor-alpha (TNF-) in Skeletal Muscle Regeneration: Studies in TNF-(-) and TNF-(-) LT-(-) Mice. *J. Histochem. Cytochem.* **49**, 989–1001 (2001).

144. Bakkar, N. & Guttridge, D. C. NF-κB signaling: A tale of two pathways in skeletal myogenesis. *Physiol. Rev.* **90**, 495–511 (2010).

145. Bakkar, N. *et al.* IKK/NF-κB regulates skeletal myogenesis via a signaling switch to inhibit differentiation and promote mitochondrial biogenesis. *J. Cell Biol.* **180**, 787–802 (2008).

146. Enwere, E. K. *et al.* TWEAK and cIAP1 regulate myoblast fusion through the noncanonical NF-κB signaling pathway. *Sci. Signal.* **5**, (2012).

147. Bakkar, N. *et al.* IKKα and alternative NF-κB regulate PGC-1β to promote oxidative muscle metabolism. *J. Cell Biol.* **196**, 497–511 (2012).

148. Shintaku, J. *et al.* MyoD Regulates Skeletal Muscle Oxidative Metabolism Cooperatively with Alternative NF-κ B. *Cell Rep.* **17**, 514 (2016).

149. Li, H., Malhotra, S. & Kumar, A. Nuclear Factor-kappa B Signaling in Skeletal Muscle Atrophy. *J. Mol. Med. (Berl).* **86**, 1113 (2008).

150. Londhe, P. *et al.* Classical NF-κB metabolically reprograms sarcoma cells through regulation of hexokinase 2. *Front. Oncol.* **8**, 104 (2018).

151. Cai, D. *et al.* IKKβ/NF-κB Activation Causes Severe Muscle Wasting in Mice. *Cell* **119**, 285–298 (2004).

152. He, W. A. *et al.* NF-κB-mediated Pax7 dysregulation in the muscle microenvironment promotes cancer cachexia. *J. Clin. Invest.* **123**, 4821–4835 (2013).

153. Acharyya, S. *et al.* Interplay of IKK/NF-κB signaling in macrophages and myofibers promotes muscle degeneration in Duchenne muscular dystrophy. *J. Clin. Invest.* **117**, 889 (2007).

154. Kumar, A. & Boriek, A. M. Mechanical stress activates the nuclear factor-kappaB pathway in skeletal muscle fibers: a possible role in Duchenne muscular dystrophy. *FASEB J.* **17**, 386–396 (2003).

155. Peterson, J. M. *et al.* Peptide-based inhibition of NF-κB rescues diaphragm muscle contractile dysfunction in a murine model of duchenne muscular dystrophy. *Mol. Med.* **17**, 508–515 (2011).

156. Tichy, E. D. *et al.* Persistent NF-κB activation in muscle stem cells induces proliferation-independent telomere shortening. *Cell Rep.* **35**, 109098 (2021).

157. Hammers, D. W. *et al.* Disease-modifying effects of orally bioavailable NF-κB inhibitors in dystrophin-deficient muscle. *JCI Insight* **1**, e90341 (2016).

158. Finkel, R. S. *et al.* Disease-modifying effects of edasalonexent, an NF-κB inhibitor, in

young boys with Duchenne muscular dystrophy: Results of the MoveDMD phase 2 and open label extension trial. *Neuromuscul. Disord.* **31**, 385–396 (2021).

159. Donovan, J. M., Zimmer, M., Offman, E., Grant, T. & Jirousek, M. A Novel NF-κB Inhibitor, Edasalonexent (CAT-1004), in Development as a Disease-Modifying Treatment for Patients With Duchenne Muscular Dystrophy: Phase 1 Safety, Pharmacokinetics, and Pharmacodynamics in Adult Subjects. *J. Clin. Pharmacol.* **57**, 627 (2017).

160. Finkel, R. S. *et al.* A Randomized, Double-Blind, Placebo-Controlled, Global Phase 3 Study of Edasalonexent in Pediatric Patients with Duchenne Muscular Dystrophy: Results of the PolarisDMD Trial. *J. Neuromuscul. Dis.* **8**, 769–784 (2021).

161. Hinds, M. G., Norton, R. S., Vaux, D. L. & Day, C. L. Solution structure of a baculoviral inhibitor of apoptosis (IAP) repeat. *Nat. Struct. Biol.* **6**, 648–651 (1999).

162. Yang, Y., Fang, S., Jensen, J. P., Weissman, A. M. & Ashwell, J. D. Ubiquitin protein ligase activity of IAPs and their degradation in proteasomes in response to apoptotic stimuli. *Science* **288**, 874–877 (2000).

163. Gyrd-Hansen, M. *et al.* IAPs contain an evolutionarily conserved ubiquitin-binding domain that regulates NF-kappaB as well as cell survival and oncogenesis. *Nat. Cell Biol.* **10**, 1309–1317 (2008).

164. Lopez, J. *et al.* CARD-Mediated Autoinhibition of cIAP1's E3 Ligase Activity Suppresses Cell Proliferation and Migration. *Mol. Cell* **42**, 569–583 (2011).

165. Feltham, R. *et al.* Smac mimetics activate the E3 ligase activity of cIAP1 protein by promoting RING domain dimerization. *J. Biol. Chem.* **286**, 17015–17028 (2011).

166. Graber, T. E. & Holcik, M. Distinct roles for the cellular inhibitors of apoptosis proteins 1 and 2. *Cell Death Dis. 2011 23* **2**, (2011).

167. Zadoroznyj, A. & Dubrez, L. Cytoplasmic and Nuclear Functions of cIAP1. (2022) doi:10.3390/biom12020322.

168. Mahoney, D. J. *et al.* Both cIAP1 and cIAP2 regulate TNFα-mediated NF-κB activation. *Proc. Natl. Acad. Sci. U. S. A.* **105**, 11778–11783 (2008).

169. Enwere, E. K. *et al.* Loss of cIAP1 attenuates soleus muscle pathology and improves diaphragm function in mdx mice. *Hum. Mol. Genet.* **22**, 867–878 (2013).

170. Lala-Tabbert, N. *et al.* Targeted ablation of the cellular inhibitor of apoptosis 1 (cIAP1) attenuates denervation-induced skeletal muscle atrophy. *Skelet. Muscle* **9**, 1–13 (2019).

171. Whitney, R. Role of cIAP1 and cIAP2 in Skeletal Muscle. (2022).

172. Tidball, J. G. Inflammatory processes in muscle injury and repair. *Am. J. Physiol. - Regul. Integr. Comp. Physiol.* **288**, 345–353 (2005).

173. Filippin, L. I., Moreira, A. J., Marroni, N. P. & Xavier, R. M. Nitric oxide and repair of skeletal muscle injury. *Nitric Oxide* **21**, 157–163 (2009).

174. Prakash, H. *et al.* cIAP-1 Controls Innate Immunity to C. pneumoniae Pulmonary Infection. *PLoS One* **4**, e6519 (2009).

175. Sun, H. *et al.* Design of small-molecule peptidic and nonpeptidic Smac mimetics. *Acc. Chem. Res.* **41**, 1264–1277 (2008).

176. Fulda, S. Promises and Challenges of Smac Mimetics as Cancer Therapeutics. *Clin. Cancer Res.* **21**, 5030–5036 (2015).

177. Varfolomeev, E. *et al.* IAP antagonists induce autoubiquitination of c-IAPs, NF-kappaB activation, and TNFalpha-dependent apoptosis. *Cell* **131**, 669–681 (2007).

178. Lammie, A. The roles of cellular Inhibitor of Apoptosis Proteins 1 and 2 in the polarization of M1 and M2 macrophages. vol. 1 (2018).

179. McComb, S. *et al.* cIAP1 and cIAP2 limit macrophage necroptosis by inhibiting Rip1 and Rip3 activation. *Cell Death Differ. 2012 1911* **19**, 1791–1801 (2012).

180. Morón-Calvente, V. *et al.* Inhibitor of apoptosis proteins, NAIP, cIAP1 and cIAP2 expression during macrophage differentiation and M1/M2 polarization. *PLoS One* **13**, (2018).

181. Ali, H. *et al.* Selective Induction of Cell Death in Human M1 Macrophages by Smac Mimetics Is Mediated by cIAP-2 and RIPK-1/3 through the Activation of mTORC. *J. Immunol.* **207**, 2359–2373 (2021).

182. De luca, A. *et al. Use of grip strength meter to assess the limb strength of mdx mice*. (2008).

183. van Putten, M., Aartsma-Rus, A., Dorchies, O., Nagaraju, K. & Carlson, G. *The use of hanging wire tests to monitor muscle strength and condition over time*. https://treat-nmd.org/wp-content/uploads/2021/06/uncategorized-Wire-test.pdf (2011).

184. Nagaraju, K., Gordish, H., Carlson, G. & De luca, A. *Serum Creatine Kinase analysis in mouse models of muscular*. (2008).

185. Esper, M. E., Kodippili, K. & Rudnicki, M. A. Immunofluorescence Labelling of Skeletal Muscle in Development, Regeneration, and Disease. *Methods Mol. Biol.* **2566**, 113 (2023).

186. Multiplexed analysis — QuPath Documentation. https://qupath.readthedocs.io/en/stable/docs/tutorials/multiplex_analysis.html (2024).

187. Bankhead, P. *et al.* QuPath: Open source software for digital pathology image analysis. *Sci. Reports 2017 71* **7**, 1–7 (2017).

188. Hildyard, J. C. W., Wells, D. J. & Piercy, R. J. Identification of qPCR reference genes

suitable for normalising gene expression in the developing mouse embryo. *Wellcome Open Res.* **6**, 197 (2021).

189. Hildyard, J. C. W. & Wells, D. J. Identification and validation of quantitative PCR reference genes suitable for normalizing expression in normal and dystrophic cell culture models of myogenesis. *PLoS Curr.* **6**, (2014).

190. Infante, J. R. *et al.* Phase I dose-escalation study of LCL161, an oral inhibitorof apoptosis proteins inhibitor, in patients with advanced solid tumors. *J. Clin. Oncol.* **32**, 3103–3110 (2014).

191. Yang, L. *et al.* LCL161, a SMAC mimetic, Preferentially Radiosensitizes Human Papillomavirus Negative Head and Neck Squamous Cell Carcinoma. *Mol. Cancer Ther.* **18**, 1025 (2019).

192. Beug, S. T. *et al.* Smac mimetics and innate immune stimuli synergize to promote tumor death. *Nat. Biotechnol. 2014 322* **32**, 182–190 (2014).

193. West, A. C. *et al.* The SMAC mimetic, LCL-161, reduces survival in aggressive MYC-driven lymphoma while promoting susceptibility to endotoxic shock. *Oncog. 2016 54* **5**, e216–e216 (2016).

194. Yuan, Z. *et al.* Blockade of inhibitors of apoptosis (IAPs) in combination with tumor-targeted delivery of tumor necrosis factor-α leads to synergistic antitumor activity. *Cancer Gene Ther. 2013 201* **20**, 46–56 (2012).

195. Kaspar, R. W., Allen, H. D. & Montanaro, F. Current understanding and management of dilated cardiomyopathy in Duchenne and Becker muscular dystrophy. *J. Am. Acad. Nurse Pract.* **21**, 241 (2009).

196. Restrepo-Cordoba, M. A. *et al.* Prevalence and clinical outcomes of dystrophin-associated dilated cardiomyopathy without severe skeletal myopathy. *Eur. J. Heart Fail.* **23**, 1276–1286 (2021).

197. De Giorgio, D. *et al.* Characterization of the Cardiac Structure and Function of Conscious D2.B10-Dmdmdx/J (D2-mdx) mice from 16–17 to 24–25 Weeks of Age. *Int. J. Mol. Sci.* **24**, 11805 (2023).

198. Hayes, H. M. *et al.* Preserved Left Ventricular Function despite Myocardial Fibrosis and Myopathy in the Dystrophin-Deficient D2.B10-Dmdmdx/J Mouse. *Oxid. Med. Cell. Longev.* **2022**, 5362115 (2022).

199. Maier, H. J. *et al.* Cardiomyocyte-specific IκB kinase (IKK)/NF-κB activation induces reversible inflammatory cardiomyopathy and heart failure. *Proc. Natl. Acad. Sci. U. S. A.* **109**, 11794–11799 (2012).

200. Siednienko, J., Jankowska, E. A., Banasiak, W., Gorczyca, W. A. & Ponikowski, P. Nuclear factor-kappaB activity in peripheral blood mononuclear cells in cachectic and non-cachectic patients with chronic heart failure. *Int. J. Cardiol.* **122**, 111–116

(2007).

201. Hamid, T. *et al.* Cardiomyocyte NF-κB p65 promotes adverse remodelling, apoptosis, and endoplasmic reticulum stress in heart failure. *Cardiovasc. Res.* **89**, 129 (2010).

202. Webster, C., Silberstein, L., Hays, A. P. & Blau, H. M. Fast muscle fibers are preferentially affected in Duchenne muscular dystrophy. *Cell* **52**, 503–513 (1988).

203. Wang, J. F., Forst, J., Schröder, S. & Schröder, J. M. Correlation of muscle fiber type measurements with clinical and molecular genetic data in Duchenne muscular dystrophy. *Neuromuscul. Disord.* **9**, 150–158 (1999).

204. Pedrazzani, P. S. *et al.* Twenty-one days of low-intensity eccentric training improve morphological characteristics and function of soleus muscles of mdx mice. *Sci. Reports 2021 111* **11**, 1–11 (2021).

205. Kiriaev, L. *et al.* Dystrophin-negative slow-twitch soleus muscles are not susceptible to eccentric contraction induced injury over the lifespan of the mdx mouse. *Am. J. Physiol. - Cell Physiol.* **321**, C704–C720 (2021).

206. Dimitrijević, M. R. & Gračanin, F. Differential involvement of tibialis anterior, gastrocnemius and soleus in muscular dystrophy. *J. Neurol. Sci.* **6**, 105–115 (1968).

207. Mázala, D. A. G. *et al.* Altered muscle niche contributes to myogenic deficit in the D2-mdx model of severe DMD. *Cell Death Discov. 2023 91* **9**, 1–13 (2023).

208. Straughn, A. R., Hindi, S. M., Xiong, G. & Kumar, A. Canonical NF-κB signaling regulates satellite stem cell homeostasis and function during regenerative myogenesis. *J. Mol. Cell Biol.* **11**, 53–66 (2019).

209. Ogura, Y., Mishra, V., Hindi, S. M., Kuang, S. & Kumar, A. Proinflammatory Cytokine Tumor Necrosis Factor (TNF)-like Weak Inducer of Apoptosis (TWEAK) Suppresses Satellite Cell Self-renewal through Inversely Modulating Notch and NF-κB Signaling Pathways. *J. Biol. Chem.* **288**, 35159 (2013).

210. Dong, J. & Ma, Q. In Vivo Activation and Pro-Fibrotic Function of NF-κB in Fibroblastic Cells During Pulmonary Inflammation and Fibrosis Induced by Carbon Nanotubes. *Front. Pharmacol.* **10**, (2019).

211. Sieber, P. *et al.* NF-κB drives epithelial-mesenchymal mechanisms of lung fibrosis in a translational lung cell model. *JCI Insight* **8**, e154719 (2023).

212. Rahman, F. A. & Krause, M. P. PAI-1, the Plasminogen System, and Skeletal Muscle. *Int. J. Mol. Sci.* **21**, 7066 (2020).

213. Lorts, A., Schwanekamp, J. A., Baudino, T. A., McNally, E. M. & Molkentin, J. D. Deletion of periostin reduces muscular dystrophy and fibrosis in mice by modulating the transforming growth factor-β pathway. *Proc. Natl. Acad. Sci. U. S. A.* **109**, 10978–10983 (2012).

214. Trundle, J. *et al.* Expression of the Pro-Fibrotic Marker Periostin in a Mouse Model of Duchenne Muscular Dystrophy. *Biomedicines* **12**, 216 (2024).

215. Abbad, L. *et al.* Role of Periostin and Nuclear Factor-κB Interplay in the Development of Diabetic Nephropathy. *Cells* **11**, 2212 (2022).

216. Raskatov, J. A. *et al.* Modulation of NF-κB-dependent gene transcription using programmable DNA minor groove binders. *Proc. Natl. Acad. Sci. U. S. A.* **109**, 1023–1028 (2012).

217. Szołtysek, K. *et al.* RRAD, IL4I1, CDKN1A, and SERPINE1 genes are potentially co-regulated by NF-κB and p53 transcription factors in cells exposed to high doses of ionizing radiation. *BMC Genomics* **19**, 813 (2018).

218. Uezumi, A. *et al.* Identification and characterization of PDGFRα+ mesenchymal progenitors in human skeletal muscle. *Cell Death Dis. 2014 54* **5**, e1186–e1186 (2014).

219. Craver, B. M. *et al.* The SMAC mimetic LCL-161 selectively targets JAK2V617F mutant cells. *Exp. Hematol. Oncol.* **9**, 1–9 (2020).

220. Pemmaraju, N. *et al.* Final results of a phase 2 clinical trial of LCL161, an oral SMAC mimetic for patients with myelofibrosis. *Blood Adv.* **5**, 3163–3173 (2021).

221. Wong, W. W. L. *et al.* cIAPs and XIAP regulate myelopoiesis through cytokine production in an RIPK1- and RIPK3-dependent manner. *Blood* **123**, 2562–2572 (2014).

222. Kang, X. *et al.* Interleukin-15 facilitates muscle regeneration through modulation of fibro/adipogenic progenitors. *Cell Commun. Signal.* **16**, 1–11 (2018).

223. Kaviratne, M. *et al.* IL-13 Activates a Mechanism of Tissue Fibrosis That Is Completely TGF-β Independent. *J. Immunol.* **173**, 4020–4029 (2004).

224. Su, S. *et al.* miR-142-5p and miR-130a-3p are regulated by IL-4 and IL-13 and control profibrogenic macrophage program. *Nat. Commun. 2015 61* **6**, 1–19 (2015).

225. Chun Geun Lee *et al.* Interleukin-13 Induces Tissue Fibrosis by Selectively Stimulating and Activating Transforming Growth Factor β1. *J. Exp. Med.* **194**, 809 (2001).

226. Chavey, C. *et al.* CXCL5 is an adipose tissue derived factor that links obesity to insulin resistance. *Cell Metab.* **9**, 339 (2009).

227. Lee, D., Lee, K. H., Kim, D. W., Yoon, S. & Cho, J. Y. CXCL5 inhibits excessive oxidative stress by regulating white adipocyte differentiation. *Redox Biol.* **54**, (2022).

228. Besnard, A.-G. *et al.* CXCL6 antibody neutralization prevents lung inflammation and fibrosis in mice in the bleomycin model. *J. Leukoc. Biol.* **94**, 1317–1323 (2013).

229. Jin, F. *et al.* Exercise training inhibits macrophage-derived IL-17A-CXCL5-CXCR2

inflammatory axis to attenuate pulmonary fibrosis in mice exposed to silica. *Sci. Total Environ.* **902**, (2023).

230. Pilling, D., Cox, N., Vakil, V., Verbeek, J. S. & Gomer, R. H. The Long Pentraxin PTX3 Promotes Fibrocyte Differentiation. *PLoS One* **10**, e0119709 (2015).

231. Doni, A. *et al.* Cell-specific regulation of PTX3 by glucocorticoid hormones in hematopoietic and nonhematopoietic cells. *J. Biol. Chem.* **283**, 29983–29992 (2008).

232. Garlanda, C., Bottazzi, B., Bastone, A. & Mantovani, A. Pentraxins at the crossroads between innate immunity, inflammation, matrix deposition, and female fertility. *Annu. Rev. Immunol.* **23**, 337–366 (2005).

233. Shiraki, A. *et al.* Pentraxin-3 regulates the inflammatory activity of macrophages. *Biochem. Biophys. Reports* **5**, 290–295 (2016).

234. Farini, A. *et al.* PTX3 Predicts Myocardial Damage and Fibrosis in Duchenne Muscular Dystrophy. *Front. Physiol.* **11**, 403 (2020).

235. Pelosi, L. *et al.* Increased levels of interleukin-6 exacerbate the dystrophic phenotype in mdx mice. *Hum. Mol. Genet.* **24**, 6041–6053 (2015).

236. Rufo, A. *et al.* Mechanisms inducing low bone density in duchenne muscular dystrophy in mice and humans. *J. Bone Miner. Res.* **26**, 1891–1903 (2011).

237. Messina, S. *et al.* Activation of NF-kB pathway in Duchenne muscular dystrophy: relation to age.

238. Kostek, M. C. *et al.* IL-6 signaling blockade increases inflammation but does not affect muscle function in the mdx mouse. *BMC Musculoskelet. Disord.* **13**, 1–12 (2012).

239. Wada, E. *et al.* Treatment with the anti-IL-6 receptor antibody attenuates muscular dystrophy via promoting skeletal muscle regeneration in dystrophin-/utrophin-deficient mice. *Skelet. Muscle* **7**, 1–15 (2017).

240. Zhang, J. *et al.* CD8 T Cells Are Involved in Skeletal Muscle Regeneration through Facilitating MCP-1 Secretion and Gr1high Macrophage Infiltration. *J. Immunol.* **193**, 5149–5160 (2014).

241. Fu, X. *et al.* Combination of inflammation-related cytokines promotes long-term muscle stem cell expansion. *Cell Res.* **25**, 655–673 (2015).

242. Dumke, B. R. & Lees, S. J. Age-related impairment of T cell-induced skeletal muscle precursor cell function. *Am. J. Physiol. - Cell Physiol.* **300**, C1226 (2011).

243. Burzyn, D. *et al.* A Special Population of Regulatory T Cells Potentiates Muscle Repair. *Cell* **155**, 1282 (2013).

244. Jin, R. M., Warunek, J. & Wohlfert, E. A. Therapeutic administration of IL-10 and amphiregulin alleviates chronic skeletal muscle inflammation and damage induced

by infection. *ImmunoHorizons* **2**, 142 (2018).

245. Burzyn, D. *et al.* A Special Population of regulatory T Cells Potentiates muscle repair. *Cell* **155**, 1282–1295 (2013).

246. Morrison, J., Lu, Q. L., Pastoret, C., Partridge, T. & Bou-Gharios, G. T-cell-dependent fibrosis in the mdx dystrophic mouse. *Lab. Invest.* **80**, 881–891 (2000).

247. Bersini, S. *et al.* Tackling muscle fibrosis: From molecular mechanisms to next generation engineered models to predict drug delivery. *Adv. Drug Deliv. Rev.* **129**, 64–77 (2018).

248. Villalta, S. A. *et al.* Regulatory T cells suppress muscle inflammation and injury in muscular dystrophy. *Sci. Transl. Med.* **6**, 258ra142 (2014).

249. Zhang, M. & Zhang, S. T Cells in Fibrosis and Fibrotic Diseases. *Front. Immunol.* **11**, 537227 (2020).

250. Giardino Torchia, M. L., Conze, D. B., Jankovic, D. & Ashwell, J. D. Balance between NF-κB p100 and p52 Regulates T Cell Costimulation Dependence. *J. Immunol.* **190**, 549–555 (2013).

251. Gerondakis, S., Fulford, T. S., Messina, N. L. & Grumont, R. J. NF-κB control of T cell development. *Nat. Immunol. 2013 151* **15**, 15–25 (2013).

252. Oh, H. & Ghosh, S. NF-κB: Roles and Regulation In Different CD4+ T cell subsets. *Immunol. Rev.* **252**, 41 (2013).

253. Knights, A. J., Fucikova, J., Pasam, A., Koernig, S. & Cebon, J. Inhibitor of apoptosis protein (IAP) antagonists demonstrate divergent immunomodulatory properties in human immune subsets with implications for combination therapy. *Cancer Immunol. Immunother.* **62**, 321–335 (2013).

254. Rizk, J. *et al.* SMAC mimetics promote NIK-dependent inhibition of CD4+ TH17 cell differentiation. *Sci. Signal.* **12**, (2019).

255. Dougan, M. *et al.* IAP inhibitors enhance co-stimulation to promote tumor immunity. *J. Exp. Med.* **207**, 2195–2206 (2010).

256. Kim, D. S. *et al.* Smac mimetics and oncolytic viruses synergize in driving anticancer T-cell responses through complementary mechanisms. *Nat. Commun.* **8**, (2017).

257. Burton, A. M., Ligman, B. R., Kearney, C. A. & Murray, S. E. SMAC mimetics inhibit human T cell proliferation and fail to augment type 1 cytokine responses. *Cell. Immunol.* **384**, (2023).